Computational Analysis of Viscoelastic Fluid Dynamics with Applications to Heat Exchangers

Anele Mavi

A dissertation submitted in fulfillment
of the requirements for the degree of
Master of Science
at the
University of Cape Town
under the supervision of
Dr Tiri Chinyoka

Department of Mathematics and Applied Mathematics

January 2019

Declaration of Authorship

I, Anele Mavi, confirm that:

- This work was done wholly or mainly while in candidature for a research degree at this university.
- Where any part of this thesis has previously been submitted for a degree or any other qualification at this university or any other institution, this has been clearly stated.
- Where I have consulted the published work of others, this is always clearly attributed.
- Where I have quoted from the work of others, the source is always given. With the exception of such quotations, this thesis is entirely my own work.
- I have acknowledged all the main sources of help.
- Where the thesis is based on work done by myself jointly with others, I have made clear exactly what was done by others and what I have contributed myself.

Signed: Signed by candidate

Date: 16 October 2018

Abstract

In this study, the computational analysis of a pressure driven viscoelastic fluid in a double pipe heat exchanger set-up is investigated. Non-Newtonian viscoelastic fluids in heat exchanger arrangements are encountered in various industrial applications such as power generation, refrigeration and in the food processing industry where the need for cooling and heating of liquids is required.

The model problem is governed by complex, non-linear and coupled partial differential equations. These are solved using the semi-implicit finite difference method integrated with the Crank-Nicolson scheme. The pressure-velocity coupling in the momentum equations is resolved by employing the Semi-Implicit Method for Pressure Linked Equations (SIMPLE). To cope with numerical diffusion and numerical stability issues the treatment of convective terms using the upwind schemes is explored.

In this work, the behaviour of viscoelastic fluids is rigorously examined by analysing the convective heat transfer from the viscoelastic core fluid of the double pipe heat exchanger to the Newtonian or viscoelastic shell fluid in the outer annulus. In addition, the effects of pressure, momentum, extra stresses, temperature, viscosity and relaxation time on the fluid temperature are investigated; both in the counter flow and parallel flow configurations.

Graphical computational results are presented and discussed quantitatively and qualitatively with respect to several parameters involved in the problem.

Acknowledgements

First and foremost, I will bless the Lord at all times and His praises shall continually be on my lips. I am so grateful to God for this great opportunity.

I would like to express my sincere gratitude to my supervisor Dr. Tiri Chinyoka for the continuous support during my research, for his patience, motivation and immense knowledge. His guidance and expertise helped me in all the time of research and writing of this thesis. I could not have imagined having a better supervisor for my MSc study.

To the UCT Mathematics Department and Science Faculty as well as to the National Research Foundation, I extend thanks for the financial support required to accomplish this work. I would like to acknowledge, in particular, Professor Daya Reddy for providing financial assistance via the South African Research Chair in Computational Mechanics.

My sincere gratitude also goes to my mentor Prof. Thabo Legwaila, thank you for your support and for encouraging me to pursue this MSc.

Finally, I must express my very deepest gratitude to my parents and family for providing me with unfailing support and continuous encouragement throughout my MSc programme. This accomplishment would not have been possible without them. Thank you

Contents

List of Figures

Nomenclature

Dimensionless quantities	
h	convective heat transfer
De	Deborah number
δ_2	Dissipative effect parameter
α_3	Giesekus nonlinear parameter
Pr	Prandtl number
β	Ratio of polymer to total viscosity
Re	Reynolds number
δ_3	thermal expansion
Greek symbols	
τ_2	Extra stresses
σ_3	Total stress tensor
η	Total viscosity
ξ	Ratio of change in temperature and Initial temperature
γ	Energy storing ability of a viscoelastic fluid
$\bar{\lambda}$	Relaxation time
μ	Viscosity
ε_η	Reference quantity from Nahme - type law
ε_λ	Reference quantity from Nahme - type law
Subscripts	
c	Denotes core fluid
s	Denotes shell fluid
Superscripts	
$*$	Dimensional parameter

Chapter 1

Introduction

1.1 Motivation

The study of non-Newtonian fluid dynamics and its numerical simulations, has generated an abundance of literature and research interest amongst scientists and engineers. In many branches of engineering and applied sciences, non-Newtonian fluids are unequivocally of critical importance and their pivotal role is encountered in various industrial applications.

Moreover, given the growing importance of these fluids in many industries, due to their intrinsic characteristics and complex rheology, many fluid models and numerical methods have been developed to describe their behaviour under various physical and geometric conditions. This growing development of advanced, efficient and robust numerical techniques under the Computational Fluid Dynamics framework has even saved industries the cost of conducting expensive experiments.

Certainly, an in-depth understanding of non-Newtonian fluid dynamics is of fundamental importance in industries such as pharmaceutical product development, mining, food processing, power generation, refrigeration, petroleum engineering, blood rheology, polymer processing just to name a few.

In this work, we limit our attention to applications involving flows through annular ducts, particularly double pipe heat exhangers. Heat exchangers play an important role in industries where the need for cooling and heating of liquids is required. Non-Newtonian viscoelastic fluids in heat exchanger arrangements are encountered in industrial applications such as power generation, air-conditioning, refrigeration and the food processing industry. In this research, a computationally based analysis will be conducted to investigate the flow of viscoelastic fluids in the parallel flow and counter flow configurations of a double pipe heat exchanger. The relevant flow phenomena is made up of complex,

coupled and non-linear partial differential equations which cannot be solved analytically hence a purely computational methodology for the solution processes is adopted.

The goal of this study is to add to the development of numerical simulations for solving complex fluid dynamics problems of industrial relevance.

1.2 Applications of Computational Fluid Dynamics (CFD) on various types of heat exchangers

Heat exchangers in their various forms are the most widespread and commonly used equipment in the operation of many systems such as metallurgical operations, chemical and petrochemical plants, oil refineries and power generation. They are utilized in heating, cooling, condensation and boiling applications. Their ineluctable demand has necessitated work on robust, dependable and efficient designs so as to achieve optimal performance in related operations [1].

There are many types of heat exchangers namely, shell and tube heat exchanger, double-pipe heat exchanger, plate type heat exchanger, fin-and-flat tube exchanger just to name a few however for an overview on various types refer to [2] and figure 1.1. Furthermore, there are three types of flows which can occur inside a heat exchanger, i.e, parallel flow, counter flow and cross flow. Fluid flow is one of the fundamental characteristics of heat exchangers. It has an influence on the heat transfer process, the design and overall performance of a heat exchanger. In this present report, we restrict our computational analysis of a pressure driven viscoelastic fluid in a double-pipe heat exchanger set-up with both parallel flow and counter flow configurations taken into account similar to work [3].

Extensive work has been implemented on different types of heat exchangers. Carla S. Fernandes et al. [4], examined the thermal behavior of a stirred yogurt (a viscoelastic fluid) in a plate heat exchanger. In his work, the effect of Reynolds number on a local Nusslet number was investigated and the effect of fluid entry on average Nusslet number was also analysed. In addition, a correlation between Nusslet number and Reynolds number was presented. Simulations were conducted by first considering the effect of temperature on viscosity and then by neglecting its effect. Computational results concluded that, Nusslet number increased as Reynolds number increased and it was also observed that for stirred yogurt simulations, the CPU time drastically declined when the temperature effect on viscosity was ignored.

Thomas Perrontin et al. [5], investigated heat transfer and pressure drop properties using a compact louvered fin-and-flat tube heat exchanger. The louvered fin-and-flat tube heat exchangers are used in the automotive and air conditioning industries. Thomas

and fellow researchers, simulated 2D and 3D models of fin-and-flat tube heat exchangers. It was found that at high Reynolds number, increasing heat transfer rates were observed where thermal boundary layers developed. The louver geometry gives multiple edges with great heat transfer coefficients. On the other hand, at low Reynolds number the heat transfer coefficient was low and this was due to the blocked spacing between successive louvers.

Utilizing a cross-flow heat exchanger, T. Chinyoka [6] modelled conduction-convection heat transfer between two fluids. In his work, the conduction-convection heat transfer between the viscoelastic core fluid with a constant viscosity and the Newtonian fluid in the outer annulus of the heat exchanger was analysed. Computational results showed that the viscoelastic core fluid had a lower temperature as compared to the Newtonian fluid. In applications such as car radiators these results are very significant, as they show that a viscoelastic fluid makes a good coolant because it is capable of releasing heat rapidly. For a comprehensive overview on CFD applications on heat exchangers, we refer to [2] and [7]. A few treaties on the study of the performance of a heat exchanger and the impact on the overall heat transfer by analysing parameters like Prandtl number, Dean's number, Nusselt number etc we cite [8], [9], [10] and [11].

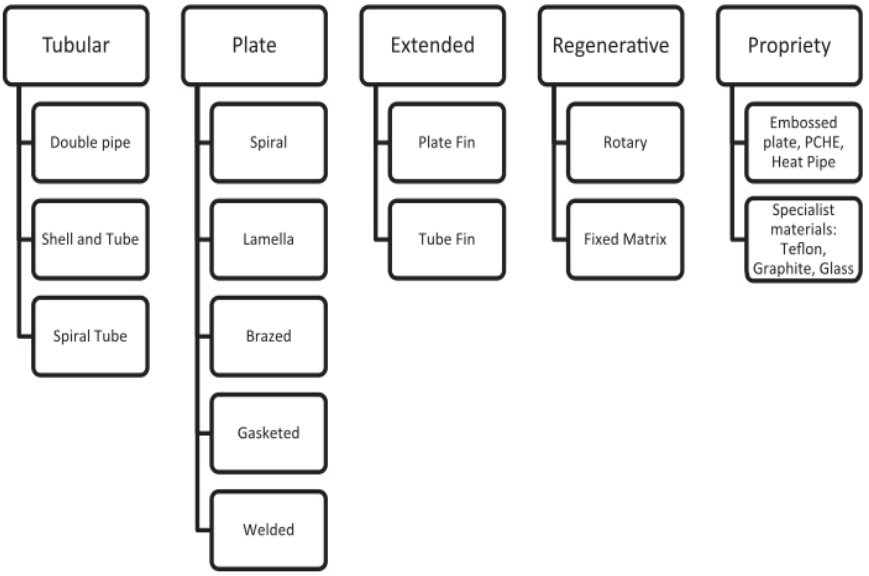

FIGURE 1.1: Classification of Heat Exchangers.

1.3 Newtonian and non-Newtonian fluids

1.3.1 Newtonian fluids

A Newtonian fluid is a fluid in which the viscosity, whilst varying with pressure, temperature and concentration, does not change with shear rate, applied stresses and time. Moreover, these fluids do not exhibit any elastic properties.

1.3.2 Non-Newtonian fluids

These are fluids which deviate from the Newtonian behaviour. In these fluids, shear stress and shear rate have a non-linear relationship. Furthermore, their viscosities depend on shear rate, applied stresses and time. Non-Newtonian fluids are divided into three classes namely [12] :

- **Viscoelastic fluids**:
  These fluids exhibit partial elastic recovery when deformation shear stress is removed. An intrinsic characteristic of a viscoelastic fluid is the simultaneous existence of viscous and elastic properties. This study will center on these type of fluids.
- **Time-dependent fluids**:
  In these type of fluids the share rate is a function of time and the size of shear stress.
- **Time-independent fluids**:
  In these fluids, share rate at a given point depends only on the instantaneous shear stress at that particular point. See figure 1.2 for different behaviours of these type of fluids.

Non-Newtonian and Newtonian fluids have complex rheology. Their complex physics has presented a rather challenging yet exciting task for numerical simulations. They are mathematically modelled using partial differential equations which are then solved using numerical methods. In the next section we will discuss three numerical methods which have been developed in this direction.

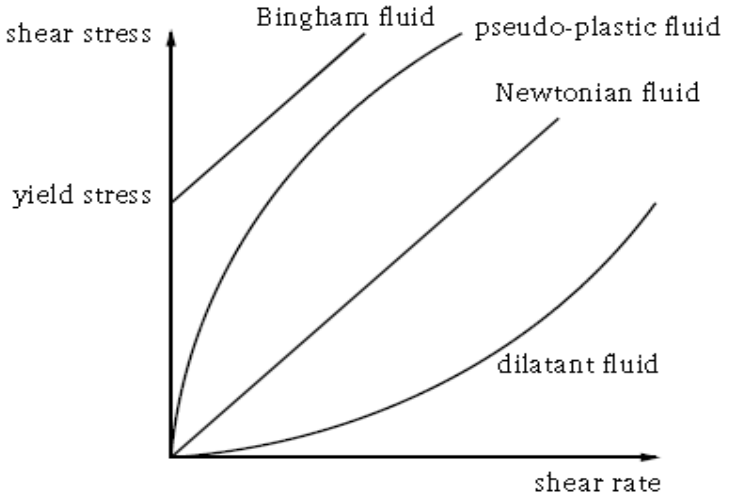

FIGURE 1.2: Different behaviours of Time-Independent fluids.

1.4 Numerical Methods

1.4.1 Finite Difference Scheme

Finite difference methods are widely used in simulating non-Newtonian and Newtonian fluid dynamics under different geometric and physical conditions. T. Chinyoka [3], modelled the conduction-convection heat transfer from a viscoelastic core fluid to a Newtonian fluid flowing in the outer annulus of the double pipe heat exchanger. Computational results showed that the viscoelastic core fluid had a slightly lower temperature than the Newtonian shell fluid and these observations are significant in industrial heating and cooling applications. In this research article, he employed the semi-implicit finite difference scheme and modified it to accommodate the Crank-Nicolson scheme for the treatment of implicit terms. In addition, second and first order derivatives were approximated with second order central differences. This approach, was echoed in his article on modelling of cross-flow heat exchangers with viscoelastic fluids [6]. As previously hinted in section 1.2 simulation results showed that again, viscoelastic fluids release heat more rapidly than Newtonian fluids. At this juncture, it is important to mention that the successful modelling results in these two articles are of great significance as they form an underpinning for this thesis.

This numerical approach has been successfully applied in other works; I.E Ireka and T. Chinyoka [13], examined the unsteady, non-isothermal and axi-symmetric flow of a viscoelastic Johnson-Segalman liquid in a lubricated pipe with a wall slip; O.D Makinde and T. Chinyoka [14] simulated the unsteady hydromagnetic flow of a third grade fluid with reactive variable viscosity and electrical conductivity. This flow was in between a moving and a fixed wall with asymmetric convective cooling and unvarying magnetic field. V. Casulli and R.T. Cheng [15], also successfully implemented the semi-implicit

finite difference scheme to obtain a numerical solution for three-dimensional shallow water flows.

M.Devakar et al. [16], analysed a fully developed flow of a non-Newtonian fluid in a linear duct through a porous medium. In their research article, the finite difference method was employed and a classical Gaussian elimination was used to solve the obtained algebraic equations. In the analysis of the flow and temperature fields which are simulated in an annulus possessing a porous lining between two concentric rotating cylinders, G. Nagaraju and fellow researchers [17] also opted for finite difference scheme. M.F Tomé et al. [18], when modelling unsteady viscoelastic free surface flows, further incorporated the marker-and-cell (MAC) method. NIU Jun et al. [19], successfully applied the finite difference method when investigating a buoyancy driven convection process of a viscoelastic fluid. This process was modelled in an open top square porous box which is subject to an unvarying heat flux boundary condition.

The finite difference method is unconditionally stable and convergent. However, a drawback with this scheme specifically when implemented on engineering problems, care should be taken in approximations in order to ensure conservation properties.

1.4.2 Finite Volume Scheme

The finite volume method gained its momentum and further established a prominent role in the numerical simulation of fluid dynamics problems as a consequence of research done by Professor Spalding [20] and fellow researchers S.V. Patankar [21], A.D. Gosman [22] just to name a few. This numerical method is one of the most flexible discretization methods used in Computational Fluid Dynamics (CFD). This is due to its ability to execute discretizations directly into the physical space without any transformation between the computational coordinate system and the physical. Furthermore, it is also well suited for solving flows in complex geometries because it seamlessly adopts to collocated arrangements [23]. A large number of numerical analysis has been successfully performed using this method.

S. De et al. [24], used the finite volume method with a staggered grid to simulate an unsteady three dimensional viscoelastic fluid flow through a porous medium. Furthermore, they used the Immersed Boundary Method(IBM) to impose boundary conditions at the walls of the porous medium. S-C. Xue et al. [25], numerically investigated the strength and pattern of secondary flows of a viscoelastic fluid in straight pipes over a range of ratios and material parameters. In this work, S-C. Xue and co-workers employed the implicit finite volume method based on the SIMPLE algorithm with splitting technique (SIMPLEST algorithm). When simulating a steady laminar flow of an Oldroyd-B fluid in a lid driven square cavity with a range of Weissenberg and Reynolds numbers, K. Yapici et al. [26], integrated the finite volume method with second order central difference scheme for the treatment of convection terms in the momentum equations whilst

employing the first order upwind approximation to deal with viscoelastic stresses. For pressure-velocity decoupling in the momentum equations they opted for SIMPLE algorithm. FU Chun-quan et al. [27], in their research paper, the mathematical modelling of a viscoelastic fluid flow through an expansion channel was considered. Their governing equations were solved using the finite volume method on a staggered grid and hybrid schemes were used for solving velocities. In agreement with K. Yapici et al. [26], they also used upwind schemes to handle viscoelastic stresses.

The finite volume method is also available on OpenFOAM software. F. Pimenta and M.A. Alves [28], their research article took a different approach in that, they looked into the stabilization of an open-source finite volume solver for viscoelastic fluid dynamics. In their study, they successfully modified the viscoelastic solver available on the OpenFOAM software toolbox so as to improve its stability for solving differentiated-type constitutive equations. To achieve this an Oldroyd-B constitutive equation was solved using the log-confirmation method and the component-wise and deffered correction approach were proposed for the discretization of convective terms. In addition, the SIMPLEC algorithm was also adopted as one of the solution techniques.

It is also important to mention that the finite volume method can also be used in phase-change related problems. J.Rigola et al. [29], in their paper, a numerical study of the thermal and fluid dynamic behaviour of two-phase flow in double pipe condensers and evaporators was conducted. Similar to S. De and fellow researchers [24], they also employed the pressure based method SIMPLEC for solving discretized governing equations and also giving special attention on the handling of the transition from one phase to another.

The finite volume has certainly been implemented successfully on many fluid dynamics models with complex geometries.

1.4.3 Finite Elements Scheme

The genesis of the finite element method can be traced back to structural mechanics in the early and mid sixties [30] and [31]. In fact the first research article on this method was published by M.J. Turner et al. [32] and Professor R.W. Clough conceived the term finite element in one of his articles in 1960. However, in later years O.C. Zienkiewicz and Y.K. Cheung [33], realized the potential of implementing the finite element method beyond structural mechanics to general field problems. This paved a way for further utilizing this method for fluid dynamics related problems. Since then indeed this numerical method has been used to solve a wide range of fluid dynamics tasks.

M. Vibiyayuthakorn and B. Caswbll [34], in their research paper, the finite element method was used to simulate the flow of a memory fluid, i.e, viscoelastic fluid with significant relaxation effects. P. Yue et al. [35], simulated phase-fields of interfacial dynamics

in viscoelastic fluids and in their algorithm they incorporated an adoptive meshing. M. Mellal et al. [36], examined the three dimensional simulation of a heat transfer in a shell side of a shell-and-tube heat exchanger and a turbulent fluid flow. Their analysis was carried out using the Computational Fluid Dynamics(CFD) COSMOL multiphysics 5.1 software utilizing finite element method.

R.Keunings and M.J.Crochet [37], simulated a viscoelastic fluid flow through a contraction geometry. Y.J. Choi et al, [38], modelled a viscoelastic fluid with suspended particles. A.W. Liu et al. [39] in their research article they carried out investigations on a viscoelastic fluid flow of polymer solutions around a periodic linear array of cylinders. Three models were used to carry out this simulation, namely the Giesekus model, finite extensible non-linear elastic dumbbell model with Peterlin's approximations (FENE-P) and the FENE dumbbell model of Chilcott-Rallison (CR). E. Castillo and R. Codina [40], performed a finite element method approximation of a viscoelastic fluid flow. In this article, they numerically tested a three-field finite element stabilization formulation for an incompressible viscoelastic flow problem.

Over the years to date literature has seen a great influx of various types of fluid dynamics problem solved using the finite element method.

1.5 Objective and organization of the thesis

This dissertation, is concerned with the computational analysis of a pressure driven viscoelastic fluid in a double pipe heat exchanger. The analysis is achieved by examining the heat transfer from the core viscoelastic fluid of the heat exchanger to the shell fluid (which can either be Newtonian or viscoelastic) in the outer annulus. The organization of this thesis is as follows: In chapter 2, the governing equations, physical description and thermodynamical modelling of the problem are presented. In the subsequent chapter 3, the numerical modelling using the semi-implicit finite difference method integrated with the Crank-Nicolson scheme, SIMPLE algorithm and Upwind scheme is discussed in detail. In addition, the discretized form of all the governing equations described in chapter 2 are presented therein. Followed by chapter 4, which provides a brief graphical presentation of the spatial and temporal convergence of the numerical method used. Next, computational results are presented and discussed in chapter 5. Finally, chapter 6 ends this thesis with a summary of work presented.

Chapter 2

Mathematical Model Formulation

This chapter describes the physical description, governing equations and thermodynamical modelling of the problem presented.

2.1 Model Description

2.1.1 Physical Description of the Model Problem

In this study, the geometry of the problem is the shell-and-tube heat exchangers set-up. The model consists of an inner circular straight pipe symmetrically surrounded by an outer pipe. The inner pipe (which will be referred to as the core) has dimensions, radius R_c where $0 < R_c \leq 1$ and a length L. The outer pipe (which will be referred to as the shell) has a radius R_s and the same length as the core pipe, L. For mathematical modelling we employ the polar cylindrical coordinate system, (r, θ, z) when the flow occurs under the rotational symmetry. However all the quantities do not depend on θ i.e. $\frac{\partial}{\partial \theta} = 0$ therefore the azimuthal component (v) of velocity $V = (u, v, w)$ vanishes identically. Thus the cylindrical coordinate system used is (r, z) and is chosen such that the z-axis is on the horizontal plane and the r-axis on the vertical plane.

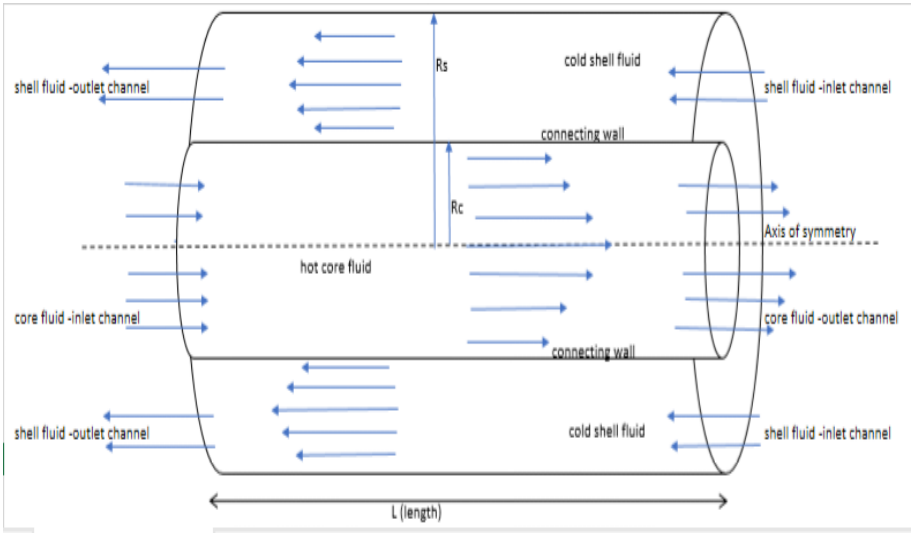

FIGURE 2.1: Schematics of the model problem.

2.1.2 Flow Pattern

The motion of both the core-fluid and shell-fluid is considered to be a Poiseuille flow where the motion is induced by different pressure gradients. The flow is assumed to be dynamically fully developed over the entire length of the pipes and the velocity distribution across each pipe will be parabolic. It is also assumed that at the initial stage of the model problem, the core-fluid is hot and the shell-fluid cold thus the heat transfer by convection is investigated. It is further assumed that the core-fluid flow depends on a two-dimensional flow velocity and the shell-fluid flow on a one-dimensional flow velocity. In shell-and-tube heat exchangers, the two fluids in their respective compartments can have either a counter flow, parallel flow or cross flow configuration. However in this computational analysis only the parallel and counter flow configurations are examined. For a counter flow arrangement, the core-fluid moves from left to right in response to the negative pressure gradient $-G_c$ and the shell-fluid moves from right to left due to the positive pressure gradient G_s. On the other hand, the parallel flow arrangement both fluids move from left to right driven by negative pressure gradient $-G$.

2.1.3 Fluid Rheology

A laminar flow of an incompressible non-Newtonian viscoelastic fluid and a Newtonian fluid is considered. This analysis examines two cases firstly, when the core-fluid is viscoelastic and the shell-fluid is Newtonian. Secondly, when the core-fluid is viscoelastic and the shell-fluid is non-Newtonian. Furthermore in both cases an isothermal and a non-isothermal study will be investigated.

2.2 Governing equations

The core and shell fluid systems are governed by the Navier-Stokes equations which are the continuity, momentum and energy conservation equations for incompressible flows together with the constitutive equations describing the fluid stress behavior. Since the two fluids are separated by a connecting solid wall through which a heat exchange or convection occurs, the temperature of the wall is governed by a one-dimensional heat equation.

2.2.1 Governing equations for the core and shell fluids

The mass balance equation :

$$\nabla^* \cdot V^* = 0. \tag{2.1}$$

The momentum balance equation:

$$\rho \frac{DV^*}{Dt^*} = \nabla^* \cdot \underline{\underline{\tau}}^* + F^*. \tag{2.2}$$

The energy balance equation:

$$\rho^* C_p^* \frac{DT^*}{Dt^*} = Q_D^* - \nabla^* \Phi_q^* + C_\beta^* T^* V^* \cdot \nabla^* p + h^*(T_w^* - T^*). \tag{2.3}$$

The equation governing the viscoelastic extra-stresses follows the non-isothermal Giesekus model [3], [41] and [42] and is given by,

$$\underline{\underline{\tau}}^* + \alpha^* \underline{\underline{\tau}}^{*2} + \lambda^* \left(\overset{\nabla}{\underline{\underline{\tau}}}^* - \underline{\underline{\tau}}^* \frac{D}{Dt^*} \ln \left[\frac{T^*}{T_{so}^*} \right] \right) = \eta^*{}_p(T^*) \underline{\underline{S}}_\nu{}^*, \tag{2.4}$$

where α^* is Giesekus nonlinear term and $\overset{\nabla}{\underline{\underline{\tau}}}^*$ is the upper convected time derivative which is defined as,

$$\overset{\nabla}{\underline{\underline{\tau}}}^* = \frac{\partial \underline{\underline{\tau}}^*}{\partial t^*} + (V^* \cdot \nabla^*) \underline{\underline{\tau}}^* - (\nabla^* V^*) \underline{\underline{\tau}}^* - \underline{\underline{\tau}}^* (\nabla^* V^*)^T. \tag{2.5}$$

Here

$$\frac{D()}{Dt} = \frac{\partial}{\partial t} + (V^* \cdot \nabla^*)() \tag{2.6}$$

is the material derivative and () represents the physical quantity. In the momentum equation, F^* is the body force due to friction factors and will be neglected. The total

stress is hereby divided into a solvent (Newtonian) and a polymer (viscoelastic) and it is given by,

$$\underline{\underline{\sigma}}^* = -p^* \underline{\underline{I}}^* + \underline{\underline{\tau}}^* + \eta^* \underline{\underline{S}}^* \tag{2.7}$$

where $\underline{\underline{S}}^* = [\nabla^* V^* + (\nabla^* V^*)^T]$ is the deformation rate tensor, $\underline{\underline{I}}^*$ is the unit tensor and $\underline{\underline{\tau}}^*$ is the extra stress tensor.

The internal heat production is given by,

$$Q_D^* = \gamma \underline{\underline{\tau}}^* : \underline{\underline{S}}^* + (1-\gamma)\eta_{sol}^* \underline{\underline{S}}^* : \underline{\underline{S}}^* \tag{2.8}$$

which is composed of an irreversible component $\eta_{sol}^* \underline{\underline{S}}^* : \underline{\underline{S}}^*$ called mechanical dissipation [42],[43],[44] and [45] and a reversible part $\underline{\underline{\tau}}^* : \underline{\underline{S}}^*$. Gamma, denoted by $0 \leq \gamma \leq 1$ describes the energy storing ability of a viscoelastic fluid. In the case of $\gamma = 1$, this represents pure entropy elasticity [46],[43],[44] and [45] in which the mechanical energy released as heat corresponds to pure viscous material behavior. On the other hand, $\gamma = 0$ corresponds to mechanical energy stored as elastic energy which matches pure elastic material behavior[46] and [45].

The heat flow rate which is referred to as heat flux is mathematically expressed by a Fourier law of heat conduction as follows,

$$\Phi_q^* = -k^* \nabla^* T^*, \tag{2.9}$$

where k is the thermal conductivity.

The viscosity and relaxation time are assumed to vary with temperature. Thus total viscosity is mathematically expressed as

$$\eta_{sol}^*(T^*) + \eta^*{}_p(T^*), \tag{2.10}$$

where $\eta_{sol}^*(T^*)$ is the solvent viscosity and $\eta^*{}_p(T^*)$ the polymer viscosity. The relaxation time which is defined as the time required for a fluid to return to its base state after deformation is denoted as $\lambda^*(T^*)$. Their temperature dependency follows Nahmes-type law [47][48],[49] and [50] which reads,

$$\lambda^* = \lambda_0 \bar{\lambda}(T^*), \qquad \eta_{sol}^* = \eta_{sol_0} \mu(T^*), \qquad \eta_p^* = \eta_{p0} \mu(T^*), \qquad \eta_s^* = \eta_{s0} \mu(T^*)$$

where

$$\bar{\lambda}(T^*) = (1-\delta_\lambda) + \delta_\lambda \frac{T_0^*}{T_c^*} \exp(-\varepsilon_\lambda \Theta_c), \qquad \mu(T^*) = \exp(-\varepsilon_\eta \Theta_c)$$

with $\Theta = (\frac{T^* - T^*_0}{\Delta T^*})$ and $\Delta T^* = T^*_{c0} - T^*_{s0}$. The zero subscripted quantities indicate constant reference values and $\delta_\lambda \in \{0, 1\}$ is a delta function such that

$$\delta_\lambda = \begin{cases} 0 & \text{if } \varepsilon_\lambda = 0 \\ 1 & \text{otherwise} \end{cases}$$

The temperature of the connecting wall is governed by the one-dimensional heat equation which is defined as follows,

$$\frac{\partial T^*_w}{\partial t^*} = K^*_w \frac{\partial^2 T^*_w}{\partial z^{*2}} + h^*_c(T^*_c - T^*_w) + h^*_s(T^*_s - T^*_w). \tag{2.11}$$

We now introduce the following dimensionless variables and parameters to the governing equations;

$$\begin{aligned}
t &= \frac{U^*_0}{L^*}t^*, & \underline{\underline{\tau}} &= \frac{L^*}{\eta^*_0}U^*_0, & p &= \rho^* U^{*2}_0 P^*, & V &= \frac{V^*}{U^*_0}, \\
z &= \frac{z^*}{L^*}, & \nabla &= L^*\nabla^*, & \underline{\underline{S}} &= \frac{L^*}{U^*_0}\underline{\underline{S}}^*, & \bar{\lambda} &= \frac{\lambda^*}{\lambda^*_0}, \\
\mu &= \frac{\eta^*}{\eta^*_0} & Re &= \frac{\rho^* U^*_0 L^*}{\eta^*_0}, & Pr &= \frac{C^*_p \eta^*_0}{K^*}, & \beta &= \frac{\eta^*_{p0}}{\eta^*_0}, \\
De &= \frac{\lambda^*_0 U^*_0}{L^*}, & h &= \frac{L^{*2}}{K^*}h^*, & \delta_3 &= C^*_\beta T^*_0, & \delta_2 &= \frac{\eta^*{}_0 U^{*2}_0}{K^* \Delta T^{*2}}, \\
\alpha &= \frac{L^*}{\eta^*_0 \mu^* U^*_0}, & t &= \frac{K^*_w t^*}{L^{*2}}.
\end{aligned}$$

In dimensionless form, the governing equations (2.1), (2.2) and (2.3) become,

$$\nabla \cdot V = 0, \tag{2.12}$$

$$\frac{DV}{Dt} = -\nabla p + \frac{1}{Re}\nabla \cdot [(\mu \underline{\underline{\tau}}) + (\mu \underline{\underline{S}})], \tag{2.13}$$

$$\begin{aligned}
RePr\frac{DT}{Dt} = \nabla^2 T + \delta_2 \mu[\gamma(\tau : \underline{\underline{S}}) + (1-\gamma)(1-\beta)\underline{\underline{S}} : \underline{\underline{S}}] \\
+ Re\delta_2\delta_3\Big(T + \frac{1}{\xi}\Big)V \cdot \nabla p + h(T_w - T).
\end{aligned} \tag{2.14}$$

The non-dimensional non-isothermal Giesekus equation for the viscoelastic extra stresses reduces to,

$$\underline{\underline{\tau}} + \alpha \underline{\underline{\tau}}^2 + De\frac{\bar{\lambda}}{\mu}\Big(\overset{\nabla}{[\mu \underline{\underline{\tau}}]} - \mu \underline{\underline{\tau}}\frac{D}{Dt}\ln[\xi T + 1]\Big) = \beta \underline{\underline{S}} \tag{2.15}$$

where

$$\xi = \frac{\Delta T}{T_{s0}}, \qquad \mu = \exp(-\varepsilon_\eta T), \qquad \bar{\lambda} = (1-\delta_\lambda) + \delta_\lambda \frac{1+\xi}{1+\xi T}\exp(-\varepsilon_\lambda T).$$

2.2.2 Equations in cylindrical form

We now recast the governing equations to cylindrical coordinates and this is in accordance with the geometry of the problem presented. This transformation is crucial for solving the equations using the finite difference numerical method.

Furthermore these equations are subject to initial and boundary conditions. The boundary conditions will either be prescribed or linearly extrapolated using neighbourhood values. At unprescribed boundaries the linear extrapolation processes will be done using the following expressions, similar to works [3], [6], [51], [52], [53], [54] and [55],

inlet channel:

$$\frac{\partial()_{i,j}}{\partial z}(t, r_0^+, z_0^+) = \frac{\partial()_{i,j}}{\partial z}(t, r_1^-, z_1^-), \tag{2.16}$$

outlet channel:

$$\frac{\partial()_{i,j}}{\partial z}(t, r_{M-1}^+, z_{N-1}^+) = \frac{\partial()_{i,j}}{\partial z}(t, r_M^-, z_N^-), \tag{2.17}$$

top solid wall:

$$\frac{\partial()_{i,j}}{\partial r}(t, r_0^+, z_0^+) = \frac{\partial()_{i,j}}{\partial r}(t, r_1^-, z_1^-), \tag{2.18}$$

bottom solid wall:

$$\frac{\partial()_{i,j}}{\partial r}(t, r_{M-1}^+, z_{N-1}^+) = \frac{\partial()_{i,j}}{\partial r}(t, r_M^-, z_N^-), \tag{2.19}$$

where $()_{i,j}$ denotes the physical quantity, $r = r_0^+$, $r = r_1^-$, $z = z_0^+$, $z = z_1^-$,$r = r_{M-1}^+$, $r = r_M^-$, $z = z_{N-1}^+$ and $z = z_N^-$ represent grid points on subintervals M and N of the interval [0,1]. The superscripts on the partial derivatives $\frac{\partial()_{i,j}}{\partial z}(t, r_{M-1}^+, z_{N-1}^+)$, $\frac{\partial()_{i,j}}{\partial z}(t, r_0^+, z_0^+)$, $\frac{\partial()_{i,j}}{\partial r}(t, r_0^+, z_0^+)$ and $\frac{\partial()_{i,j}}{\partial r}(t, r_{M-1}^+, z_{N-1}^+)$ denote the forward differences. On the other hand partial derivatives $\frac{\partial()_{i,j}}{\partial z}(t, r_M^-, z_N^-)$, $\frac{\partial()_{i,j}}{\partial z}(t, r_1^-, z_1^-)$, $\frac{\partial()_{i,j}}{\partial r}(t, r_1^-, z_1^-)$ and $\frac{\partial()_{i,j}}{\partial r}(t, r_M^-, z_N^-)$ denote the backward differences. These are constructed using the finite difference method.

2.2.2.1 Core fluid Equations

The continuity equation is given by,

$$\frac{\partial u_c}{\partial r} + \frac{u_c}{r} + \frac{\partial w_c}{\partial z} = 0. \tag{2.20}$$

The momentum equation reads,
$z - component$:

$$\frac{\partial w_c}{\partial t} + u_c\frac{\partial w_c}{\partial r} + w_c\frac{\partial w_c}{\partial z} = -\frac{\partial p}{\partial z} + \frac{1}{Re_c}\Big(\mu_c\frac{\partial^2 w_c}{\partial r^2} + \frac{\mu_c}{r}\frac{\partial w_c}{\partial r} + 2\mu_c\frac{\partial^2 w_c}{\partial z^2} + 2\mu_c\frac{\partial^2 u_c}{\partial r\partial z}\Big) + \frac{1}{Re_c}\Big(2\frac{\partial \mu_c}{\partial z}\frac{\partial w_c}{\partial z} + \frac{\partial \mu_c}{\partial r}\frac{\partial w_c}{\partial r} + \mu_c\frac{\partial \tau_{rz}}{\partial r} + \mu_c\frac{\partial \tau_{zz}}{\partial z} + \mu_c\frac{\tau_{rz}}{r}\Big), \tag{2.21}$$

$r - component$:

$$\frac{\partial u_c}{\partial t} + u_c\frac{\partial u_c}{\partial r} + w_c\frac{\partial u_c}{\partial z} = -\frac{\partial p}{\partial r} + \frac{1}{Re_c}\Big(2\mu_c\frac{\partial^2 u_c}{\partial r^2} + \frac{2\mu_c}{r}\frac{\partial u_c}{\partial r} + \mu_c\frac{\partial^2 u_c}{\partial z^2} + 2\mu_c\frac{\partial^2 w_c}{\partial z\partial r}\Big) + \frac{1}{Re_c}\Big(2\frac{\partial \mu_c}{\partial z}\frac{\partial u_c}{\partial z} + \frac{\partial \mu_c}{\partial r}\frac{\partial u_c}{\partial r} + \mu_c\frac{\partial \tau_{rr}}{\partial r} + \mu_c\frac{\partial \tau_{rz}}{\partial z} + \mu_c\frac{\tau_{rr}}{r}\Big). \tag{2.22}$$

It assumed that the flow is fully developed and therefore the initial velocity condition is given by ,

$$w_c(r) = \frac{-G_c Re_c}{2\mu_c}(R_c^2 - r), \tag{2.23}$$

where $0 \leqq r \leqq 1$ and $G_c = \frac{G_c^* L^*}{\rho_c^* w^{*2}_{c0}}$ is the dimensionless pressure gradient [3], [6] and [56] which drives the fluid into motion.

Boundary conditions to be satisfied are the following,

no-slip condition:

$$\begin{aligned} w_c(t,1,z) &= 0, \\ u_c(t,1,z) &= 0, \end{aligned} \tag{2.24}$$

axisymmetric (centerline)condition:

$$\begin{aligned} \frac{\partial w_c}{\partial r}(t,0,z) &= 0, \\ \frac{\partial u_c}{\partial r}(t,0,z) &= 0, \end{aligned} \tag{2.25}$$

inlet channel:

$$\frac{\partial w_{c_{i,j}}}{\partial z}(t, r_0^+, z_0^+) = \frac{\partial u_{c_{i,j}}}{\partial z}(t, r_1^-, z_1^-), \tag{2.26}$$

$$\frac{\partial w_{c_{i,j}}}{\partial z}(t, r_0^+, z_0^+) = \frac{\partial u_{c_{i,j}}}{\partial z}(t, r_1^-, z_1^-), \tag{2.27}$$

outlet channel:

$$\frac{\partial w_{c_{i,j}}}{\partial z}(t, r_{M-1}^+, z_{N-1}^+) = \frac{\partial u_{c_{i,j}}}{\partial z}(t, r_M^-, z_N^-), \tag{2.28}$$

$$\frac{\partial w_{c_{i,j}}}{\partial z}(t, r_{M-1}^+, z_{N-1}^+) = \frac{\partial u_{c_{i,j}}}{\partial z}(t, r_M^-, z_N^-). \tag{2.29}$$

The energy equation in cylindrical coordinates is as follows,

$$\begin{aligned} Re_c Pr_c\Big(\frac{\partial T_c}{\partial t} + u_c\frac{\partial T_c}{\partial r} + w_c\frac{\partial T_c}{\partial z}\Big) &= \Big(\frac{\partial^2 T_c}{\partial r^2} + \frac{1}{r}\frac{\partial T_c}{\partial r} + \frac{\partial^2 T_c}{\partial z^2}\Big) \\ &+ Re_c\delta_{c2}\delta_{c3}\Big(1+\frac{1}{\xi}\Big)\Big(u_c\frac{\partial p}{\partial r} + w_c\frac{\partial p}{\partial z}\Big) + h_c(T_w - T_c) \\ &+ \delta_{c2}\mu_c\Big[\gamma\Big(2\tau_{rr}\frac{\partial w_c}{\partial z} + 2\tau_{rz}\Big(\frac{\partial u_c}{\partial z} + \frac{\partial w_c}{\partial r}\Big) + 2\tau_{zz}\frac{\partial u_c}{\partial r} + 2\frac{u_c}{r}\Big) \\ &+ (1-\gamma)(1-\beta)\Big(2\Big(\frac{\partial u_c}{\partial r}\Big)^2 + 2\Big(\frac{u_c}{r}\Big)^2 + 2\Big(\frac{\partial w_c}{\partial z}\Big)^2 + \Big(\frac{\partial u_c}{\partial z} + \frac{\partial w_c}{\partial r}\Big)^2\Big)\Big] \end{aligned} \tag{2.30}$$

subject to an initial condition given by,

$$T_c(0, r, w) = 1, 0 \leqq r \leqq 1. \tag{2.31}$$

Boundary condition are presented as follows,

solid wall :

$$\frac{\partial T_{ci,j}}{\partial r}(t, r_{M-1}^+, z_{N-1}^+) = \frac{\partial T_{ci,j}}{\partial r}(t, r_M^-, z_N^-), \tag{2.32}$$

axisymmetric (centreline) condition:

$$\frac{\partial T_c}{\partial r}(t, 0, z) = 0, \tag{2.33}$$

inlet channel condition:

$$T_c(t, 0, z) = 1 = T_c(t, 1, z), \tag{2.34}$$

outlet channel condition:

$$\frac{\partial T_{ci,j}}{\partial z}(t, r^+_{M-1}, z^+_{N-1}) = \frac{\partial T_{ci,j}}{\partial z}(t, r^-_M, z^-_N). \tag{2.35}$$

The viscoelastic stresses are expressed in cylindrical coordinates as,

$$\begin{aligned}&\mu_c\tau_{rr} + \alpha\mu_c{\tau_{rr}}^2 + De\bar{\lambda}\Big[\Big(\frac{\partial}{\partial t}\mu_c\tau_{rr} + u_c\frac{\partial}{\partial r}\mu_c\tau_{rr} + w_c\frac{\partial}{\partial z}\mu_c\tau_{rr}\Big)\\ &-\mu_c\Big(2\tau_{rr}\frac{\partial u_c}{\partial r} + 2\tau_{rz}\frac{\partial u_c}{\partial z}\Big) - \mu_c\tau_{rr}\frac{D}{Dt}\ln[\xi T_c + 1]\Big] = 2\mu_c\beta\frac{\partial u_c}{\partial r},\end{aligned} \tag{2.36}$$

$$\begin{aligned}&\mu_c\tau_{rz} + \alpha\mu_c{\tau_{rz}}^2 + De\bar{\lambda}\Big[\big(\frac{\partial}{\partial t}\mu_c\tau_{rz} + u_c\frac{\partial}{\partial r}\mu_c\tau_{rz} + w_c\frac{\partial}{\partial z}\mu_c\tau_{rz}\Big)\\ &-\mu_c\Big(\tau_{rr}\frac{\partial w_c}{\partial r} + \tau_{rz}\Big(\frac{\partial u_c}{\partial r} + \frac{\partial w_c}{\partial z}\Big) + \tau_{zz}\frac{\partial u_c}{\partial z}\Big) - \mu_c\tau_{rz}\frac{D}{Dt}\ln[\xi T_c + 1]\Big]\\ &= \mu_c\beta\Big(\frac{\partial u_c}{\partial z} + \frac{\partial w_c}{\partial r}\Big),\end{aligned} \tag{2.37}$$

$$\begin{aligned}&\mu_c\tau_{zz} + \alpha\mu_c{\tau_{zz}}^2 + De\bar{\lambda}\Big[\big(\frac{\partial}{\partial t}\mu_c\tau_{zz} + u_c\frac{\partial}{\partial r}\mu_c\tau_{zz} + w_c\frac{\partial}{\partial z}\mu_c\tau_{zz}\Big)\\ &-\mu_c\Big(2\tau_{rz}\frac{\partial w_c}{\partial r} + 2\tau_{rz}\frac{\partial w_c}{\partial z}\Big) - \mu_c\tau_{zz}\frac{D}{Dt}\ln[\xi T_c + 1]\Big] = 2\mu_c\beta\frac{\partial w_c}{\partial z}.\end{aligned} \tag{2.38}$$

The equations are subject to the following initial condition,

$$\tau_{i,j} = 0, 0 \leq r \leq 1. \tag{2.39}$$

Boundary conditions are implemented at the walls, centreline, inlet channel and outlet channel of the pipe. These are mathematically expressed as,

solids walls :

$$\frac{\partial \tau_{i,j}}{\partial r}(t, r^+_0, z^+_0) = \frac{\partial \tau_{i,j}}{\partial r}(t, r^-_1, z^-_1), \tag{2.40}$$

$$\frac{\partial \tau_{i,j}}{\partial r}(t, r^+_{M-1}, z^+_{N-1}) = \frac{\partial \tau_{i,j}}{\partial r}(t, r^-_M, z^-_N), \tag{2.41}$$

inlet channel:

$$\frac{\partial \tau_{i,j}}{\partial z}(t, r^+_0, z^+_0) = \frac{\partial \tau_{i,j}}{\partial z}(t, r^-_1, z^-_1), \tag{2.42}$$

outlet channel :

$$\frac{\partial \tau_{i,j}}{\partial z}(t, r^{+}_{M-1}, z^{+}_{N-1}) = \frac{\partial \tau_{i,j}}{\partial z}(t, r^{-}_{M}, z^{-}_{N}). \tag{2.43}$$

2.2.2.2 Shell-fluid Equations

The shell-fluid is subject to a one dimensional flow velocity w_s therefore, velocity in the radial direction $u_s = (0, u_s(r))$ is neglected. The fluid is assumed to be Newtonian however a non-Newtonian case will be considered as well in our investigations. The Newtonian case equations will be similar to the below non-Newtonian fluid equations but without the extra stress components.

The continuity equation is given by,

$$\frac{\partial w_s}{\partial z} = 0. \tag{2.44}$$

The momentum equation reads,

$$\begin{aligned} \frac{\partial w_s}{\partial t} + w_s \frac{\partial w_s}{\partial z} &= -G_s + \frac{1}{Re_c}\Big(\mu_s \frac{\partial^2 w_s}{\partial r^2} + \frac{\mu_s}{r}\frac{\partial w_s}{\partial r} + 2\mu_s \frac{\partial^2 w_s}{\partial z^2}\Big) \\ &+ \frac{1}{Re_s}\Big(2\frac{\partial \mu_s}{\partial z_s}\frac{\partial w_s}{\partial z} + \frac{\partial \mu_s}{\partial r}\frac{\partial w_s}{\partial r} + \mu_s \frac{\partial \tau_{rz}}{\partial r} + \mu_s \frac{\partial \tau_{zz}}{\partial z} + \mu_s \frac{\tau_{rz}}{r}\Big). \end{aligned} \tag{2.45}$$

The equation is subject to the following initial condition,

$$w_s(r) = -\frac{G_s Re_s}{2\mu_s}(R_s^2 - r), \tag{2.46}$$

where $G_s = \frac{G_s^* L^*}{\rho_s^* {w_{s0}^*}^2}$ is the dimensionless pressure gradient.

The boundary conditions which are imposed at the walls, centerline, inlet channel and outlet channel of the pipe are given by the following mathematical expressions,

the no-slip condition at the wall of the pipe :

$$w_s(t, 1, z) = 0, \tag{2.47}$$

inlet channel:

$$\frac{\partial w_{si,j}}{\partial z}(t, r^{+}_{0}, z^{+}_{0}) = \frac{\partial w_{si,j}}{\partial z}(t, r^{-}_{1}, z^{-}_{1}), \tag{2.48}$$

outlet channel:

$$\frac{\partial w_{si,j}}{\partial z}(t, r^{+}_{M-1}, z^{+}_{N-1}) = \frac{\partial w_{si,j}}{\partial z}(t, r^{-}_{M}, z^{-}_{N}). \tag{2.49}$$

The energy equation is expressed as,

$$\begin{aligned} Re_s Pr_s\Big(\frac{\partial T_s}{\partial t} + w_s\frac{\partial T_s}{\partial z}\Big) &= \Big(\frac{\partial^2 T_s}{\partial r^2} + \frac{1}{r}\frac{\partial T_s}{\partial r} + \frac{\partial^2 T_s}{\partial z^2}\Big) \\ &+ Re_s\delta_{s2}\delta_{s3}\Big(1+\frac{1}{\xi}\Big)\Big(+w_s G_s) + h_s(T_w - T_s\Big) \\ +\delta_{s2}\mu_s\Big[\gamma\big(2\tau_{rr}\frac{\partial w_c}{\partial z} + 2\tau_{rz}\Big(\frac{\partial u_s}{\partial z} + \frac{\partial w_s}{\partial r}\Big) + 2\tau_{zz}\frac{\partial u_s}{\partial r} + 2\frac{u_s}{r}\Big) \\ +(1-\gamma)(1-\beta)\Big(2\Big(\frac{\partial u_s}{\partial r}\Big)^2 + 2\Big(\frac{u_s}{r}\Big)^2 + 2\Big(\frac{\partial w_s}{\partial z}\Big)^2 + \Big(\frac{\partial u_s}{\partial z} + \frac{\partial w_s}{\partial r}\Big)^2\Big)\Big], \end{aligned} \tag{2.50}$$

subject to the following initial conditions,

$$T_s(0, r, z) = 0, 0 \leqq r \leqq 1. \tag{2.51}$$

It is further subject to boundary conditions which are denoted by,

Solid walls:

$$\frac{\partial T_{si,j}}{\partial r}(t, r_0^+, z_0^+) = \frac{\partial T_{si,j}}{\partial r}(t, r_1^-, z_1^-), \tag{2.52}$$

$$\frac{\partial T_{si,j}}{\partial r}(t, r_{M-1}^+, z_{N-1}^+) = \frac{\partial T_{si,j}}{\partial r}(t, r_M^-, z_N^-), \tag{2.53}$$

axisymmetric condition:

$$\frac{\partial T_s}{\partial r}(t, 0, z) = 0, \tag{2.54}$$

inlet channel condition :

$$T_s(t, 0, z) = 0 = T_s(t, 1, z), \tag{2.55}$$

outlet channel condition:

$$\frac{\partial T_{si,j}}{\partial z}(t, r_{M-1}^+, z_{N-1}^+) = \frac{\partial T_{si,j}}{\partial z}(t, r_M^-, z_N^-). \tag{2.56}$$

The extra stresses equations read,

$$\mu_s\tau_{rr} + \alpha\mu_s{\tau_{rr}}^2 + De\bar{\lambda}\Big[\Big(\frac{\partial}{\partial t}\mu_s\tau_{rr} + w_s\frac{\partial}{\partial z}\mu_s\tau_{rr}\Big) - \mu_s\tau_{rr}\frac{D}{Dt}\ln[\xi T_s + 1]\Big] = 0, \tag{2.57}$$

$$\mu_s\tau_{rz} + \alpha\mu_s{\tau_{rz}}^2 + De\bar{\lambda}\Big[\Big(\frac{\partial}{\partial t}\mu_s\tau_{rz} + w_s\frac{\partial}{\partial z}\mu_s\tau_{rz}\Big) - \mu_s\Big(\tau_{rr}\frac{\partial w_s}{\partial r} + \tau_{rz}\frac{\partial w_s}{\partial z}\Big) - \mu_s\tau_{rz}\frac{D}{Dt}\ln[\xi T_s + 1]\Big] = \mu_s\beta\Big(\frac{\partial w_s}{\partial r}\Big), \tag{2.58}$$

$$\mu_s\tau_{zz} + \alpha\mu_s{\tau_{zz}}^2 + De\bar{\lambda}\Big[\Big(\frac{\partial}{\partial t}\mu_s\tau_{zz} + w_s\frac{\partial}{\partial z}\mu_s\tau_{zz}\Big) - \mu_s\Big(2\tau_{rz}\frac{\partial w_s}{\partial r} + 2\tau_{rz}\frac{\partial w_s}{\partial z}\Big) - \mu_s\tau_{zz}\frac{D}{Dt}\ln[\xi T_s + 1]\Big] = 2\mu_s\beta\frac{\partial w_s}{\partial z}. \tag{2.59}$$

The equations are subject to an initial condition which is given by,

$$\tau_{i,j} = 0, 0 \leq r \leq 1. \tag{2.60}$$

Boundary conditions are imposed at the walls, inlet channel and outlet channel of the pipe. They are linearly extrapolated and expressed by the following equations,

inlet channel:

$$\frac{\partial\tau_{i,j}}{\partial z}(t, r_0^+, z_0^+) = \frac{\partial\tau_{i,j}}{\partial z}(t, r_1^-, z_1^-), \tag{2.61}$$

outlet channel :

$$\frac{\partial\tau_{i,j}}{\partial z}(t, r_{M-1}^+, z_{N-1}^+) = \frac{\partial\tau_{i,j}}{\partial z}(t, r_M^-, z_N^-), \tag{2.62}$$

boundary condition at the wall of the pipe :

$$\frac{\partial\tau_{i,j}}{\partial r}(t, r_0^+, z_0^+) = \frac{\partial\tau_{i,j}}{\partial r}(t, r_1^-, z_1^-), \tag{2.63}$$

$$\frac{\partial\tau_{i,j}}{\partial r}(t, r_{M-1}^+, z_{N-1}^+) = \frac{\partial\tau_{i,j}}{\partial r}(t, r_M^-, z_N^-). \tag{2.64}$$

2.2.2.3 Connecting wall Equation

The equation is given by,

$$\frac{\partial T_w}{\partial t} = \frac{\partial^2 T_w}{\partial z^2} + h_c(T_c - T_w) + h_s(T_s - T_c), \tag{2.65}$$

and it is subject to boundary conditions at $z = 0$ which is the left end point and $z = 1$ right point end of the rod [3] and [6],

$$T_w|_{z=0,1} = \Big[(h_c(T_c - T_w) + h_s(T_s - T_c))_{r=0.1}/(h_c + h_s)\Big]_{z=0,1}. \tag{2.66}$$

2.2.2.4 Poisson equation for Pressure

It is mathematically expressed as,

$$\frac{\partial^2 P}{\partial r^2} + \frac{1}{r}\frac{\partial P}{\partial r} + \frac{\partial^2 P}{\partial z^2} = \frac{1}{\Delta t}\Big(\frac{\partial \bar{u_c}}{\partial r} + \frac{1}{r}u_c + \frac{\partial \bar{w_c}}{\partial z}\Big). \tag{2.67}$$

The equation subject to the following initial condition,

$$P_c = -G_c + 1. \tag{2.68}$$

Pressure is further subject to boundary conditions which are imposed at the walls, inlet channel and outlet channel of the pipe. They are linearly extrapolated and mathematically expressed by the following equations,

inlet channel condition:

$$\frac{\partial P_{ci,j}}{\partial z}(t, r_0^+, z_0^+) = \frac{\partial P_{ci,j}}{\partial z}(t, r_1^-, z_1^-), \tag{2.69}$$

outlet channel condition :

$$\frac{\partial P_{ci,j}}{\partial z}(t, r_{M-1}^+, z_{N-1}^+) = \frac{\partial P_{ci,j}}{\partial z}(t, r_M^-, z_N^-), \tag{2.70}$$

solid walls :

$$\frac{\partial P_{ci,j}}{\partial r}(t, r_0^+, z_0^+) = \frac{\partial P_{ci,j}}{\partial r}(t, r_1^-, z_1^-), \tag{2.71}$$

$$\frac{\partial P_{ci,j}}{\partial r}(t, r_{M-1}^+, z_{N-1}^+) = \frac{\partial P_{ci,j}}{\partial r}(t, r_M^-, z_N^-). \tag{2.72}$$

Chapter 3

Numerical Implementation

This chapter is concerned with the numerical modelling of viscoelastic fluid dynamics with applications to heat exchangers via the semi-implicit finite difference method. This numerical scheme, similar to finite difference method, transforms each component of the partial derivatives into finite difference approximations (derived using Taylor theorem) which are made at discrete values of independent variables. At its simplest the transformation process reduces the problem into solving a system of algebraic equations at some set of discrete locations in space and time. The solution procedure is an iterative process which involves pentadiagonal and tridiagonal matrix manipulation. The governing equations which mathematically describe the problem to be solved are complex ,non-linear and coupled. To address the pressure-velocity coupling in the momentum equations the Semi-Implicit Method for Pressure Linked Equations (SIMPLE) [57] is employed.

3.1 Numerical Scheme Overview

3.1.1 Numerical Grid

The discrete positions at which the dependent variables are to be computed are defined by the numerical grid. For this problem we select a two dimensional structured numerical grid, i.e., the Cartesian mesh grid.

3.1.2 Coordinate System

To solve the model problem using semi-implicit finite difference method, the governing equations are expressed in the cylindrical coordinate system, see equations (2.20- 2.22, 2.30, 2.36 - 2.38, 2.44, 2.45, 2.50, 2.57 - 2.59, 2.65, 2.67). This is because the problem described in the previous chapter involves a flow in the pipe.

3.1.3 Semi-Implicit Finite Difference Technique

The governing equations expressed in cylindrical form are discretized using the semi-implicit finite difference technique integrated with the Crank-Nicolson scheme. This technique is numerically unconditionally stable because it combines the stability of an implicit method with the accuracy of a method that is second order in both space and time. Semi-implicit time integration schemes are considered efficient due to their ability to use long time steps [58] and [59]. Furthermore a factorization technique, [3], [60] and [61], can be applied to the left-hand side ,i.e., the implicit side of the discretized equations. The presented method is based on works [3], [6], [62] and [63]. Here the first and second spatial derivatives are discretized with the second order central differences and the time derivative with the Euler forward difference scheme. The implicit terms are handled by utilizing the Crank-Nicolson scheme, here terms are taken at an intermediate time level $(n + \xi)$ where $0 \leq \xi \leq 1$. The choice of ξ is such that, for $\xi = 1/2$ accuracy in time is increased to second order [54], $\xi = 1$ provides the freedom to use larger time steps and still achieve convergence [62] and in the case of $\xi = 0$ the terms on the right hand side of the governing equations reduce an explicit discretization. In this study $\xi = 1$ is used in the momentum equation, energy equation and Poisson equation for pressure. For the constitutive equation, extra stress tensor terms which involve spacial derivatives utilize $\xi = 1/2$. In the calculation of the connecting wall temperature, a full Crank-Nicolson scheme is employed [3].

The numerical diffusion and numerical stability issues are addressed by the treatment of convective terms using the first order upwind differential scheme [64] and [65].

3.1.4 Finite Approximations

In approximating the partial derivatives by algebraic expressions a discretization error is incurred. The error is due to the infinite Taylor series truncated after a number of terms to derive an expression for the partial derivatives approximated. The approximation is improved by decreasing the step size of the spacial domain, which means that the discretization error will go to zero as the step size tends to zero. The order of the step size with which the error tends to zero is called the order of accuracy of the finite difference approximation. This indicates that the discretization error plays a crucial role in the numerical accuracy of the solution of the partial differential equation to be solved [66]. To achieve optimal or good accuracy the discretization method must yield a second or higher order accuracy [67], [68], [69] and [57]. It is for this reason that in this study both the second and first spacial derivatives are approximated with second order central differences. The full discretization of all the governing equations is shown in section 3.2.

3.1.5 Semi-Implicit Method for Pressure Linked Equations (SIMPLE)

The partial equations derived in the previous chapter are non-linear, complex and intricately coupled. In particular the momentum equation is the most complex and requires special techniques in order to be solved. The reason is that:

- The pressure and velocity in the momentum equations are coupled.
- All the velocity components exist in both the momentum and continuity equations.
- The convective terms in the momentum equation possess a non-linearity property.
- The pressure term which appears in the momentum equation does not have an explicit equation.

In the above mentioned concerns the most difficult issue to resolve is the pressure aspect in the momentum equation. Firstly, if the flow is compressible then the continuity and energy equations can be used to derive a solution for pressure using the equation of state, i.e., $p = \rho \bar{R} T$ where $\bar{R}$ is a gas constant, given by R /M, where R is the universal gas constant and M is the molecular weight of the gas. Secondly, if it is an incompressible flow then density is constant therefore the equation of state cannot be used to solve for pressure because there is no connection between pressure and density. In this work only the incompressible flow case is investigated.

To resolve these issues, the Semi-Implicit Method for Pressure Linked Equations (SIMPLE) by Patankar and Spalding (1972) is employed. The Algorithm elegantly decouples the pressure from the momentum equation and also resolves the non-linearity by sequentially solving the equations in an iterative procedure. A more detailed description can be found in [57], [70], [71] and [72].

The algorithm can be recapitulated as follows :

1. Set initial conditions or values for pressure (p) and velocity (V^n).
2. Decouple pressure from the below momentum equation

$$\frac{\partial V}{\partial t} = -\nabla p + \nabla \cdot \underline{\underline{\tau}} + F \tag{3.1}$$

as follows:

$$\frac{\overline{V} - V^n}{\Delta t} = \nabla \cdot \underline{\underline{\tau}} + F, \tag{3.2}$$

$$\frac{V^{n+1} - \overline{V}}{\Delta t} = -\nabla p. \tag{3.3}$$

3. Next solve for the intermediate velocity $\overline{V}$ in equation (3.2). Here the Navier-Stokes equations are solved for an intermediate velocity without pressure. The solution procedure will lead to an inversion of tridiagonal matrices.

4. The solution for V^n and V^{n+1} must satisfy the incompressibility condition, $\nabla \cdot V^n = \nabla \cdot V^{n+1} = 0$. Using this condition an equation for pressure is derived by taking the divergence of equation (3.3) as follows:

$$\frac{\nabla \cdot V^{n+1} - \nabla \cdot \overline{V}}{\Delta t} = \nabla \cdot (-\nabla p), \tag{3.4}$$

this then leads to a Poisson equation for pressure given by

$$\nabla^2 p = \frac{\nabla \cdot \overline{V}}{\Delta t}. \tag{3.5}$$

The equation (3.5) is then solved to find the pressure field. The solution procedure to this equation reduces to an inversion of a pentadiagonal matrix .

5. Now solve for the updated velocity V^{n+1} from equation (3.3) by correcting the intermediate velocity $\overline{V}$ using the pressure field in (3.5). The updated velocity equation (3.3) can be rewritten as

$$V^{n+1} = \overline{V} - \Delta t \nabla p. \tag{3.6}$$

6. Then solve for other discretized equations, namely energy (2.30), extra stress components τ_{rr}, τ_{rz}, τ_{zz} (2.36 - 2.38) and wall temperature T_w (2.65) equations. This will also involve an inversion of tridiagonal matrices. Also solve for relaxation time and viscosity using the below equations respectively

$$\bar{\lambda} = (1 - \delta_\lambda) + \delta_\lambda \frac{1 + \xi}{1 + \xi T} \exp(-\varepsilon_\lambda T) \tag{3.7}$$

where $\xi = \frac{\Delta T}{T_{s0}}$,

$$\mu(T) = \exp(-\varepsilon_\lambda T). \tag{3.8}$$

7. Finally update all the physical quantities solved u, v, p, T, T_w, τ_{rr}, τ_{rz}, τ_{zz}, $\bar{\lambda}$ and μ.

8. Repeat the process from step 2 until convergence is reached.

In this research the SIMPLE algorithm is only implemented on the core pipe fluid flow.

3.1.6 Implementation of boundary conditions

The solution procedure relies heavily on matrix operations some of which involve the inversion of tridiagonal and pentadiagonal matrices. Therefore care should be taken in imposing boundary conditions as these will greatly influence matrix dimensions which will inevitably affect the numerical solution. Matrix dimensions are of vital importance when it comes to numerical solution procedures implemented on computational platforms such as MATLAB. To elaborate on this, we revisit the key aspect discussed in chapter 2 concerning boundary conditions.

Pressure and extra stress boundary conditions are extrapolated at the inlet channel, outlet channel and solid walls by using neighborhood values meaning that these will be determined as the solution process progresses. Therefore, the equations need only to be solved for (n-2) and (m-2) unknown values on the mesh grid. As a result matrix dimensions for pressure and extra stress will be (n-2) by (m-2).

For velocity components, boundary conditions are similarly extrapolated at inlet and outlet channels. At the solid walls the no-slip condition is prescribed and since the geometry of the problem is a pipe, the symmetry boundary condition is imposed at the centreline of the pipe. Likewise both the channels and centreline boundary values will be determined as the solution process progresses. This implies that there are (n-2) unknown values on z plane and (m-1) unknown values on the radial plane of the mesh grid. Thus the matrix to be solved has (n-2) by (m-1) dimensions.

Temperature is prescribed at the inlet channel. At the centreline, the boundary condition will be imposed the same way as it as done for velocity. The outlet channel and solid walls values will be determined as the solution process progresses by extrapolating neighborhood values. In contrast to velocity, equations need only to be solved for (n-1) and (m-2) unknown values on the mesh grid and this means that the matrix dimensions for temperature will be (n-1) by (m-2).

Boundary conditions can be incorporated in two ways. Firstly, at the inception of the solution process which will lead to operations of non- square matrices meaning that the solution procedure will involve solving matrices with dimension described above. And secondly it would be to incorporate them at the end of the solution process which will entail solving only interior unknown points of the mesh grid first. In this study we choose the latter similar to woks [6] and [3], as it circumvents matrix dimension issues elegantly by solving (n-2) by (m-2) matrices and then impose boundary conditions immediately thereafter.

3.2 Discretization and Matrix Formulation

3.2.1 Discretization of Core-Fluid Equations

3.2.1.1 Momentum Equation

z- component is given by;

$$\begin{aligned}
\overline{w}_{ci,j} - w^n_{c\,i,j} = -\Delta t\Big[u^n_{c\,i,j}\Big(\frac{w^n_{c\,i+1,j} - w^n_{c\,i,j}}{2\Delta r}\Big) - \Big(w^n_{c\,i,j}\frac{w^n_{c\,i,j+1} - w^n_{c\,i,j}}{2\Delta z}\Big)\Big] \\
+\frac{\Delta t}{2Re_c\Delta r\Delta z}\Big[\Big((\mu^n_{c\,i+1,j})(u^n_{c\,i+1,j+1} - u^n_{c\,i+1,j-1}) - (\mu^n_{c\,i-1,j})(u^n_{c\,i-1,j+1} - u^n_{c\,i-1,j-1})\Big)\Big] \\
+\frac{\Delta t}{Re_c}\Big[\frac{(\mu^n_{c\,i+1,j} - \mu^n_{c\,i-1,j})(w^n_{c\,i+1,j} - w^n_{c\,i-1,j})}{\Delta r} + \frac{(\mu^n_{c\,i,j+1} - \mu^n_{c\,i,j-1})(w^n_{c\,i,j+1} - w^n_{c\,i,j-1})}{2\Delta z}\Big] \\
+\frac{\Delta t}{Re_c}\Big[\mu^n_{c\,i,j}\Big(\frac{\overline{w}_{ci+1,j} - 2\overline{w}_{ci,j} + \overline{w}_{ci-1,j}}{(\Delta r)^2}\Big) + 2\mu^n_{c\,i,j}\Big(\frac{\overline{w}_{ci,j+1} - 2\overline{w}_{ci,j} + \overline{w}_{ci,j-1}}{(\Delta z)^2}\Big)\Big] \\
+\frac{\Delta t}{2Re_c}\Big[\mu^n_{c\,i,j}\Big(\frac{w^n_{c\,i+1,j} - 2w^n_{c\,i,j} + w^n_{c\,i-1,j}}{(\Delta r)^2}\Big) + \mu^n_{c\,i,j}\Big(\frac{w^n_{c\,i,j+1} - 2w^n_{c\,i,j} + w^n_{c\,i,j-1}}{(\Delta z)^2}\Big)\Big] \\
+\frac{\Delta t}{2Re_c}\Big[\Big(\frac{\mu^n_{c\,i+1,j}\tau^n_{rzi+1,j} - \mu^n_{c\,i-1,j}\tau^n_{rzi-1,j}}{2\Delta r}\Big) + \Big(\frac{\mu^n_{c\,i,j+1}\tau^n_{zzi,j+1} - \mu^n_{c\,i,j-1}\tau^n_{zzi,j-1}}{2\Delta z}\Big)\Big] \\
+\frac{\Delta r}{Re_c}\Big[\mu^n_{c\,i,j}\frac{\tau^n_{rzi,j}}{r_{ci}}\Big] + \frac{1}{Re_c}\Big[\frac{\mu_c}{r_{ci}}\Big(\frac{w^n_{c\,i+1,j} - w^n_{c\,i-1,j}}{2\Delta r}\Big)\Big].
\end{aligned} \tag{3.9}$$

Factorization of implicit terms is as follows:

$$\Big(1 - \frac{\mu_{ci,j}\Delta t}{Re_c}\frac{\partial^2}{\partial z^2} - \frac{\mu_{ci,j}\Delta t}{2Re_c}\frac{\partial^2}{\partial r^2}\Big)\overline{w}_{ci,j} = \text{Explicit terms}, \tag{3.10}$$

$$\Big(1 - \frac{\mu_{ci,j}\Delta t}{Re_c}\frac{\partial^2}{\partial z^2}\Big)\Big(1 - \frac{\mu_{ci,j}\Delta t}{2Re_c}\frac{\partial^2}{\partial r^2}\Big)\overline{w}_{ci,j} = \text{Explicit terms}, \tag{3.11}$$

with a discretization error of $O((\Delta t/Re_c)^2)$. This factorization reduces (3.11) into two tridiagonal matrices.

r-component is given by,

$$\begin{aligned}
\overline{u}_{ci,j} - u^n_{c\,i,j} = -\Delta t\Big[u^n_{c\,i,j}\Big(\frac{u^n_{c\,i+1,j} - u^n_{c\,i,j}}{2\Delta r}\Big) - \Big(w^n_{c\,i,j}\frac{u^n_{c\,i,j+1} - u^n_{c\,i,j}}{\Delta z}\Big)\Big] \\
+\frac{\Delta t}{2Re_c\Delta r\Delta z}\Big[\Big((\mu^n_{c\,i+1,j})(w^n_{c\,i+1,j+1} - w^n_{c\,i+1,j-1}) - (\mu^n_{c\,i-1,j})(w^n_{c\,i-1,j+1} - w^n_{c\,i-1,j-1})\Big)\Big] \\
+\frac{\Delta t}{Re_c}\Big[\frac{(\mu^n_{c\,i+1,j} - \mu^n_{c\,i-1,j})(u^n_{c\,i+1,j} - u^n_{c\,i-1,j})}{2\Delta r} + \frac{(\mu^n_{c\,i,j+1} - \mu^n_{c\,i,j-1})(u^n_{c\,i,j+1} - u^n_{c\,i,j-1})}{\Delta z}\Big] \\
+\frac{\Delta t}{Re_c}\Big[\mu^n_{c\,i,j}\Big(\frac{\overline{u}_{ci+1,j} - 2\overline{u}_{ci,j} + \overline{u}_{ci-1,j}}{(\Delta r)^2}\Big) + 2\mu^n_{c\,i,j}\Big(\frac{\overline{u}_{ci,j+1} - 2\overline{u}_{ci,j} + \overline{u}_{ci,j-1}}{(\Delta z)^2}\Big)\Big] \\
+\frac{\Delta t}{2Re_c}\Big[\mu^n_{c\,i,j}\Big(\frac{u^n_{c\,i+1,j} - 2u^n_{c\,i,j} + u^n_{c\,i-1,j}}{(\Delta r)^2}\Big) + \mu^n_{c\,i,j}\Big(\frac{u^n_{c\,i,j+1} - 2u^n_{c\,i,j} + u^n_{c\,i,j-1}}{(\Delta z)^2}\Big)\Big] \\
+\frac{\Delta t}{2Re_c}\Big[\Big(\frac{\mu^n_{c\,i+1,j}\tau^n_{rri+1,j} - \mu^n_{c\,i-1,j}\tau^n_{rri-1,j}}{2\Delta r}\Big) + \Big(\frac{\mu^n_{c\,i,j+1}\tau^n_{rzi,j+1} - \mu^n_{c\,i,j-1}\tau^n_{rzi,j-1}}{2\Delta z}\Big)\Big] \\
+\frac{\Delta r}{Re_c}\Big[\mu^n_{c\,i,j}\frac{\tau^n_{rri,j}}{r_{ci}}\Big] + \frac{1}{Re_c}\Big[\frac{\mu_c}{r_{ci}}\Big(\frac{u^n_{c\,i+1,j} - u^n_{c\,i-1,j}}{2\Delta r}\Big)\Big].
\end{aligned} \tag{3.12}$$

Factorization of implicit terms with a discretization error of $O((\Delta t/Re_c)^2)$ is given by,

$$\Big(1 - \frac{\mu^n_{c\,i,j}\Delta t}{Re_c}\frac{\partial^2}{\partial z^2} - \frac{\mu^n_{c\,i,j}\Delta t}{2Re_c}\frac{\partial^2}{\partial r^2}\Big)\overline{u}_{ci,j} = \text{Explicit terms}, \tag{3.13}$$

$$\Big(1 - \frac{\mu^n_{c\,i,j}\Delta t}{Re_c}\frac{\partial^2}{\partial z^2}\Big)\Big(1 - \frac{\mu^n_{c\,i,j}\Delta t}{2Re_c}\frac{\partial^2}{\partial r^2}\Big)\overline{u}_{ci,j} = \text{Explicit terms}. \tag{3.14}$$

This reduces into a solution of tridiagonal matrices.

3.2.1.2 Energy Equation

$$
\begin{aligned}
{T_c^{n+1}}_{i,j} - {T_c^n}_{i,j} = -\Delta t\Big[{u_c^n}_{i,j}\Big(\frac{{T_c^n}_{i+1,j} - {T_c^n}_{i,j}}{2\Delta r}\Big) - {w_c^n}_{i,j}\Big(\frac{{T_c^n}_{i,j+1} - {T_c^n}_{i,j}}{2\Delta z}\Big)\Big] \\
+h_c(T_{w\,i,j}^n - {T_c^n}_{i,j}) + \frac{\Delta t}{Re_c Pr_c}\Big[\frac{1}{r_{ci}}\Big(\frac{{T_c^n}_{i+1,j} - {T_c^n}_{i-1,j}}{2\Delta r}\Big)\Big] \\
+\frac{\Delta t}{2Re_c Pr_c}\Big[\Big(\frac{{T_c^{n+1}}_{i+1,j} - 2{T_c^{n+1}}_{i,j} + {T_c^{n+1}}_{i-1,j}}{(\Delta r)^2}\Big) + \Big(\frac{{T_c^{n+1}}_{i,j+1} - 2{T_c^{n+1}}_{i,j} + {T_c^{n+1}}_{i,j-1}}{(\Delta z)^2}\Big)\Big] \\
+\frac{\Delta t}{2Re_c Pr_c}\Big[\Big(\frac{{T_c^n}_{i+1,j} - 2{T_c^n}_{i,j} + {T_c^n}_{i-1,j}}{(\Delta r)^2}\Big) + \Big(\frac{{T_c^n}_{i,j+1} - 2{T_c^n}_{i,j} + {T_c^n}_{i,j-1}}{(\Delta z)^2}\Big)\Big] \\
+\frac{\Delta t Re_c \delta_{c2}\delta_{c3}}{Pr_c}\Big(1+\frac{1}{\xi}\Big)\Big[\Big({u_c^n}_{i,j}\frac{{P_c^n}_{i+1,j} - {P_c^n}_{i-1,j}}{2\Delta r}\Big) + \Big({w_c^n}_{i,j}\frac{{P_c^n}_{i,j+1} - {P_c^n}_{i,j-1}}{2\Delta z}\Big)\Big] \\
+\frac{2\Delta\gamma t\delta_{c2}}{Re_c Pr_c}\Big[\Big({\mu_c^n}_{i,j}{\tau_{rr}^n}_{i,j}\frac{{w_c^n}_{i,j+1} - {w_c^n}_{i,j-1}}{2\Delta r}\Big) + \Big({\mu_c^n}_{i,j}{\tau_{zz}^n}_{i,j}\frac{{u_c^n}_{i+1,j} - {u_c^n}_{i-1,j}}{2\Delta r}\Big)\Big] \\
+\frac{2\Delta\gamma t\delta_{c2}}{Re_c Pr_c}{\mu_c^n}_{i,j}{\tau_{rz}^n}_{i,j}\Big[\Big(\frac{{u_c^n}_{i,j+1} - {u_c^n}_{i,j-1}}{2\Delta z}\Big) + \Big(\frac{{w_c^n}_{i+1,j} - {w_c^n}_{i-1,j}}{2\Delta r}\Big) + \frac{{u^n}_{i,j}}{r_{ci}}\Big] \\
+\frac{\Delta t\delta_{c2}(1-\gamma)(1-\beta)}{Re_c Pr_c}{\mu_c^n}_{i,j}\Big[2\Big(\frac{{u_c^n}_{i+1,j} - {u_c^n}_{i-1,j}}{2\Delta r}\Big)^2 + 2\Big(\frac{{u^n}_{i,j}}{r_{ci}}\Big)^2 \\
+2\Big(\frac{{w_c^n}_{i,j+1} - {w_c^n}_{i,j-1}}{2\Delta z}\Big)^2 + \Big(\frac{{w_c^n}_{i+1,j} - {w_c^n}_{i-1,j}}{2\Delta r} + \frac{{u_c^n}_{i,j+1} - {u_c^n}_{i,j-1}}{2\Delta z}\Big)^2\Big]
\end{aligned}
\tag{3.15}
$$

Similarly the factorization of implicit terms are given by,

$$
\Big(1 - \frac{\Delta t}{2Re_c Pr_c}\frac{\partial^2}{\partial z^2} - \frac{\Delta t}{2Re_c Pr_c}\frac{\partial^2}{\partial r^2}\Big){T_c^{n+1}}_{i,j} = \text{Explicit terms}, \tag{3.16}
$$

$$
\Big(1 - \frac{\Delta t}{Re_c Pr_c}\frac{\partial^2}{\partial z^2}\Big)\Big(1 - \frac{\Delta t}{2Re_c Pr_c}\frac{\partial^2}{\partial r^2}\Big){T_c^{n+1}}_{i,j} = \text{Explicit terms}, \tag{3.17}
$$

with a discretization error of $O((\Delta t/Re_c Pr_c)^2)$.

3.2.1.3 Pressure Equation

$$
\begin{aligned}
\Big(\frac{{P_c^{n+1}}_{i+1,j} - 2{P_c^{n+1}}_{i,j} + {P_c^{n+1}}_{i-1,j}}{(\Delta r)^2}\Big) + \Big(\frac{{P_c^{n+1}}_{i+1,j} - {P_c^{n+1}}_{i-1,j}}{2\Delta r}\Big) \\
+\Big(\frac{{P_c^{n+1}}_{i,j+1} - 2{P_c^{n+1}}_{i,j} + {P_c^{n+1}}_{i,j-1}}{\big(\Delta z\big)^2}\Big) = \\
\frac{1}{\Delta t}\Big(\frac{\overline{u}_{c\,i+1,j}^n - \overline{u}_{ci-1,j}}{2\Delta r}\Big) + \frac{1}{\Delta t}\Big(\frac{\overline{u}_{ci,j}}{r_{ci}}\Big) + \frac{1}{\Delta t}\Big(\frac{\overline{u}_{c\,i,j+1}^n - \overline{u}_{ci,j-1}}{2\Delta z}\Big).
\end{aligned}
\tag{3.18}
$$

Rearranging the left hand side of equation (3.18), will result in the formulation of a pentadiagonal matrix:

$$\begin{aligned}\left(\frac{\Delta t}{(\Delta z)^2}\right){P_c^{n+1}}_{i+1,j}+\left(\frac{\Delta t}{(\Delta z)^2}\right){P_c^{n+1}}_{i-1,j}+\left(\frac{2\Delta t}{(\Delta r)^2}+\frac{2\Delta t}{(\Delta z)^2}\right){P_c^{n+1}}_{i,j}\\ +\left(\frac{\Delta t}{(\Delta r)^2}+\frac{\Delta t}{(2r_{ci}\Delta r)}\right){P_c^{n+1}}_{i,j+1}-\left(\frac{\Delta t}{(2r_{ci}\Delta r)}\right){P_c^{n+1}}_{i,j-1}=\\ \left(\frac{\overline{u}^n_{c\,i+1,j}-\overline{u}_{ci-1,j}}{2\Delta r}\right)+\left(\frac{\overline{u}_{ci,j}}{r_{ci}}\right)+\left(\frac{\overline{u}^n_{c\,i,j+1}-\overline{u}_{ci,j-1}}{2\Delta z}\right).\end{aligned} \tag{3.19}$$

3.2.1.4 Stress Equations

τ_{rr} - component:

$$\begin{aligned}(\mu_c\tau_{rr})^{n+1}+De\bar{\lambda}\left(\frac{(\mu_c\tau_{rr})^{n+1}-(\mu_c\tau_{rr})^n}{\Delta t}\right)+De\bar{\lambda}u_c^n\frac{\partial}{\partial r}(\mu_c\tau_{rr})^{n+1}+De\bar{\lambda}w_c^n\frac{\partial}{\partial r}(\mu_c\tau_{rr})^{n+1}\\ =\mu_cDe\bar{\lambda}\left[2\tau_{rr}\frac{\partial u_c}{\partial r}+2\tau_{rz}\frac{\partial u_c}{\partial z}+\tau_{rr}\frac{D}{Dt}\ln(\xi T_c+1)\right]^n-\alpha\mu_c(\tau_{rr}^n)^2+2\mu_c\beta\frac{\partial u_c}{\partial r}.\end{aligned} \tag{3.20}$$

By applying the Crank-Nicolson scheme on spacial derivatives of extra stresses using the transformation $\tau_{rr}^{n+\xi}=\xi\tau_{rr}^{n+1}+(1-\xi)\tau_{rr}^n$, where is $\xi=\frac{1}{2}$ [3] we obtain,

$$\begin{aligned}\mu_c\tau_{rr}^{n+\xi}+De\bar{\lambda}\left(\frac{(\mu_c\tau_{rr})^{n+1}-(\mu_c\tau_{rr})^n}{\Delta t}\right)+De\bar{\lambda}u_c^n\frac{\partial}{\partial r}(\mu_c\tau_{rr})^{n+\xi}+De\bar{\lambda}w_c^n\frac{\partial}{\partial r}(\mu_c\tau_{rr})^{n+\xi}\\ =\mu_cDe\bar{\lambda}\left[2\tau_{rr}\frac{\partial u_c}{\partial r}+2\tau_{rz}\frac{\partial u_c}{\partial z}+\tau_{rr}\frac{D}{Dt}\ln(\xi T_c+1)\right]^n-\alpha\mu_c(\tau_{rr}^n)^2+2\mu_c\beta\frac{\partial u_c}{\partial r},\end{aligned} \tag{3.21}$$

next by multiplying Δt (3.21) then becomes,

$$\begin{aligned}\Delta t\xi(\mu_c\tau_{rr}^{n+1})+\Delta t(1-\xi)(\mu_c\tau_{rr}^n)+De\bar{\lambda}[(\mu_c\tau_{rr})^{n+1}-(\mu_c\tau_{rr})^n]\\ +\Delta t\xi De\bar{\lambda}u_c^n\frac{\partial}{\partial r}(\mu_c\tau_{rr})^{n+1}+\Delta t(1-\xi)De\bar{\lambda}u_c^n\frac{\partial}{\partial r}(\mu_c\tau_{rr})^n\\ +\Delta t\xi De\bar{\lambda}w_c^n\frac{\partial}{\partial r}(\mu_c\tau_{rr})^{n+1}+\Delta t(1-\xi)De\bar{\lambda}w_c^n\frac{\partial}{\partial r}(\mu_c\tau_{rr})^n\\ =\Delta t\mu_cDe\bar{\lambda}\left[2\tau_{rr}\frac{\partial u_c}{\partial r}+2\tau_{rz}\frac{\partial u_c}{\partial z}+\tau_{rr}\frac{D}{Dt}\ln(\xi T_c+1)\right]^n-\Delta t\alpha\mu_c(\tau_{rr}^n)^2+2\Delta t\mu_c\beta\frac{\partial u_c}{\partial r}.\end{aligned} \tag{3.22}$$

Simplifying equation (3.22) we obtain,

$$\begin{aligned}
&(\Delta t\xi + De\bar{\lambda})(\mu_c\tau_{rr})^{n+1} + (\Delta t(1-\xi) - De\bar{\lambda})(\mu_c\tau_{rr})^{n} \\
&+\Big(\Delta t\xi De\bar{\lambda}u_c^n\frac{\partial}{\partial r} + +\Delta t\xi De\bar{\lambda}w_c^n\frac{\partial}{\partial r}\Big)(\mu_c\tau_{rr})^{n+1} \\
&+\Big(\Delta t(1-\xi)De\bar{\lambda}u_c^n\frac{\partial}{\partial r} + \Delta t(1-\xi)De\bar{\lambda}w_c^n\frac{\partial}{\partial r}\Big)(\mu_c\tau_{rr})^{n} \\
= \Delta t\mu_c De\bar{\lambda}&\left[2\tau_{rr}\frac{\partial u_c}{\partial r} + 2\tau_{rz}\frac{\partial u_c}{\partial z} + \tau_{rr}\frac{D}{Dt}\ln(\xi T_c + 1)\right]^n - \Delta t\alpha\mu_c(\tau_{rr}^n)^2 + 2\Delta t\mu_c\beta\frac{\partial u_c}{\partial r}.
\end{aligned} \tag{3.23}$$

Finally by rearranging equation (3.23) in terms of implicit and explicit terms we obtain the following equation for τ_{rr} - component,

$$\begin{aligned}
(\mu_c\tau_{rr})^{n+1} &+ \left(\frac{\Delta t\xi De\bar{\lambda}}{\Delta t\xi + De\bar{\lambda}}u_c^n\frac{\partial}{\partial r} + \frac{\Delta t\xi De\bar{\lambda}}{\Delta t\xi + De\bar{\lambda}}w_c^n\frac{\partial}{\partial r}\right)(\mu_c\tau_{rr})^{n+1} \\
&= -\left(\frac{\Delta t(1-\xi)De\bar{\lambda}}{\Delta t\xi + De\bar{\lambda}}u_c^n\frac{\partial}{\partial r} + \frac{\Delta t(1-\xi)De\bar{\lambda}}{\Delta t\xi + De\bar{\lambda}}w_c^n\frac{\partial}{\partial r}\right)(\mu_c\tau_{rr})^{n} \\
&\quad -\frac{\Delta t\mu_c De\bar{\lambda}}{\Delta t\xi + De\bar{\lambda}}\left[2\tau_{rr}\frac{\partial u_c}{\partial r} + 2\tau_{rz}\frac{\partial u_c}{\partial z} + \tau_{rr}\frac{D}{Dt}\ln(\xi T_c + 1)\right]^n \\
-\frac{(\Delta t(1-\xi) - De\bar{\lambda})}{\Delta t\xi + De\bar{\lambda}}&(\mu_c\tau_{rr})^{n} - \frac{\Delta t\alpha\mu_c}{\Delta t\xi + De\bar{\lambda}}(\tau_{rr}^n)^2 + \frac{2\Delta t\mu_c\beta}{\Delta t\xi + De\bar{\lambda}}\frac{\partial u_c^n}{\partial r}.
\end{aligned} \tag{3.24}$$

The implicit terms can be factorized into [3],[6],

$$\left[1 + \Big(\frac{\Delta tDe\bar{\lambda}}{2\Delta t + De\bar{\lambda}}u_c^n\frac{\partial}{\partial r} + \frac{\Delta tDe\bar{\lambda}}{2\Delta t + De\bar{\lambda}}w_c^n\frac{\partial}{\partial r}\Big)\right](\mu_c\tau_{rr})^{n+1}, \tag{3.25}$$

$$\left(1 + \frac{\Delta tDe\bar{\lambda}}{2\Delta t + De\bar{\lambda}}u_c^n\frac{\partial}{\partial r}\right)\left(1 + \frac{\Delta tDe\bar{\lambda}}{2\Delta t + De\bar{\lambda}}w_c^n\frac{\partial}{\partial r}\right)(\mu_c\tau_{rr})^{n+1}. \tag{3.26}$$

Similar to the energy and momentum equations this factorization has produced tridiagonal matrices with an associated error term of $O\Big(\frac{(\Delta t\|u_c\|_{max})^2De\bar{\lambda}}{2\Delta t+De\bar{\lambda}}\Big)$.

The fully discretized form of (3.26) reads,

$$\begin{aligned}
&\Big(-\frac{\Delta t De\bar{\lambda}^n_{i,j}}{(2\Delta t + De\bar{\lambda}^n_{i,j})2\Delta r}u^n_{c\,i,j}(\mu_c\tau_{rr\,i,j-1})^{n+1} + (\mu_c\tau_{rr\,i,j})^{n+1} \\
&\qquad + \frac{\Delta t De\bar{\lambda}^n_{i,j}}{(2\Delta t + De\bar{\lambda}^n_{i,j})2\Delta r}u^n_{c\,i,j}(\mu_c\tau_{rr\,i,j+1})^{n+1}\Big) \\
&\Big(-\frac{\Delta t De\bar{\lambda}^n_{i,j}}{(2\Delta t + De\bar{\lambda}^n_{i,j})2\Delta r}w^n_{c\,i,j}(\mu_c\tau_{rr\,i,j-1})^{n+1} + (\mu_c\tau_{rr\,i,j})^{n+1} \\
&\qquad + \frac{\Delta t De\bar{\lambda}^n_{i,j}}{(2\Delta t + De\bar{\lambda}^n_{i,j})2\Delta r}w^n_{c\,i,j}(\mu_c\tau_{rr\,i,j+1})^{n+1}\Big).
\end{aligned} \tag{3.27}$$

The discretized explicit terms are of the form,

$$\begin{aligned}
RHS_{\tau_{rr}} = &-\frac{(\Delta t(1-\xi) - De\bar{\lambda}^n_{i,j})}{\Delta t\xi + De\bar{\lambda}^n_{i,j}}(\mu_c\tau^n_{rr\,i,j}) \\
&-\frac{\Delta t(1-\xi)De\bar{\lambda}^n_{i,j}}{\Delta t\xi + De\bar{\lambda}^n_{i,j}}\Big[u^n_{c\,i,j}\Big(\frac{\mu^n_{c\,i+1,j}\tau^n_{rri+1,j} - \mu^n_{c\,i-1,j}\tau^n_{rri-1,j}}{2\Delta r}\Big)\Big] \\
&-\frac{\Delta t(1-\xi)De\bar{\lambda}^n_{i,j}}{\Delta t\xi + De\bar{\lambda}^n_{i,j}}\Big[w^n_{c\,i,j}\Big(\frac{\mu^n_{c\,i,j+1}\tau^n_{rri,j+1} - \mu^n_{c\,i,j-1}\tau^n_{rri,j-1}}{2\Delta z}\Big)\Big] \\
&+\frac{\Delta t De\bar{\lambda}^n_{i,j}}{\Delta t\xi + De\bar{\lambda}^n_{i,j}}\Big[2\tau^n_{rr\,i,j}\Big(\frac{u^n_{c\,i+1,j} - u^n_{c\,i-1,j}}{2\Delta r}\Big) + 2\tau^n_{rz\,i,j}\Big(\frac{u^n_{c\,i,j+1} - u^n_{c\,i,j-1}}{2\Delta z}\Big)\Big] \\
&+\frac{\Delta t De\bar{\lambda}^n_{i,j}}{\Delta t\xi + De\bar{\lambda}^n_{i,j}}\Bigg[\mu^n_{c\,i,j}\tau^n_{rr\,i,j}\Big(\frac{\log(\xi T^n{}_{cold\,i,j}+1) - \log(\xi T^n{}_{cnew\,i,j}+1)}{\Delta t}\Big) \\
&\qquad +(\tau^n_{rr\,i,j})(u^n_{c\,i,j})\Big(\frac{\log(\xi T^n{}_{ci+1,j}+1) - log(\xi T^n{}_{ci-1,j}+1)}{2\Delta r}\Big) \\
&\qquad +(\tau^n_{rr\,i,j})(w^n_{c\,i,j})\Big(\frac{\log(\xi T^n{}_{ci,j+1}+1) - log(\xi T^n{}_{ci,j-1}+1)}{2\Delta z}\Big)\Bigg] \\
&-\frac{\Delta t\alpha\mu_c}{\Delta t\xi + De\bar{\lambda}^n_{i,j}}(\tau^n_{rr\,i,j})^2 + \frac{\Delta t\mu_c\beta}{\Delta t\xi + De\bar{\lambda}^n_{i,j}}\Big(\frac{u^n_{c\,i+1,j} - u^n_{c\,i-1,j}}{2\Delta r}\Big).
\end{aligned} \tag{3.28}$$

τ_{rz} - component:

$$\begin{aligned}
(\mu_c\tau_{rz})^{n+1} + De\bar{\lambda}\left(\frac{(\mu_c\tau_{rz})^{n+1} - (\mu_c\tau_{rz})^n}{\Delta t}\right) + De\bar{\lambda}u^n_c\frac{\partial}{\partial r}(\mu_c\tau_{rz})^{n+1} + De\bar{\lambda}w^n_c\frac{\partial}{\partial r}(\mu_c\tau_{rz})^{n+1} \\
= \mu_c De\bar{\lambda}\left[\tau_{rr}\frac{\partial w_c}{\partial r} + \tau_{rz}\Big(\frac{\partial u_c}{\partial r} + \frac{\partial w_c}{\partial z}\Big) + \tau_{zz}\frac{\partial u_c}{\partial z} + \tau_{rz}\frac{D}{Dt}\ln(\xi T_c + 1)\right]^n \\
-\alpha\mu_c(\tau^n_{rz})^2 + \mu_u\beta\Big(\frac{\partial u_c}{\partial z} + \frac{\partial w_c}{\partial r}\Big).
\end{aligned} \tag{3.29}$$

By similarly applying Crank-Nicolson on derivatives involving spacial of extra stresses we obtain,

$$\begin{aligned}(\mu_c\tau_{rz})^{n+\xi} + De\bar{\lambda}\left(\frac{(\mu_c\tau_{rz})^{n+1} - (\mu_c\tau_{rz})^n}{\Delta t}\right) + De\bar{\lambda}u_c^n\frac{\partial}{\partial r}(\mu_c\tau_{rz})^{n+\xi} + De\bar{\lambda}w_c^n\frac{\partial}{\partial r}(\mu_c\tau_{rz})^{n+\xi}\\ = \mu_c De\bar{\lambda}\left[\tau_{rr}\frac{\partial w_c}{\partial r} + \tau_{rz}\Big(\frac{\partial u_c}{\partial r} + \frac{\partial w_c}{\partial z}\Big) + \tau_{zz}\frac{\partial u_c}{\partial z} + \tau_{rz}\frac{D}{Dt}\ln(\xi T_c + 1)\right]^n\\ -\alpha\mu_c(\tau_{rz}^n)^2 + \mu_c\beta\Big(\frac{\partial u_c}{\partial z} + \frac{\partial w_c}{\partial r}\Big).\end{aligned} \tag{3.30}$$

Multiplying by ΔT and rearranging equation (3.30) in the same way as the τ_{rr}- component the equation reduces to,

$$\begin{aligned}(\mu_c\tau_{rz})^{n+1} + \left(\frac{\Delta t\xi De\bar{\lambda}}{\Delta t\xi + De\bar{\lambda}}u_c^n\frac{\partial}{\partial r} + \frac{\Delta t\xi De\bar{\lambda}}{\Delta t\xi + De\bar{\lambda}}w_c^n\frac{\partial}{\partial r}\right)(\mu_c\tau_{rz})^{n+1}\\ = -\left(\frac{\Delta t(1-\xi)De\bar{\lambda}}{\Delta t\xi + De\bar{\lambda}}u_c^n\frac{\partial}{\partial r} + \frac{\Delta t(1-\xi)De\bar{\lambda}}{\Delta t\xi + De\bar{\lambda}}w_c^n\frac{\partial}{\partial r}\right)(\mu_c\tau_{rz})^n\\ -\frac{\Delta t\mu_c De\bar{\lambda}}{\Delta t\xi + De\bar{\lambda}}\left[\tau_{rr}\frac{\partial w_c}{\partial r} + \tau_{rz}\Big(\frac{\partial u_c}{\partial r} + \frac{\partial w_c}{\partial z}\Big) + \tau_{zz}\frac{\partial u_c}{\partial z} + \tau_{rz}\frac{D}{Dt}\ln(\xi T_c + 1)\right]^n\\ -\frac{(\Delta t(1-\xi) - De\bar{\lambda})}{\Delta t\xi + De\bar{\lambda}}(\mu_c\tau_{rz})^n - \frac{\Delta t\alpha\mu_c}{\Delta t\xi + De\bar{\lambda}}{\tau_{rz}^n}^2 + \frac{\Delta t\mu_c\beta}{\Delta t\xi + De\bar{\lambda}}\Big(\frac{\partial u_c}{\partial z} + \frac{\partial w_c}{\partial r}\Big).\end{aligned} \tag{3.31}$$

The implicit terms of equation 3.31 also factorize into tridiagonal matrices,

$$\left(1 + \frac{\Delta tDe\bar{\lambda}}{2\Delta t + De\bar{\lambda}}u_c^n\frac{\partial}{\partial r}\right)\left(1 + \frac{\Delta tDe\bar{\lambda}}{2\Delta t + De\bar{\lambda}}w_c^n\frac{\partial}{\partial r}\right)(\mu_c\tau_{rz})^{n+1}, \tag{3.32}$$

with an associated error term of $O\Big(\frac{(\Delta t\|u_c\|_{max})^2De\bar{\lambda}}{2\Delta t + De\bar{\lambda}}\Big)$.

The fully discretized form reads as,

$$\begin{aligned}\Big(-\frac{\Delta tDe\bar{\lambda}^n_{i,j}}{(2\Delta t + De\bar{\lambda}^n_{i,j})2\Delta r}u^n_{c\,i,j}(\mu_c\tau_{rzi,j-1})^{n+1} + (\mu_c\tau_{rzi,j})^{n+1}\\ + \frac{\Delta tDe\bar{\lambda}^n_{i,j}}{(2\Delta t + De\bar{\lambda}^n_{i,j})2\Delta r}u^n_{c\,i,j}(\mu_c\tau_{rzi,j+1})^{n+1}\Big)\\ \Big(-\frac{\Delta tDe\bar{\lambda}^n_{i,j}}{(2\Delta t + De\bar{\lambda}^n_{i,j})2\Delta r}w^n_{c\,i,j}(\mu_c\tau_{rzi,j-1})^{n+1} + (\mu_c\tau_{rzi,j})^{n+1}\\ + \frac{\Delta tDe\bar{\lambda}^n_{i,j}}{(2\Delta t + De\bar{\lambda}^n_{i,j})2\Delta r}w^n_{c\,i,j}(\mu_c\tau_{rzi,j+1})^{n+1}\Big).\end{aligned} \tag{3.33}$$

The explicit terms are discretized as;

$$
\begin{aligned}
RHS_{\tau_{rz}} = &-\frac{(\Delta t(1-\xi) - De\bar{\lambda}^n_{i,j})}{\Delta t\xi + De\bar{\lambda}^n_{i,j}}(\mu_c\tau^n_{rzi,j}) \\
&-\frac{\Delta t(1-\xi)De\bar{\lambda}^n_{i,j}}{\Delta t\xi + De\bar{\lambda}^n_{i,j}}\Big[u^n_{c\,i,j}\Big(\frac{\mu^n_{c\,i+1,j}\tau^n_{rzi+1,j} - \mu^n_{c\,i-1,j}\tau^n_{rzi-1,j}}{2\Delta r}\Big)\Big] \\
&-\frac{\Delta t(1-\xi)De\bar{\lambda}^n_{i,j}}{\Delta t\xi + De\bar{\lambda}^n_{i,j}}\Big[w^n_{c\,i,j}\Big(\frac{\mu^n_{c\,i,j+1}\tau^n_{rzi,j+1} - \mu^n_{c\,i,j-1}\tau^n_{rzi,j-1}}{2\Delta z}\Big)\Big] \\
&+\frac{\Delta tDe\bar{\lambda}^n_{i,j}}{\Delta t\xi + De\bar{\lambda}^n_{i,j}}\Big[\tau^n_{rri,j}\Big(\frac{w^n_{c\,i+1,j} - w^n_{c\,i-1,j}}{2\Delta r}\Big) + \tau^n_{rzi,j}\Big((\frac{u^n_{c\,i+1,j} - u^n_{c\,i-1,j}}{2\Delta r}\Big) + (\frac{w^n_{c\,i,j+1} - w^n_{c\,i,j-1}}{2\Delta z})\Big) \\
&+\tau^n_{zzi,j}(\frac{u^n_{c\,i,j+1} - u^n_{c\,i,j-1}}{2\Delta z}\Big)\Big] \\
&+\frac{\Delta tDe\bar{\lambda}^n_{i,j}}{\Delta t\xi + De\bar{\lambda}^n_{i,j}}\Bigg[\mu^n_{c\,i,j}\tau^n_{rzi,j}(\frac{\log(\xi T^n{}_{coldi,j}+1) - \log(\xi T^n{}_{cnewi,j}+1)}{\Delta t}) \\
&+(\tau^n_{rzi,j})(u^n_{c\,i,j})(\frac{\log(\xi T^n{}_{ci+1,j}+1) - log(\xi T^n{}_{ci-1,j}+1)}{2\Delta r}) \\
&+(\tau^n_{rzi,j})(w^n_{c\,i,j})(\frac{\log(\xi T^n{}_{ci,j+1}+1) - log(\xi T^n{}_{ci,j-1}+1)}{2\Delta z})\Bigg] \\
&-\frac{\Delta t\alpha\mu_c}{\Delta t\xi + De\bar{\lambda}^n_{i,j}}(\tau^n_{rzi,j})^2 + \frac{2\Delta t\mu_c\beta}{\Delta t\xi + De\bar{\lambda}^n_{i,j}}\Big((\frac{u^n_{c\,i,j+1} - u^n_{c\,i,j-1}}{2\Delta z}) + (\frac{w^n_{c\,i+1,j} - w^n_{c\,i-1,j}}{2\Delta r})\Big).
\end{aligned}
\tag{3.34}
$$

τ_{zz}-component:

$$
\begin{aligned}
(\mu_c\tau_{zz})^{n+1} + De\bar{\lambda}\left(\frac{(\mu_c\tau_{zz})^{n+1} - (\mu_c\tau_{zz})^n}{\Delta t}\right) + De\bar{\lambda}u^n_c\frac{\partial}{\partial r}(\mu_c\tau_{zz})^{n+1} + De\bar{\lambda}w^n_c\frac{\partial}{\partial r}(\mu_c\tau_{zz})^{n+1} \\
= \mu_c De\bar{\lambda}\left[2\tau_{rz}\frac{\partial w_c}{\partial r} + 2\tau_{zz}\frac{\partial w_c}{\partial z} + \tau_{zz}\frac{D}{Dt}\ln(\xi T_c + 1)\right]^n - \alpha\mu_c(\tau^n_{zz})^2 + 2\mu_c\beta\frac{\partial w_c}{\partial z}
\end{aligned}
\tag{3.35}
$$

by also applying Crank-Nicolson on derivatives involving spacial of extra stresses (3.35) becomes,

$$
\begin{aligned}
\mu_c\tau^{n+\xi}_{zz} + De\bar{\lambda}\left(\frac{(\mu_c\tau_{zz})^{n+1} - (\mu_c\tau_{zz})^n}{\Delta t}\right) + De\bar{\lambda}u^n_c\frac{\partial}{\partial r}(\mu_c\tau_{zz})^{n+\xi} + De\bar{\lambda}w^n_c\frac{\partial}{\partial r}(\mu_c\tau_{zz})^{n+\xi} \\
= \mu_c De\bar{\lambda}\left[2\tau_{rz}\frac{\partial w_c}{\partial r} + 2\tau_{zz}\frac{\partial w_c}{\partial z} + \tau_{zz}\frac{D}{Dt}\ln(\xi T_c + 1)\right]^n - \alpha\mu_c(\tau^n_{zz})^2 + 2\mu_c\beta\frac{\partial w_c}{\partial z}.
\end{aligned}
\tag{3.36}
$$

Simplifying equation (3.36) similar to components τ_{rr} and τ_{rz} we obtain the following equation for τ_{zz} - component

$$\begin{aligned}(\mu_c\tau_{zz})^{n+1} + \left(\frac{\Delta t\xi De\bar{\lambda}}{\Delta t\xi + De\bar{\lambda}}u_c^n\frac{\partial}{\partial r} + \frac{\Delta t\xi De\bar{\lambda}}{\Delta t\xi + De\bar{\lambda}}w_c^n\frac{\partial}{\partial r}\right)(\mu_c\tau_{zz})^{n+1} \\ = -\left(\frac{\Delta t(1-\xi)De\bar{\lambda}}{\Delta t\xi + De\bar{\lambda}}u_c^n\frac{\partial}{\partial r} + \frac{\Delta t(1-\xi)De\bar{\lambda}}{\Delta t\xi + De\bar{\lambda}}w_c^n\frac{\partial}{\partial r}\right)(\mu_c\tau_{zz})^n \\ -\frac{\Delta t\mu_c De\bar{\lambda}}{\Delta t\xi + De\bar{\lambda}}\left[2\tau_{rz}\frac{\partial w_c}{\partial r} + 2\tau_{zz}\frac{\partial w_c}{\partial z} + \tau_{zz}\frac{D}{Dt}\ln(\xi T_c + 1)\right]^n \\ -\frac{(\Delta t(1-\xi) - De\bar{\lambda})}{\Delta t\xi + De\bar{\lambda}}(\mu_c\tau_{zz})^n - \frac{\Delta t\alpha\mu_c}{\Delta t\xi + De\bar{\lambda}}(\tau_{zz}^n)^2 + \frac{2\Delta t\mu_c\beta}{\Delta t\xi + De\bar{\lambda}}\frac{\partial w_c^n}{\partial z}.\end{aligned} \tag{3.37}$$

The implicit terms of equation 3.37 factorize into tridiagonal matrices

$$\left(1 + \frac{\Delta tDe\bar{\lambda}}{2\Delta t + De\bar{\lambda}}u_c^n\frac{\partial}{\partial r}\right)\left(1 + \frac{\Delta tDe\bar{\lambda}}{2\Delta t + De\bar{\lambda}}w_c^n\frac{\partial}{\partial r}\right)(\mu_c\tau_{zz})^{n+1}, \tag{3.38}$$

with an associated error term of $O\Big(\frac{(\Delta t\|u_c\|_{max})^2 De\bar{\lambda}}{2\Delta t + De\bar{\lambda}}\Big)$.

The fully discretized form reads,

$$\begin{aligned}\Big(-\frac{\Delta tDe\bar{\lambda}^n_{i,j}}{(2\Delta t + De\bar{\lambda}^n_{i,j})2\Delta r}u^n_{c\,i,j}(\mu_c\tau_{zzi,j-1})^{n+1} + (\mu_c\tau_{zzi,j})^{n+1} \\ + \frac{\Delta tDe\bar{\lambda}^n_{i,j}}{(2\Delta t + De\bar{\lambda}^n_{i,j})2\Delta r}u^n_{c\,i,j}(\mu_c\tau_{zzi,j+1})^{n+1}\Big) \\ \Big(-\frac{\Delta tDe\bar{\lambda}^n_{i,j}}{(2\Delta t + De\bar{\lambda}^n_{i,j})2\Delta r}w^n_{c\,i,j}(\mu_c\tau_{zzi,j-1})^{n+1} + (\mu_c\tau_{zzi,j})^{n+1} \\ + \frac{\Delta tDe\bar{\lambda}^n_{i,j}}{(2\Delta t + De\bar{\lambda}^n_{i,j})2\Delta r}w^n_{c\,i,j}(\mu_c\tau_{zzi,j+1})^{n+1}\Big).\end{aligned} \tag{3.39}$$

The discretized version of explicit terms is given by,

$$
\begin{aligned}
RHS_{\tau_{zz}} = &-\frac{(\Delta t(1-\xi) - De\bar{\lambda}^n_{i,j})}{\Delta t\xi + De\bar{\lambda}^n_{i,j}}(\mu_c \tau^n_{zz\,i,j}) \\
&-\frac{\Delta t(1-\xi)De\bar{\lambda}^n_{i,j}}{\Delta t\xi + De\bar{\lambda}^n_{i,j}}\Big[u^n_{c\,i,j}\Big(\frac{\mu^n_{c\,i+1,j}\tau^n_{zzi+1,j} - \mu^n_{c\,i-1,j}\tau^n_{zzi-1,j}}{2\Delta r}\Big)\Big] \\
&-\frac{\Delta t(1-\xi)De\bar{\lambda}^n_{i,j}}{\Delta t\xi + De\bar{\lambda}^n_{i,j}}\Big[w^n_{c\,i,j}\Big(\frac{\mu^n_{c\,i,j+1}\tau^n_{zzi,j+1} - \mu^n_{c\,i,j-1}\tau^n_{zzi,j-1}}{2\Delta z}\Big)\Big] \\
&+\frac{\Delta t De\bar{\lambda}^n_{i,j}}{\Delta t\xi + De\bar{\lambda}^n_{i,j}}\Big[2\tau^n_{rzi,j}\Big(\frac{w^n_{c\,i+1,j} - w^n_{c\,i-1,j}}{2\Delta r}\Big) + 2\tau^n_{zzi,j}\Big(\frac{w^n_{c\,i,j+1} - w^n_{c\,i,j-1}}{2\Delta z}\Big)\Big] \\
&+\frac{\Delta t De\bar{\lambda}^n_{i,j}}{\Delta t\xi + De\bar{\lambda}^n_{i,j}}\Bigg[\mu^n_{c\,i,j}\tau^n_{zzi,j}\Big(\frac{\log(\xi T^n{}_{cold\,i,j}+1) - \log(\xi T^n{}_{cnew\,i,j}+1)}{\Delta t}\Big) \\
&+(\tau^n_{zzi,j})(u^n_{c\,i,j})\Big(\frac{\log(\xi T^n{}_{ci+1,j}+1) - log(\xi T^n{}_{ci-1,j}+1)}{2\Delta r}\Big) \\
&+(\tau^n_{zzi,j})(w^n_{c\,i,j})\Big(\frac{\log(\xi T^n{}_{ci,j+1}+1) - log(\xi T^n{}_{ci,j-1}+1)}{2\Delta z}\Big)\Bigg] \\
&-\frac{\Delta t\alpha\mu_c}{\Delta t\xi + De\bar{\lambda}^n_{i,j}}(\tau^n_{zzi,j})^2 + \frac{2\Delta t\mu_c\beta}{\Delta t\xi + De\bar{\lambda}^n_{i,j}}\Big(\frac{w^n_{c\,i,j+1} - w^n_{c\,i,j-1}}{2\Delta z}\Big).
\end{aligned}
\tag{3.40}
$$

3.2.2 Discretization of Shell-Fluid Equations

Momentum Equation:

$$
\begin{aligned}
{w_s^{n+1}}_{i,j} - w^n_{s\,i,j} = &-\Delta t\Big(w^n_{s\,i,j}\frac{w^n_{s\,i,j+1} - w^n_{s\,i,j-1}}{2\Delta z}\Big) - \Delta t G_s \\
&+\frac{\Delta t}{Re_s}\Big[\mu^n_{s\,i,j}\Big(\frac{w_{si+1,j} - 2w_{si,j} + w_{si-1,j}}{(\Delta r)^2}\Big) + 2\mu^n_{s\,i,j}\Big(\frac{w_{si,j+1} - 2w_{si,j} + w_{si,j-1}}{(\Delta z)^2}\Big)\Big] \\
&+\frac{\Delta t}{2Re_s}\Big[\mu^n_{s\,i,j}\Big(\frac{w^n_{s\,i+1,j} - 2w^n_{s\,i,j} + w^n_{s\,i-1,j}}{(\Delta r)^2}\Big) + \mu^n_{s\,i,j}\Big(\frac{w^n_{s\,i,j+1} - 2w^n_{s\,i,j} + w^n_{s\,i,j-1}}{(\Delta z)^2}\Big)\Big] \\
&+\frac{\Delta t}{2Re_s}\Big[\Big(\frac{\mu^n_{s\,i+1,j}\tau^n_{rzi+1,j} - \mu^n_{s\,i-1,j}\tau^n_{rzi-1,j}}{2\Delta r}\Big) + \Big(\frac{\mu^n_{s\,i,j+1}\tau^n_{zzi,j+1} - \mu^n_{s\,i,j-1}\tau^n_{zzi,j-1}}{2\Delta z}\Big)\Big] \\
&+\frac{\Delta t}{Re_s}\Big[\frac{\tau^n_{rzi,j}}{r_{si}}\Big] + \frac{\Delta t}{Re_s}\Big[\frac{\mu_s}{r_{si}}\Big(\frac{w^n_{s\,i+1,j} - w^n_{s\,i-1,j}}{2\Delta r}\Big)\Big].
\end{aligned}
\tag{3.41}
$$

Energy Equation:

$$
\begin{aligned}
{T_s^{n+1}}_{i,j} - {T_s^n}_{i,j} &= -\Delta t {w_s^n}_{i,j}\Big(\frac{{T_s^n}_{i,j+1} - {T_s^n}_{i,j-1}}{2\Delta z}\Big) + \frac{\Delta t}{Re_s Pr_s}\Big[\frac{1}{r_{si}}\Big(\frac{{T_s^n}_{i+1,j} - {T_s^n}_{i-1,j}}{2\Delta r}\Big)\Big] \\
&+ \frac{\Delta t}{2Re_s Pr_s}\Big[\Big(\frac{{T_s^{n+1}}_{i+1,j} - 2{T_s^{n+1}}_{i,j} + {T_s^{n+1}}_{i-1,j}}{(\Delta r)^2}\Big) + \Big(\frac{{T_s^{n+1}}_{i,j+1} - 2{T_s^{n+1}}_{i,j} + {T_s^{n+1}}_{i,j-1}}{(\Delta z)^2}\Big)\Big] \\
&+ \frac{\Delta t}{2Re_s Pr_s}\Big[\Big(\frac{{T_s^n}_{i+1,j} - 2{T_s^n}_{i,j} + {T_s^n}_{i-1,j}}{(\Delta r)^2}\Big) + \Big(\frac{{T_s^n}_{i,j+1} - 2{T_s^n}_{i,j} + {T_s^n}_{i,j-1}}{(\Delta z)^2}\Big)\Big] \\
&+ \frac{\Delta t Re_s \delta_{s2}\delta_{s3}}{Pr_s}\Big(1 + \frac{1}{\xi}\Big)\Big[{w_s^n}_{i,j} G_s\Big] \\
&+ \frac{2\Delta t\gamma\delta_{s2}}{Re_s Pr_s}\Big[\Big({\mu_s^n}_{i,j}{\tau_{rr}^n}_{i,j}\frac{{w_s^n}_{i,j+1} - {w_s^n}_{i,j-1}}{2\Delta z}\Big)\Big] + \frac{2\Delta t\gamma\delta_{s2}}{Re_s Pr_s}{\mu_s^n}_{i,j}{\tau_{rz}^n}_{i,j}\Big[\Big(\frac{{w_s^n}_{i+1,j} - {w_s^n}_{i-1,j}}{2\Delta r}\Big)\Big] \\
&+ \frac{\Delta t\delta_{s2}(1-\gamma)(1-\beta)}{Re_s Pr_s}{\mu_s^n}_{i,j}\Big[2\Big(\frac{{w_s^n}_{i,j+1} - {w_s^n}_{i,j-1}}{2\Delta z}\Big)^2 + \Big(\frac{{w_s^n}_{i+1,j} - {w_s^n}_{i-1,j}}{2\Delta r}\Big)^2\Big] + h_s(T_{w\,i,j}^n - {T_s^n}_{i,j}).
\end{aligned}
\tag{3.42}
$$

Stress Equations:

$\tau_{rr} - component$:

$$
\begin{aligned}
(\mu_s\tau_{rr})^{n+1} + De\bar{\lambda}\left(\frac{(\mu_s\tau_{rr})^{n+1} - (\mu_s\tau_{rr})^n}{\Delta t}\right) + De\bar{\lambda}w_s^n\frac{\partial}{\partial r}(\mu_s\tau_{rr})^{n+1} \\
= \mu_s De\bar{\lambda}\left[\tau_{rr}\frac{D}{Dt}\ln(\xi T_s + 1)\right]^n - \alpha\mu_s(\tau_{rr}^n)^2.
\end{aligned}
\tag{3.43}
$$

Applying Crank-Nicolson scheme on spacial derivatives of extra stresses (3.43) becomes,

$$
\begin{aligned}
\mu_s\tau_{rr}^{n+\xi} + De\bar{\lambda}\left(\frac{(\mu_s\tau_{rr})^{n+1} - (\mu_s\tau_{rr})^n}{\Delta t}\right) + De\bar{\lambda}w_s^n\frac{\partial}{\partial r}(\mu_s\tau_{rr})^{n+\xi} \\
= \mu_s De\bar{\lambda}\left[\tau_{rr}\frac{D}{Dt}\ln(\xi T_s + 1)\right]^n - \alpha\mu_s(\tau_{rr}^n)^2.
\end{aligned}
\tag{3.44}
$$

When simplifying (3.44) it reduces to;

$$
\begin{aligned}
(\mu_s\tau_{rr})^{n+1} + \left(\frac{\Delta t\xi De\bar{\lambda}}{\Delta t\xi + De\bar{\lambda}}w_s^n\frac{\partial}{\partial r}\right)(\mu_s\tau_{rr})^{n+1} \\
= -\left(\frac{\Delta t(1-\xi)De\bar{\lambda}}{\Delta t\xi + De\bar{\lambda}}w_s^n\frac{\partial}{\partial r}\right)(\mu_s\tau_{rr})^n - \frac{\Delta t\mu_s De\bar{\lambda}}{\Delta t\xi + De\bar{\lambda}}\left[\tau_{rr}\frac{D}{Dt}\ln(\xi T_s + 1)\right]^n \\
- \frac{(\Delta t(1-\xi) - De\bar{\lambda})}{\Delta t\xi + De\bar{\lambda}}(\mu_s\tau_{rr})^n - \frac{\Delta t\alpha\mu_s}{\Delta t\xi + De\bar{\lambda}}(\tau_{rr}^n)^2.
\end{aligned}
\tag{3.45}
$$

The implicit side then becomes,

$$
\left(1 + \frac{\Delta t De\bar{\lambda}}{2\Delta t + De\bar{\lambda}}w_s^n\frac{\partial}{\partial r}\right)(\mu_s\tau_{rr})^{n+1}.
\tag{3.46}
$$

This results in a tridiagonal matrix with an associated error term of $O\Big(\frac{(\Delta t\|w_s\|_{max})^2 De\bar{\lambda}}{2\Delta t+De\bar{\lambda}}\Big)$ and the fully discretized form of (3.46) is given by,

$$\begin{aligned}\Big(-\frac{\Delta t De\bar{\lambda}^n_{i,j}}{(2\Delta t+De\bar{\lambda}^n_{i,j})2\Delta r}w^n_{s\,i,j}(\mu_s\tau_{rri,j-1})^{n+1}+(\mu_s\tau_{rri,j})^{n+1}\\ +\frac{\Delta t De\bar{\lambda}^n_{i,j}}{(2\Delta t+De\bar{\lambda}^n_{i,j})2\Delta r}w^n_{s\,i,j}(\mu_s\tau_{rri,j+1})^{n+1}\Big).\end{aligned} \tag{3.47}$$

The explicit terms are discretized as follows:

$$\begin{aligned}RHS_{\tau_{rr}}=&-\frac{(\Delta t(1-\xi)-De\bar{\lambda}^n_{i,j})}{\Delta t\xi+De\bar{\lambda}^n_{i,j}}(\mu_s\tau^n_{rri,j})\\ &-\frac{\Delta t(1-\xi)De\bar{\lambda}^n_{i,j}}{\Delta t\xi+De\bar{\lambda}^n_{i,j}}\Big[w^n_{s\,i,j}\Big(\frac{\mu^n_{s\,i,j+1}\tau^n_{rri,j+1}-\mu^n_{s\,i,j-1}\tau^n_{rri,j-1}}{2\Delta z}\Big)\Big]\\ &+\frac{\Delta t De\bar{\lambda}^n_{i,j}}{\Delta t\xi+De\bar{\lambda}^n_{i,j}}\Big[\mu^n_{s\,i,j}\tau^n_{rri,j}\Big(\frac{\log(\xi T^n{}_{s-old_{i,j}}+1)-\log(\xi T^n{}_{s-new_{i,j}}+1)}{\Delta t}\Big)\\ &+(\tau^n_{rri,j})(w^n_{s\,i,j})\Big(\frac{\log(\xi T^n{}_{si,j+1}+1)-log(\xi T^n{}_{si,j-1}+1)}{2\Delta z}\Big)\Big]\\ &-\frac{\Delta t\alpha\mu_s}{\Delta t\xi+De\bar{\lambda}^n_{i,j}}(\tau^n_{rri,j})^2\end{aligned} \tag{3.48}$$

τ_{rz} - component:

$$\begin{aligned}(\mu_s\tau_{rz})^{n+1}+De\bar{\lambda}\left(\frac{(\mu_s\tau_{rz})^{n+1}-(\mu_s\tau_{rz})^n}{\Delta t}\right)+De\bar{\lambda}w^n_s\frac{\partial}{\partial r}(\mu_s\tau_{rz})^{n+1}\\ =\mu_s De\bar{\lambda}\left[\tau_{rr}\frac{\partial w_s}{\partial r}+\tau_{rz}\frac{\partial w_s}{\partial z}+\tau_{rz}\frac{D}{Dt}\ln(\xi T_s+1)\right]^n\\ -\alpha\mu_s(\tau^n_{rz})^2+\mu_s\beta\Big(\frac{\partial w_s}{\partial r}\Big).\end{aligned} \tag{3.49}$$

Similarly when applying Crank-Nicolson scheme on the derivatives spacial of extra stresses, equation (3.49) becomes,

$$\begin{aligned}(\mu_s\tau_{rz})^{n+\xi}+De\bar{\lambda}\left(\frac{(\mu_s\tau_{rz})^{n+1}-(\mu_s\tau_{rz})^n}{\Delta t}\right)+De\bar{\lambda}w^n_s\frac{\partial}{\partial r}(\mu_s\tau_{rz})^{n+\xi}\\ =\mu_s De\bar{\lambda}\left[\tau_{rr}\frac{\partial w_s}{\partial r}+\tau_{rz}\Big(\frac{\partial w_s}{\partial z}\Big)+\tau_{rz}\frac{D}{Dt}\ln(\xi T_s+1)\right]^n\\ -\alpha\mu_s(\tau^n_{rz})^2+\mu_s\beta\Big(\frac{\partial w_s}{\partial r}\Big).\end{aligned} \tag{3.50}$$

When multiplying equation (3.50) by ΔT and rearranging it similar to the τ_{rr} - component we obtain,

$$\begin{aligned}(\mu_s\tau_{rz})^{n+1} + \left(\frac{\Delta t\xi De\bar{\lambda}}{\Delta t\xi + De\bar{\lambda}} w_s^n \frac{\partial}{\partial r}\right)(\mu_s\tau_{rz})^{n+1} = -\left(\frac{\Delta t(1-\xi) De\bar{\lambda}}{\Delta t\xi + De\bar{\lambda}} w_s^n \frac{\partial}{\partial r}\right)(\mu_s\tau_{rz})^{n} \\ -\frac{\Delta t\mu_s De\bar{\lambda}}{\Delta t\xi + De\bar{\lambda}}\left[\tau_{rr}\frac{\partial w_s}{\partial r} + \tau_{rz}\Big(\frac{\partial w_s}{\partial z}\Big) + \tau_{rz}\frac{D}{Dt}\ln(\xi T_s + 1)\right]^n \\ -\frac{(\Delta t(1-\xi) - De\bar{\lambda})}{\Delta t\xi + De\bar{\lambda}}(\mu_s\tau_{rz})^n - \frac{\Delta t\alpha\mu_s}{\Delta t\xi + De\bar{\lambda}}{\tau_{rz}^n}^2 + \frac{\Delta t\mu_s\beta}{\Delta t\xi + De\bar{\lambda}}\Big(\frac{\partial w_s}{\partial r}\Big).\end{aligned} \tag{3.51}$$

The implicit terms reduce to a tridiagonal matrix

$$\left(1 + \frac{\Delta t De\bar{\lambda}}{2\Delta t + De\bar{\lambda}} w_s^n \frac{\partial}{\partial r}\right)(\mu_s\tau_{rz})^{n+1}, \tag{3.52}$$

with an associated error term of $O\Big(\frac{(\Delta t\|w_s\|_{max})^2 De\bar{\lambda}}{2\Delta t + De\bar{\lambda}}\Big)$.

The fully discretized form reads,

$$\begin{aligned}\Big(-\frac{\Delta t De\bar{\lambda}^n_{i,j}}{(2\Delta t + De\bar{\lambda}^n_{i,j})2\Delta r} {w_s}^n_{i,j}(\mu_s\tau_{rzi,j-1})^{n+1} + (\mu_s\tau_{rzi,j})^{n+1} \\ + \frac{\Delta t De\bar{\lambda}^n_{i,j}}{(2\Delta t + De\bar{\lambda}^n_{i,j})2\Delta r} {w_s}^n_{i,j}(\mu_s\tau_{rzi,j+1})^{n+1}\Big).\end{aligned} \tag{3.53}$$

The discretized version of the explicit terms leads to,

$$\begin{aligned}RHS_{\tau_{rz}} = -\frac{(\Delta t(1-\xi) - De\bar{\lambda}^n_{i,j})}{\Delta t\xi + De\bar{\lambda}^n_{i,j}}(\mu_s\tau^n_{rzi,j}) \\ -\frac{\Delta t(1-\xi) De\bar{\lambda}^n_{i,j}}{\Delta t\xi + De\bar{\lambda}^n_{i,j}}\Big[{w_s}^n_{i,j}\Big(\frac{\mu^n_{s\,i,j+1}\tau^n_{rzi,j+1} - \mu^n_{s\,i,j-1}\tau^n_{rzi,j-1}}{2\Delta z}\Big)\Big] \\ +\frac{\Delta t De\bar{\lambda}^n_{i,j}}{\Delta t\xi + De\bar{\lambda}^n_{i,j}}\Big[\tau^n_{rri,j}\Big(\frac{{w_s}^n_{i+1,j} - {w_s}^n_{i-1,j}}{2\Delta r}\Big) + \tau^n_{rzi,j}\Big(\frac{{w_s}^n_{i,j+1} - {w_s}^n_{i,j-1}}{2\Delta z})\Big) \\ +\frac{\Delta t De\bar{\lambda}^n_{i,j}}{\Delta t\xi + De\bar{\lambda}^n_{i,j}}\Big[\mu^n_{s\,i,j}\tau^n_{rzi,j}(\frac{\log(\xi {T^n}_{s-old_{i,j}} + 1) - \log(\xi {T^n}_{s-new_{i,j}} + 1)}{\Delta t} \\ +(\tau^n_{rzi,j})({w_s}^n_{i,j})(\frac{\log(\xi {T^n}_{si,j+1} + 1) - log(\xi {T^n}_{si,j-1} + 1)}{2\Delta z})\Big] \\ -\frac{\Delta t\alpha\mu_s}{\Delta t\xi + De\bar{\lambda}^n_{i,j}}(\tau^n_{rzi,j})^2 + \frac{2\Delta t\mu^n_s\beta}{\Delta t\xi + De\bar{\lambda}^n_{i,j}}\Big(\frac{{w_s}^n_{i+1,j} - {w_s}^n_{i-1,j}}{2\Delta r})\Big).\end{aligned} \tag{3.54}$$

τ_{zz} - component:

$$\begin{aligned}(\mu_s\tau_{zz})^{n+1} + De\bar{\lambda}\left(\frac{(\mu_s\tau_{zz})^{n+1} - (\mu_s\tau_{zz})^n}{\Delta t}\right) + De\bar{\lambda}w_s^n\frac{\partial}{\partial r}(\mu_s\tau_{zz})^{n+1} \\ = \mu_s De\bar{\lambda}\left[2\tau_{rz}\frac{\partial w_s}{\partial r} + 2\tau_{zz}\frac{\partial w_s}{\partial z} + \tau_{zz}\frac{D}{Dt}\ln(\xi T_s + 1)\right]^n - \alpha\mu_s(\tau_{zz}^n)^2 + 2\mu_s\beta\frac{\partial w_s}{\partial z}.\end{aligned} \tag{3.55}$$

When applying Crank-Nicolson scheme on the spacial derivatives of extra stresses, equation (3.55) then becomes,

$$\begin{aligned}\mu_s\tau_{zz}^{n+\xi} + De\bar{\lambda}\left(\frac{(\mu_s\tau_{zz})^{n+1} - (\mu_s\tau_{zz})^n}{\Delta t}\right) + De\bar{\lambda}w_s^n\frac{\partial}{\partial r}(\mu_s\tau_{zz})^{n+\xi} \\ = \mu_s De\bar{\lambda}\left[2\tau_{rz}\frac{\partial w_s}{\partial r} + 2\tau_{zz}\frac{\partial w_s}{\partial z} + \tau_{zz}\frac{D}{Dt}\ln(\xi T_s + 1)\right]^n - \alpha\mu_s(\tau_{zz}^n)^2 + 2\mu_s\beta\frac{\partial w_s}{\partial z}.\end{aligned} \tag{3.56}$$

In multiplying equation (3.56) by Δt and rearranging it similar to component τ_{rr} - component and τ_{rz} - component we obtain the following equation,

$$\begin{aligned}(\mu_s\tau_{zz})^{n+1} + \left(\frac{\Delta t\xi De\bar{\lambda}}{\Delta t\xi + De\bar{\lambda}}w_s^n\frac{\partial}{\partial r}\right)(\mu_s\tau_{zz})^{n+1} = -\left(\frac{\Delta t(1-\xi)De\bar{\lambda}}{\Delta t\xi + De\bar{\lambda}}w_s^n\frac{\partial}{\partial r}\right)(\mu_s\tau_{zz})^n \\ -\frac{\Delta t\mu_s De\bar{\lambda}}{\Delta t\xi + De\bar{\lambda}}\left[2\tau_{rz}\frac{\partial w_s}{\partial r} + 2\tau_{zz}\frac{\partial w_s}{\partial z} + \tau_{zz}\frac{D}{Dt}\ln(\xi T_s + 1)\right]^n \\ -\frac{(\Delta t(1-\xi) - De\bar{\lambda})}{\Delta t\xi + De\bar{\lambda}}(\mu_s\tau_{zz})^n - \frac{\Delta t\alpha\mu_s}{\Delta t\xi + De\bar{\lambda}}(\tau_{zz}^n)^2 + \frac{2\Delta t\mu_s\beta}{\Delta t\xi + De\bar{\lambda}}\frac{\partial w_s^n}{\partial z}.\end{aligned} \tag{3.57}$$

The implicit terms then become a tridiagonal matrix

$$\left(1 + \frac{\Delta t De\bar{\lambda}}{2\Delta t + De\bar{\lambda}}w_s^n\frac{\partial}{\partial r}\right)(\mu_s\tau_{zz})^{n+1}, \tag{3.58}$$

with an associated error term of $O\Big(\frac{(\Delta t\|w_s\|_{max})^2 De\bar{\lambda}}{2\Delta t + De\bar{\lambda}}\Big)$. The fully discretized form reads,

$$\begin{aligned}\Big(-\frac{\Delta t De\bar{\lambda}^n_{i,j}}{(2\Delta t + De\bar{\lambda}^n_{i,j})2\Delta r}w^n_{s\,i,j}(\mu_s\tau_{zzi,j-1})^{n+1} + (\mu_s\tau_{zzi,j})^{n+1} \\ + \frac{\Delta t De\bar{\lambda}^n_{i,j}}{(2\Delta t + De\bar{\lambda}^n_{i,j})2\Delta r}w^n_{s\,i,j}(\mu_s\tau_{zzi,j+1})^{n+1}\Big).\end{aligned} \tag{3.59}$$

The explicit terms are also discretized to become,

$$\begin{aligned} RHS_{\tau_{zz}} = &-\frac{(\Delta t(1-\xi) - De\bar{\lambda}^n_{i,j})}{\Delta t\xi + De\bar{\lambda}^n_{i,j}}(\mu_s \tau^n_{zzi,j}) \\ &-\frac{\Delta t(1-\xi)De\bar{\lambda}^n_{i,j}}{\Delta t\xi + De\bar{\lambda}^n_{i,j}}\Big[{w^n_s}_{i,j}\Big(\frac{{\mu^n_s}_{i,j+1}\tau^n_{zzi,j+1} - {\mu^n_s}_{i,j-1}\tau^n_{zzi,j-1}}{2\Delta z}\Big)\Big] \\ &+\frac{\Delta t De\bar{\lambda}^n_{i,j}}{\Delta t\xi + De\bar{\lambda}^n_{i,j}}\Big[2\tau^n_{rzi,j}\Big(\frac{{w^n_s}_{i+1,j} - {w^n_s}_{i-1,j}}{2\Delta r}\Big) + 2\tau^n_{zzi,j}\Big(\frac{{w^n_s}_{i,j+1} - {w^n_s}_{i,j-1}}{2\Delta z}\Big)\Big] \\ &+\frac{\Delta t De\bar{\lambda}^n_{i,j}}{\Delta t\xi + De\bar{\lambda}^n_{i,j}}\Bigg[{\mu^n_s}_{i,j}\tau^n_{zzi,j}\Big(\frac{\log(\xi {T^n}_{s-old_{i,j}} + 1) - \log(\xi {T^n}_{s-new_{i,j}} + 1)}{\Delta t}\Big) \\ &+(\tau^n_{zzi,j})({w^n_s}_{i,j})\Big(\frac{\log(\xi {T^n}_{si,j+1} + 1) - log(\xi {T^n}_{si,j-1} + 1)}{2\Delta z}\Big)\Bigg] \\ &-\frac{\Delta t\alpha\mu_s}{\Delta t\xi + De\bar{\lambda}^n_{i,j}}(\tau^n_{zzi,j})^2 + \frac{2\Delta t\mu_s\beta}{\Delta t\xi + De\bar{\lambda}^n_{i,j}}\Big(\frac{{w^n_s}_{i,j+1} - {w^n_s}_{i,j-1}}{2\Delta z}\Big). \end{aligned} \tag{3.60}$$

3.3 Discretization of the connecting wall

The full Crank-Nicolson scheme is applied to the below equation and it reduces to,

$$\begin{aligned} {T^{n+1}_w}_{i,j} = T^n_{wi,j} &+ \xi\Delta t\Bigg(\frac{{T^{n+1}_w}_{i,j+1} - 2{T^{n+1}_w}_{i,j} + {T^{n+1}_w}_{i,j-1}}{(\Delta z)^2}\Bigg) \\ +((1-\xi)\Delta t\Bigg(\frac{T^n_{wi,j+1} - 2T^n_{wi,j} + T^n_{wi,j-1}}{(\Delta z)^2}\Bigg) &+ h_c\Big[T^n_c - \Big(\xi\Delta t{T^{n+1}_w}_{i,j} + (1-\xi)\Delta t T^n_{wi,j}\Big)\Big] \\ &+h_s\Big[T^n_s - \Big(\xi\Delta t{T^{n+1}_w}_{i,j} + (1-\xi)\Delta t T^n_{wi,j}\Big)\Big]. \end{aligned} \tag{3.61}$$

When rearranging equation (3.61) into implicit and explicit terms it then becomes,

$$\begin{aligned} {T^{n+1}_w}_{i,j} - \frac{\xi\Delta t}{(\Delta z)^2}\Big({T^{n+1}_w}_{i,j+1} - 2{T^{n+1}_w}_{i,j} + {T^{n+1}_w}_{i,j-1}\Big) + h_c\xi\Delta t{T^{n+1}_w}_{i,j} \\ +h_s\xi\Delta t{T^{n+1}_w}_{i,j} = T^n_{wi,j} + \frac{(1-\xi)\Delta t}{(\Delta z)^2}\Bigg(T^n_{wi,j+1} - 2T^n_{wi,j} + T^n_{wi,j-1}\Bigg) \\ +h_c\Big[T^n_c - (1-\xi)\Delta t T^n_{wi,j}\Big] + h_s\Big[T^n_s - (1-\xi)\Delta t T^n_{wi,j}\Big] \end{aligned} \tag{3.62}$$

The implicit terms reduce to a tridiagonal matrix as follows,

$$-\Bigg(\frac{\xi\Delta t}{(\Delta z)^2}\Bigg)T^n_{wi,j-1} + \Bigg(1 + 2\frac{\xi\Delta t}{(\Delta z)^2} + h_s\xi\Delta t + h_c\xi\Delta t\Bigg)T^n_{wi,j} - \Bigg(\frac{\xi\Delta t}{(\Delta z)^2}\Bigg)T^n_{wi,j+1}. \tag{3.63}$$

The explicit terms read,

$$\begin{aligned} &T^n_{wi,j} + \frac{(1-\xi)\Delta t}{(\Delta z)^2}\left(T^n_{wi,j+1} - 2T^n_{wi,j} + T^n_{wi,j-1}\right) \\ &+h_c\Big[T^n_c - (1-\xi)\Delta t T^n_{wi,j}\Big] + h_s\Big[T^n_s - (1-\xi)\Delta t T^n_{wi,j}\Big]. \end{aligned} \tag{3.64}$$

Chapter 4

Temporal and Mesh Convergence

The numerical accuracy of results necessitates for both temporal and mesh convergence tests to be conducted on the algorithm used for computational analysis.

Temporal convergence was tested at various times at $\Delta t = 0.0001$ and the algorithm successfully converged. Results are shown in figures 4.1, 4.3 and 4.5 with corresponding surface plots. Final temporal convergence was reached when times $t = 0.3, 0.5, 0.8$ and 1 were used and this is presented in figure 4.5.

Similarly when values $\Delta r = 0.05, 0.03$ and 0.25 were employed to check for spacial convergence, the algorithm converged to the same results both qualitatively and quantitatively. Graphical results are presented in figures 4.7 and 4.9 with corresponding surface plots.

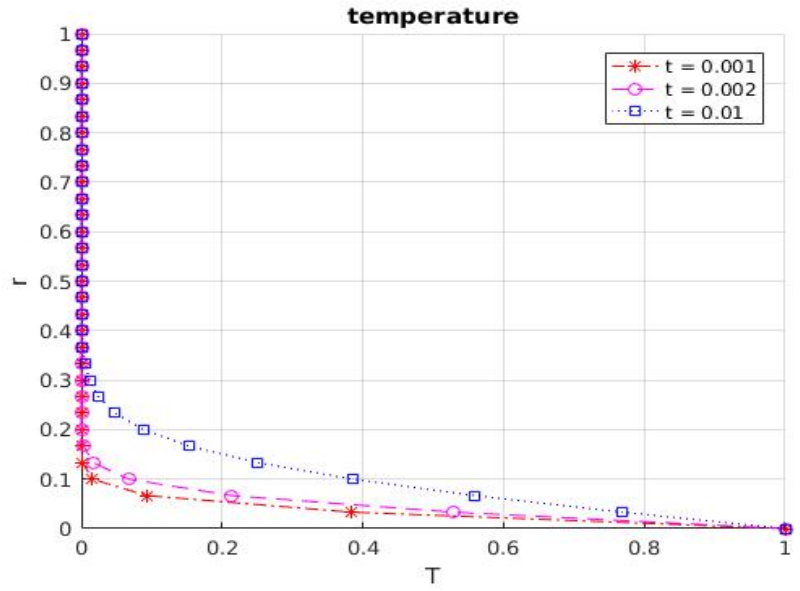

FIGURE 4.1: Temporal convergence Test 1 plot.

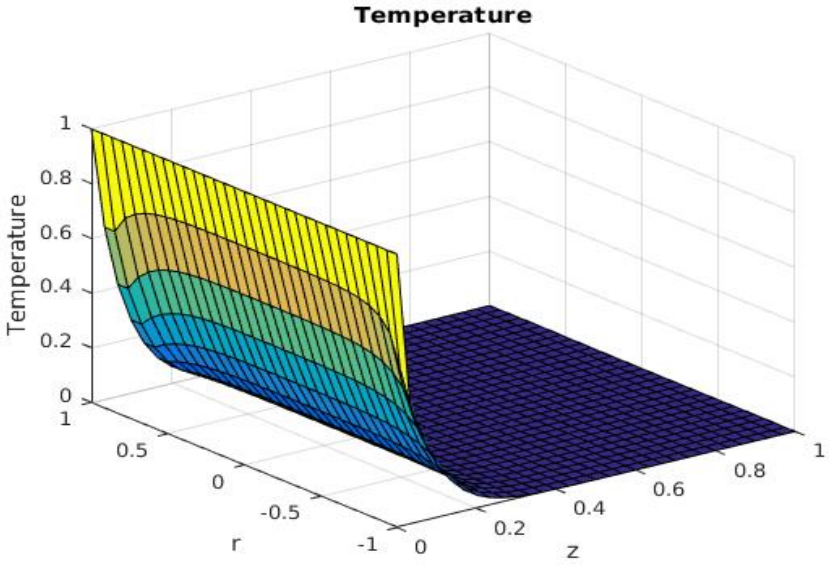

FIGURE 4.2: Temporal convergence Test 1 surface plot at t= 0.01.

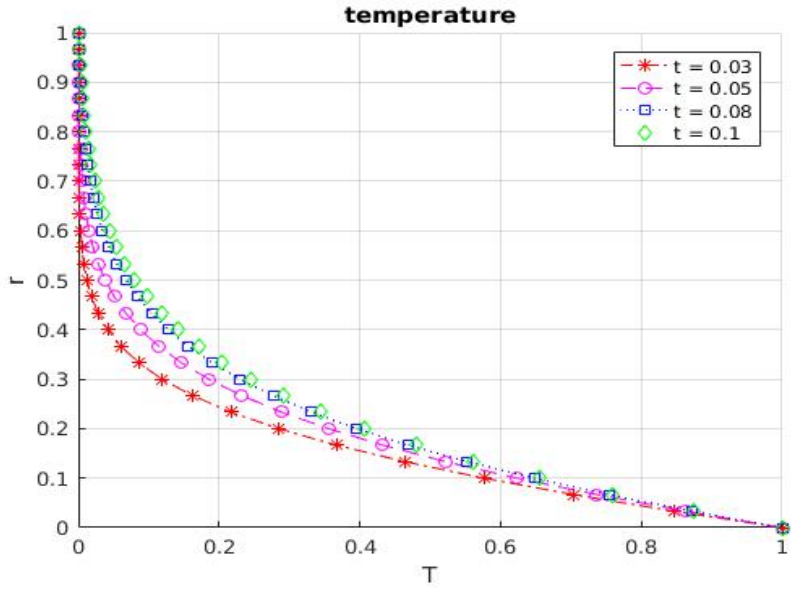

FIGURE 4.3: Temporal convergence Test 2 plot.

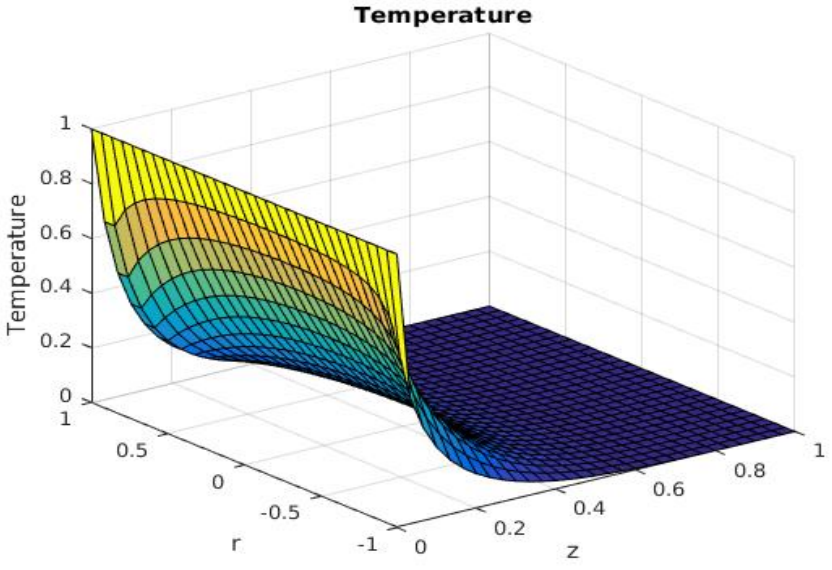

FIGURE 4.4: Temporal convergence Test 2 surface plot at t = 0.05.

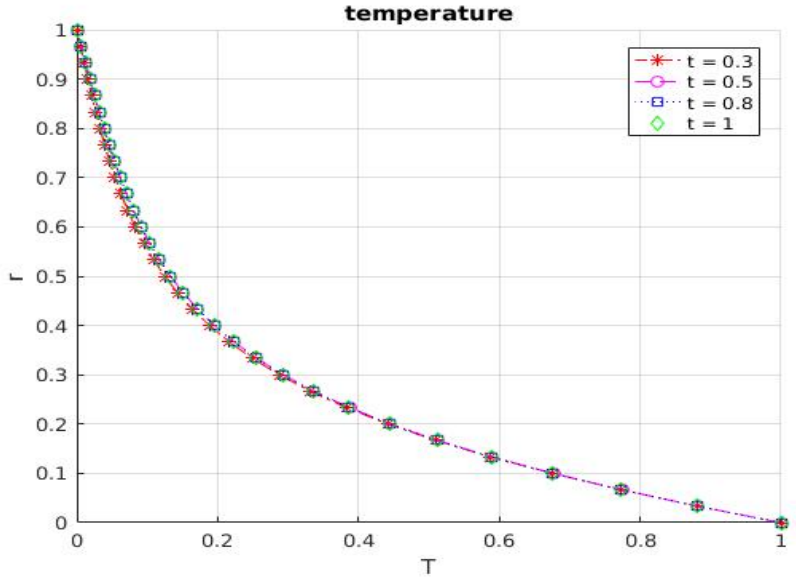

FIGURE 4.5: Temporal convergence Test 3 plot.

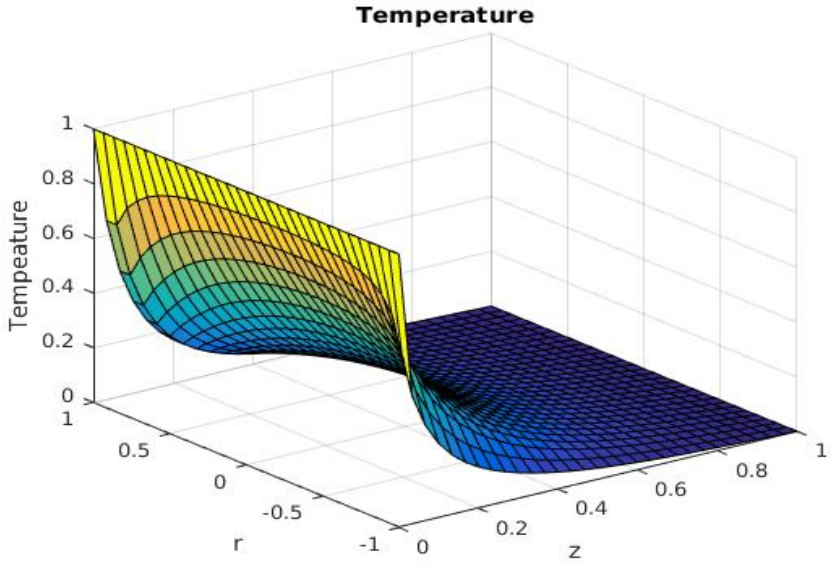

FIGURE 4.6: Temporal convergence Test 3 surface plot at t = 0.3.

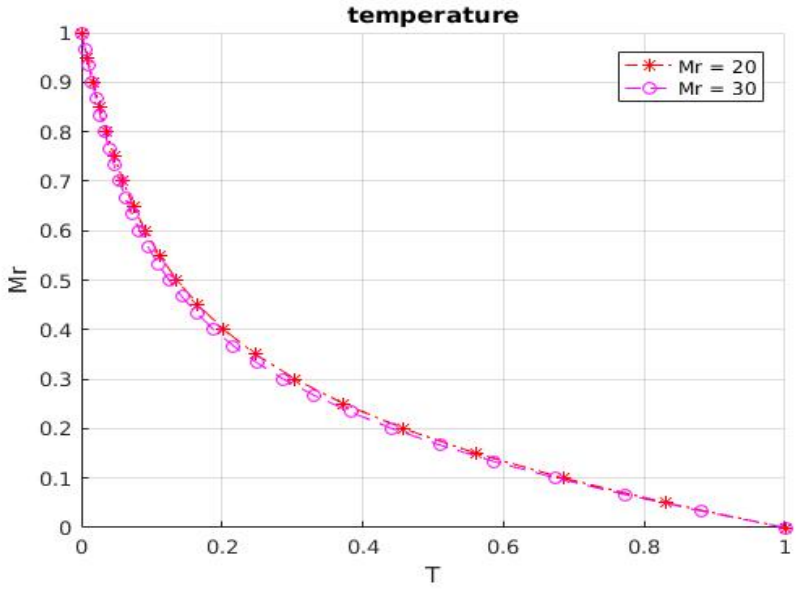

FIGURE 4.7: Mesh convergence Test 1 plot.

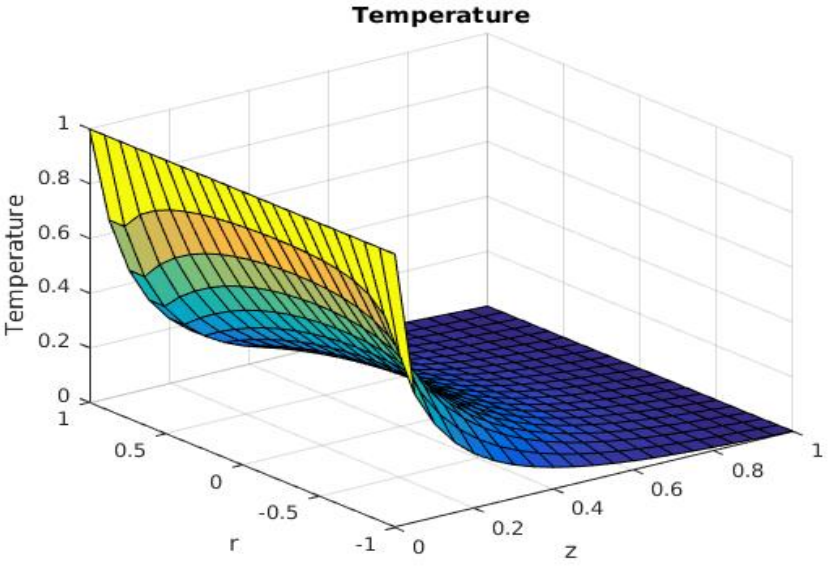

FIGURE 4.8: 20x20 Mesh surface plot.

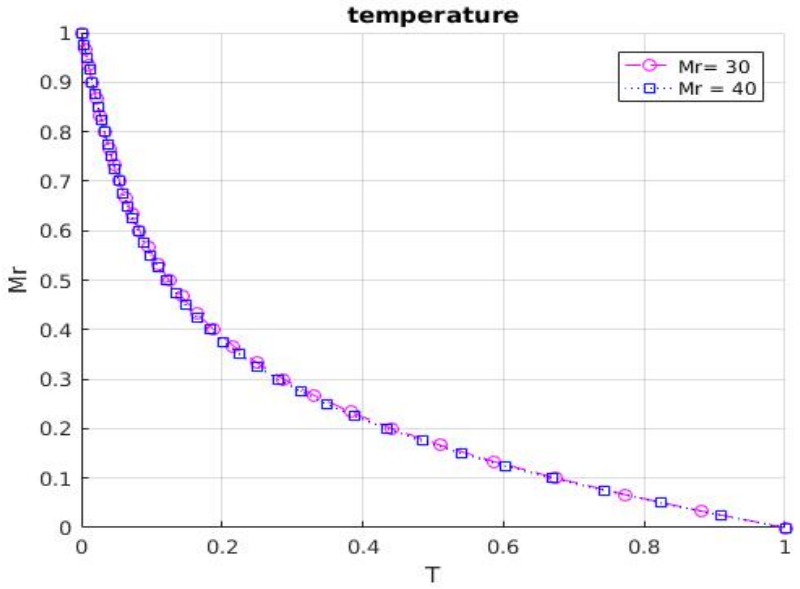

FIGURE 4.9: Mesh convergence Test 2 plot.

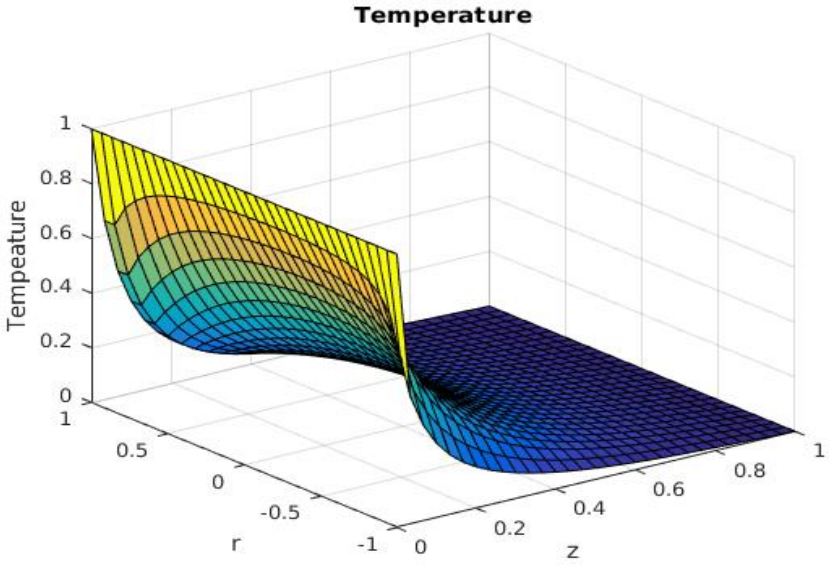

FIGURE 4.10: 30x30 Mesh surface plot.

Chapter 5

Results and Discussion

In this chapter, graphical results from numerical simulations of the research problem are discussed and interpreted both quantitatively and qualitatively with respect to dimensionless parameters that are involved in the problem. The correlation between the parameters and flow quantities is described based on the computational results and theoretical literature. Furthermore, for both core fluid and shell fluid regions the computational analysis is carried out using a 30x30 mesh grid and at t = 0.3. Unless otherwise specified the following parameter list is used for simulations:

- **core fluid**:

$$\begin{aligned} \alpha_c = 1, \quad G_c = 1, \quad \delta_{c_2} = 0.3, \quad \delta_{c_3} = 0.15, \quad De_c = 4, \quad Pr_c = 0.8, \\ Re_c = 0.9, \quad \beta = 0.6, \quad \gamma = 0.6, \quad \varepsilon_{\lambda c} = 0.1, \quad \varepsilon_{\eta_c} = 0.1, \quad dt = 0.0001. \end{aligned}$$

- **shell fluid**:

$$\begin{aligned} \alpha_s = 1, \quad G_s = 1, \quad \delta_{s_2} = 0.2, \quad \delta_{s_3} = 0.08, \quad De_s = 4, \quad Pr_s = 0.8, \\ Re_s = 150, \quad \beta = 0.6, \quad \gamma = 0.6, \quad \varepsilon_{\lambda s} = 0.1, \quad \varepsilon_{\eta_s} = 0.1, \quad dt = 0.0001. \end{aligned}$$

5.1 Simulation test for core fluid

5.1.1 Initial conditions

The plots presented in figure 5.1, depict the dimensionless basic velocities which correspond to the initial velocity condition represented by equations (2.46) and (2.23) in chapter 2 for the shell fluid and core fluid respectively. The profile is parabolic since the fluid flow is through a pipe furthermore the fluids are traversing through their respective pipes under a counter flow configuration. In figures 5.2 and 5.3 the core fluid initial velocity and pressure surface plots are shown. The initial condition for stress is taken as zero as depicted in figures 5.4 -5.6.

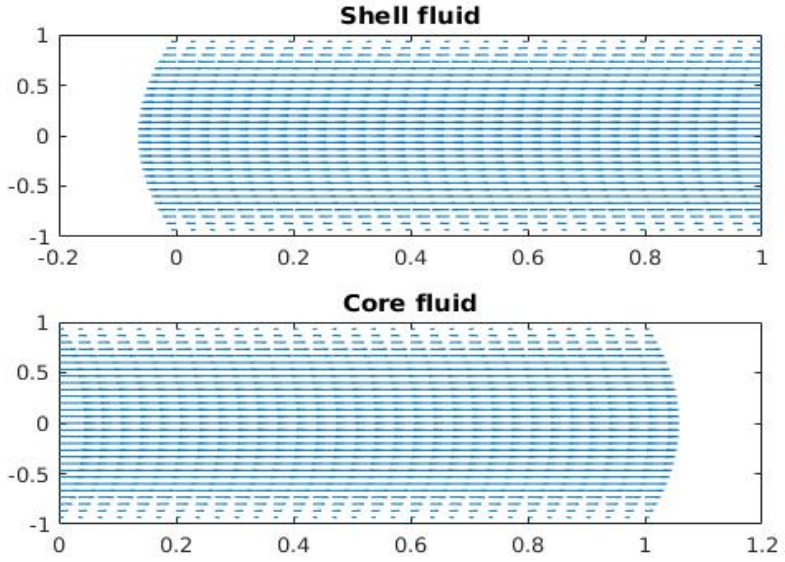

FIGURE 5.1: Initial velocity vector plot with a counter flow arrangement.

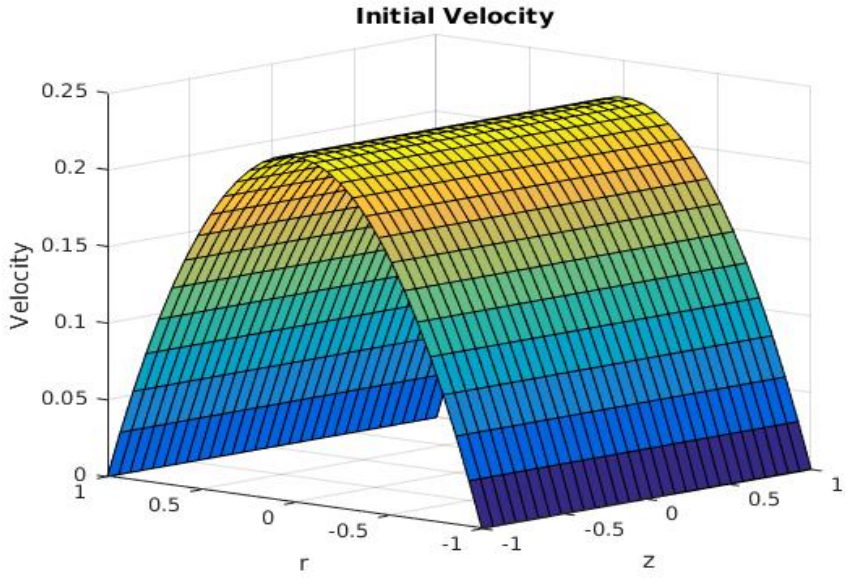

FIGURE 5.2: Core fluid initial velocity surface plot.

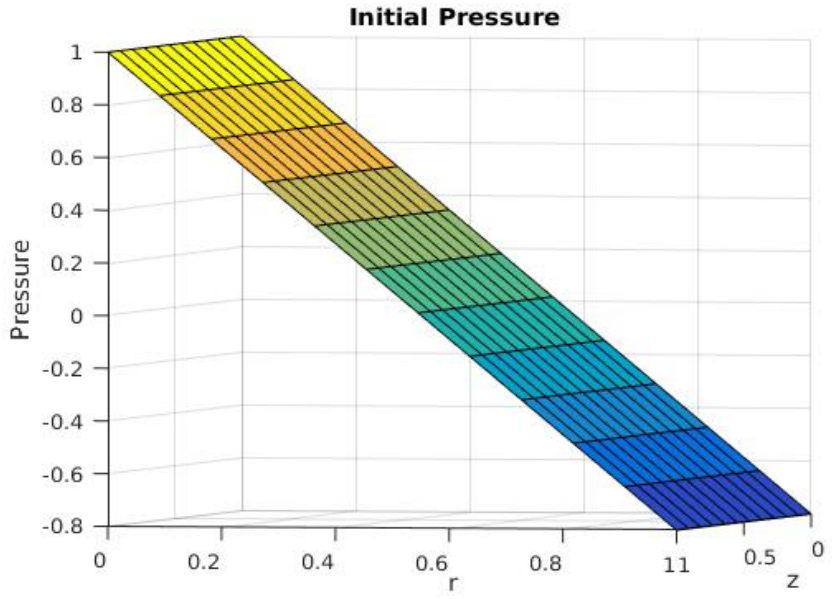

FIGURE 5.3: Core fluid initial pressure surface plot.

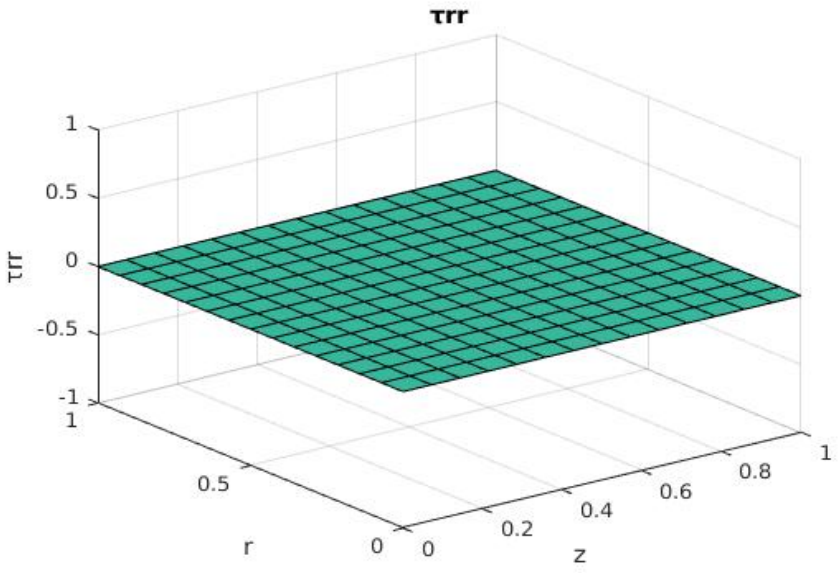

FIGURE 5.4: τ_{rr} initial condition plot.

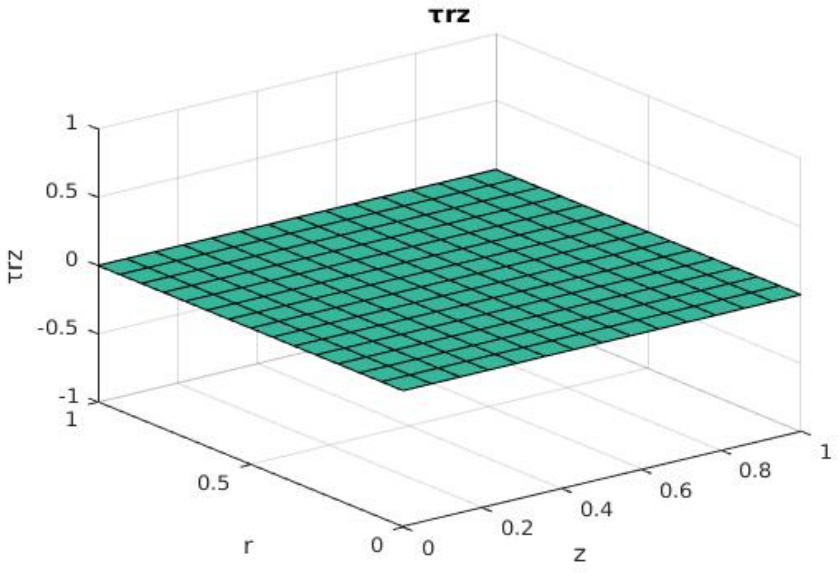

FIGURE 5.5: τ_{rz} initial condition plot.

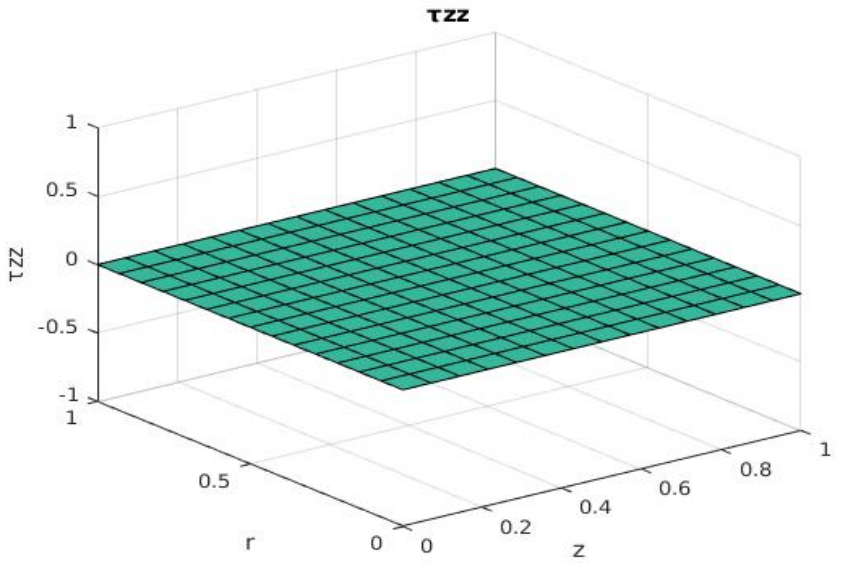

FIGURE 5.6: τ_{zz} initial condition plot.

5.2 Core fluid results

5.2.1 Isothermal case

In an isothermal case, temperature is zero and that is illustrated in figure 5.7. The relaxation time and viscosity which are temperature dependent and are mathematically described as follows,

$$\bar{\lambda} = (1 - \delta_\lambda) + \delta_\lambda \frac{1 + \xi}{1 + \xi T} \exp(-\varepsilon_\lambda T),$$
$$\mu(T^*) = \exp(-\varepsilon_\eta T),$$

respectively. At a zero temperature, both these quantities remain constant at value one as shown in figure 5.8 and 5.9.

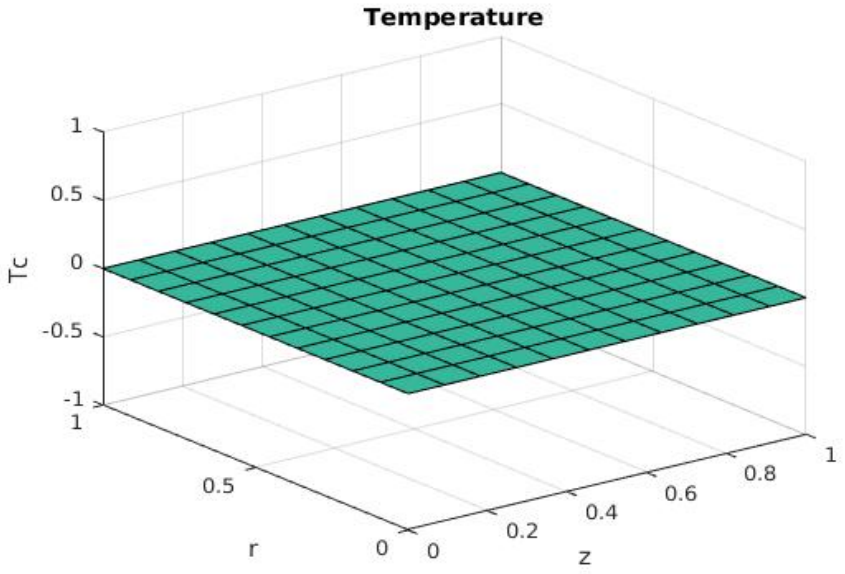

FIGURE 5.7: Temperature plot.

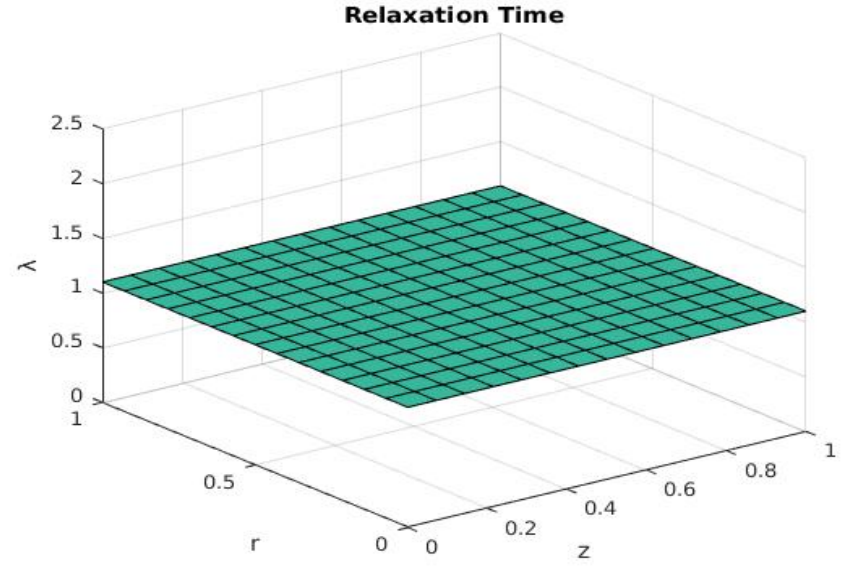

FIGURE 5.8: Relaxation time plot.

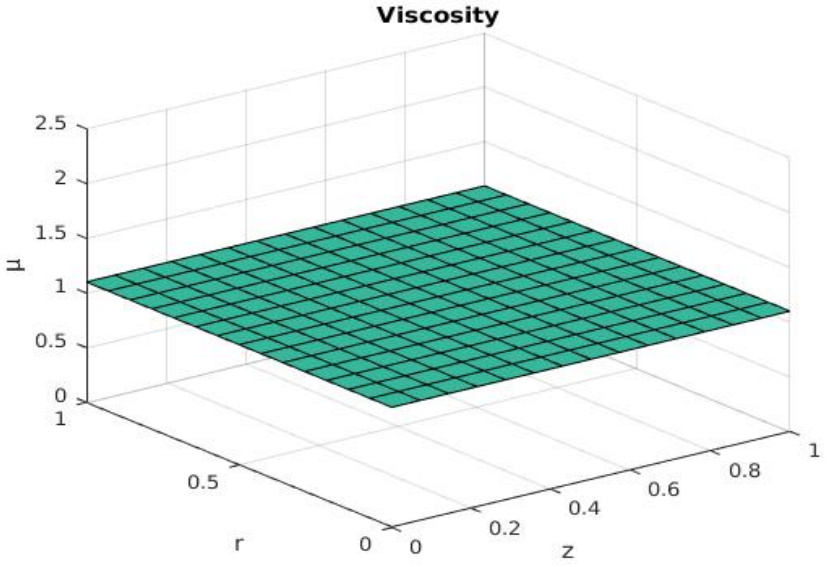

FIGURE 5.9: Viscosity plot.

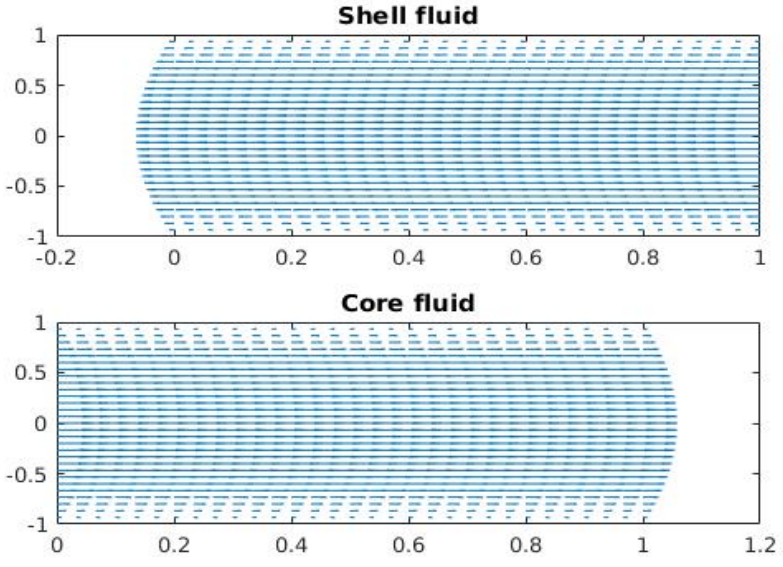

FIGURE 5.10: Vector Plots.

5.2.2 Non-isothermal case

The following results were obtained using the semi-implicit technique integrated with the Crank-Nicolson Scheme. The SIMPLE algorithm was employed for pressure-velocity decoupling in the momentum equations and the convective terms were handled using the upwind scheme. The above stated parameter list is used unless otherwise stated.

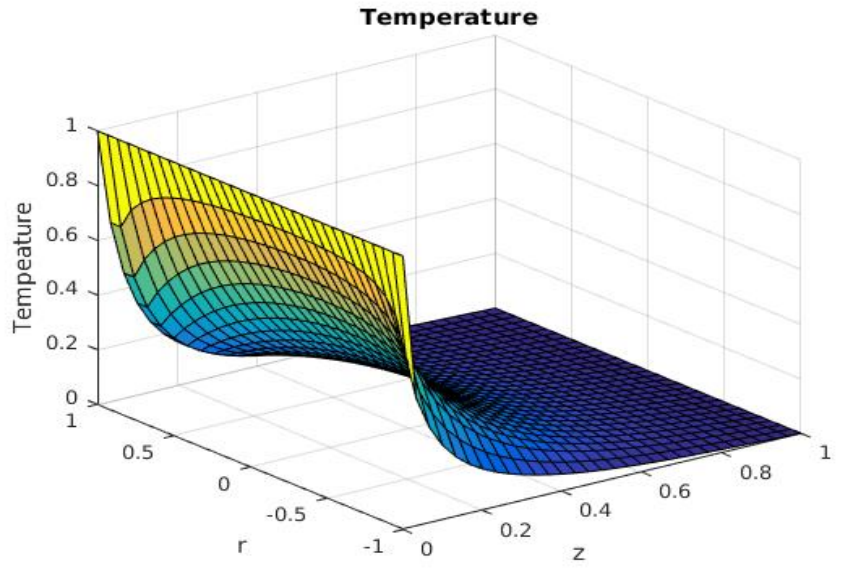

FIGURE 5.11: Core fluid temperature surface plot .

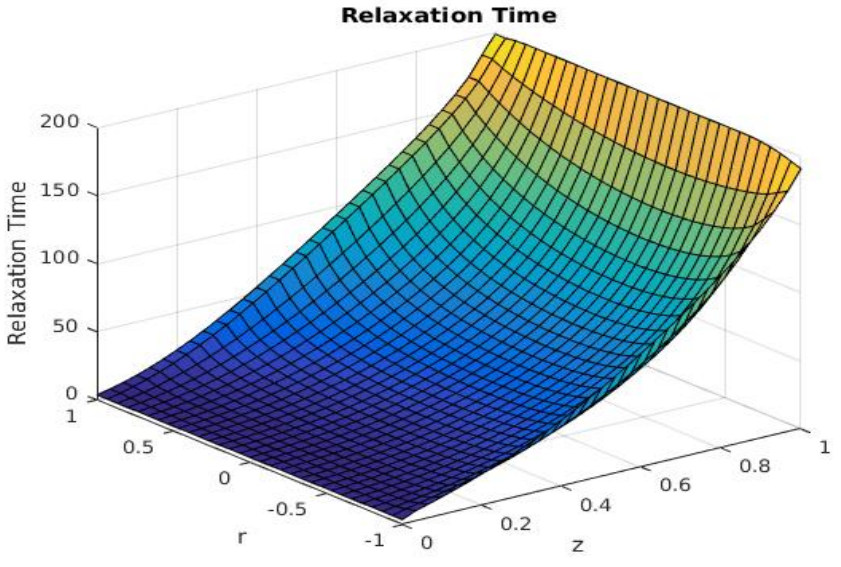

FIGURE 5.12: Relaxation time surface plot.

As the core fluid traverses through the pipe from the inlet channel to the outlet channel it looses its thermal heat hence the temperature decline. This is as a result of the convective heat transfer process and that is shown in figure 5.11.

In figure 5.12 the inverse relationship between relaxation time and temperature is illustrated.

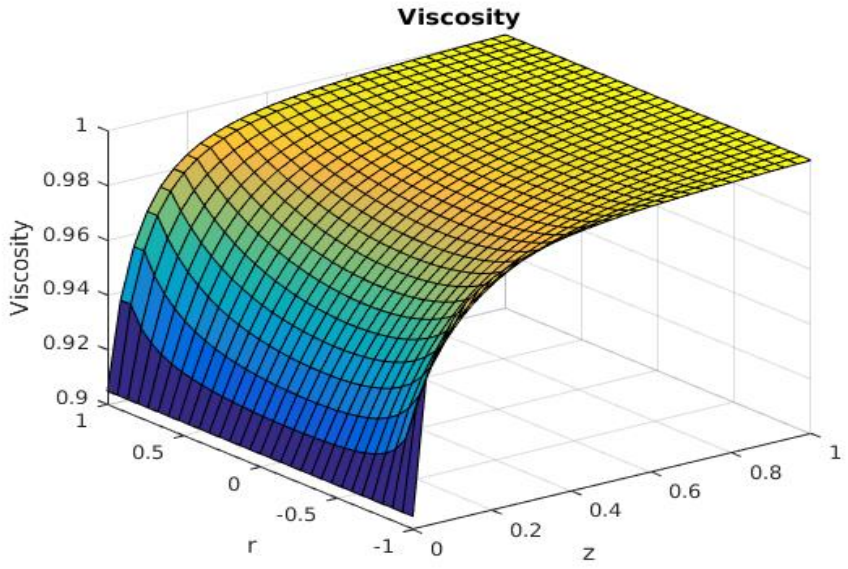

FIGURE 5.13: Viscosity surface plot.

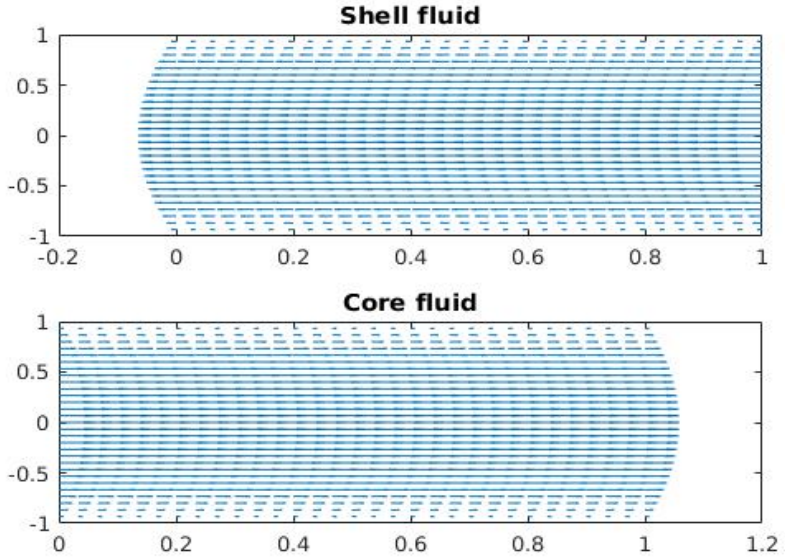

FIGURE 5.14: Vector Plots.

An inverse relationship between viscosity and temperature is illustrated in figure 5.13. As temperature decreases when the fluid is moving downstream through the pipe, viscosity on the other hand increases. Figure 5.14 illustrates the velocity vector plot. It is noticed that the parabolic profile is still preserved.

5.2.3 Parameter dependence of temperature

In figures 5.15 - 5.21, we examine the effects of Prandtl and Reynolds numbers. An increase in Prandtl number correlates with an increase in the fluid viscosity and as a result the thermal conductivity decreases. It is observed that as the Prandtl number increases, temperature decreases significantly. On the other hand, the Reynolds number describes the ratio of inertia forces to viscosity. So as the Reynolds number increases, viscosity deceases and thus velocity increases.

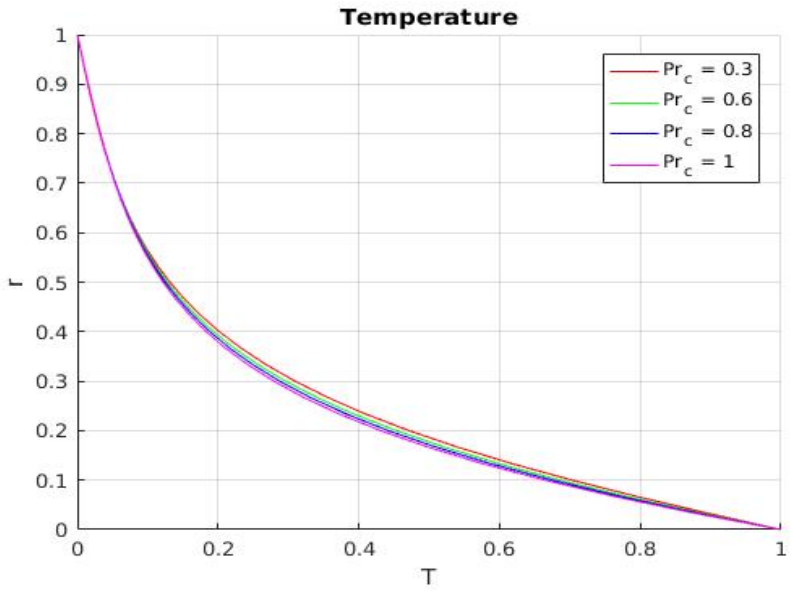

FIGURE 5.15: Prandtl vs Temperature at Re = 0.9 plot.

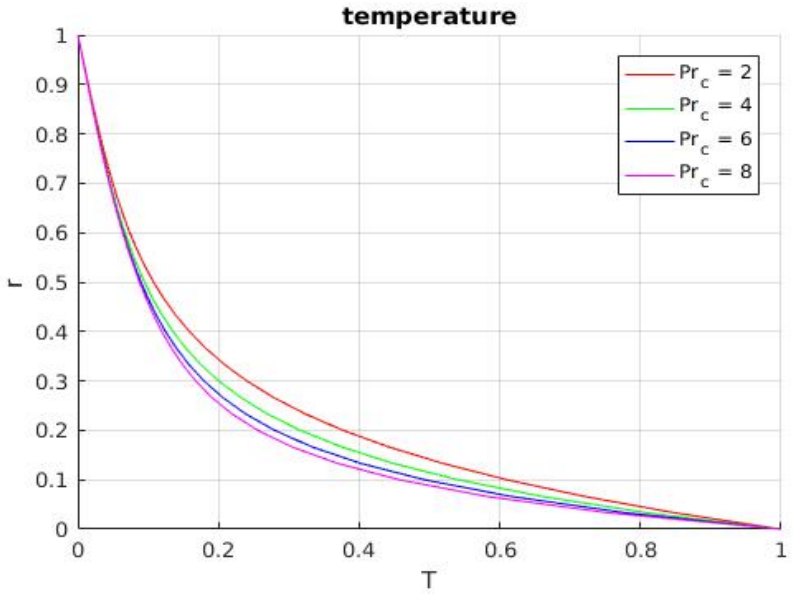

FIGURE 5.16: Prandtl vs Temperature at Re = 1 plot.

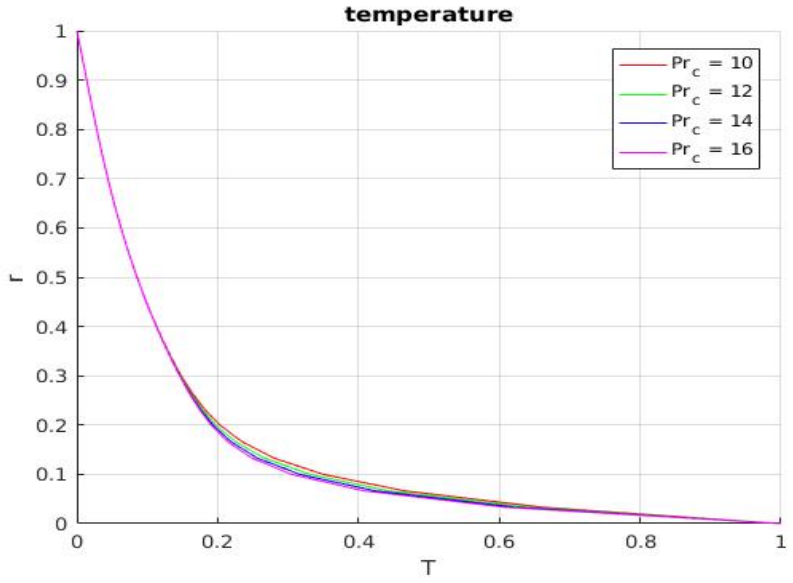

FIGURE 5.17: Prandtl vs Temperature at Re = 2 plot.

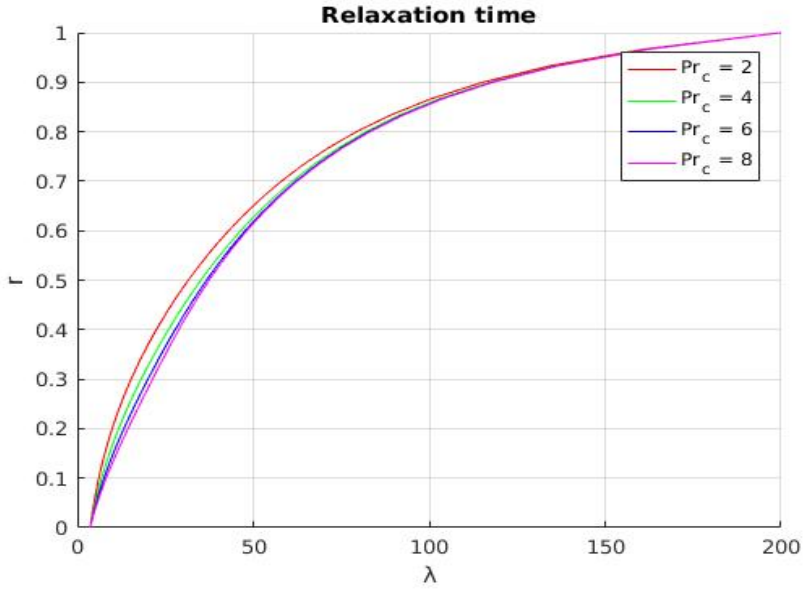

FIGURE 5.18: Prandtl vs Relaxation time at various values of Re plot.

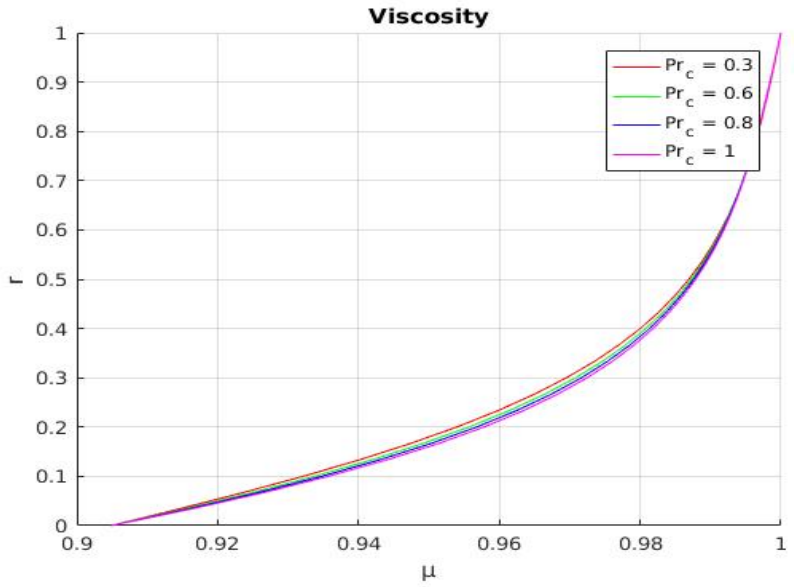

FIGURE 5.19: Prandtl vs Viscosity at Re = 0.9 plot.

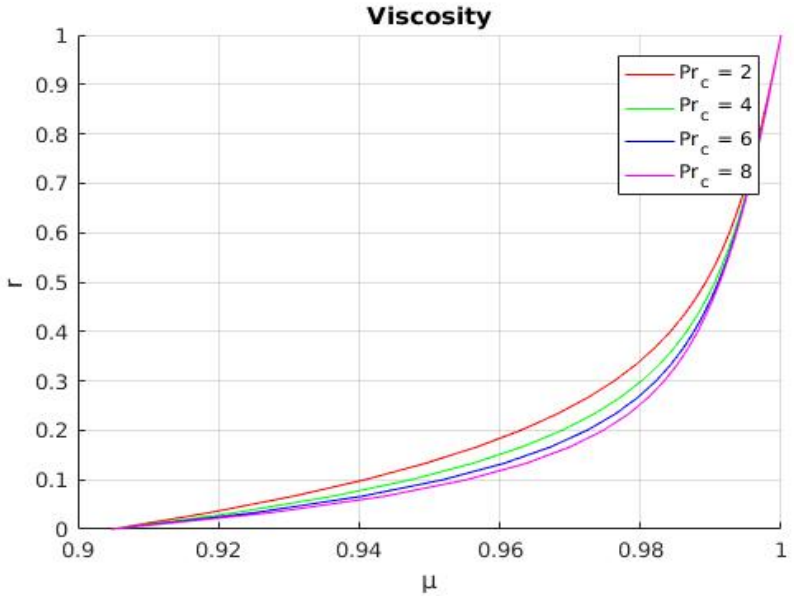

FIGURE 5.20: Prandtl vs Viscosity at Re = 1 plot.

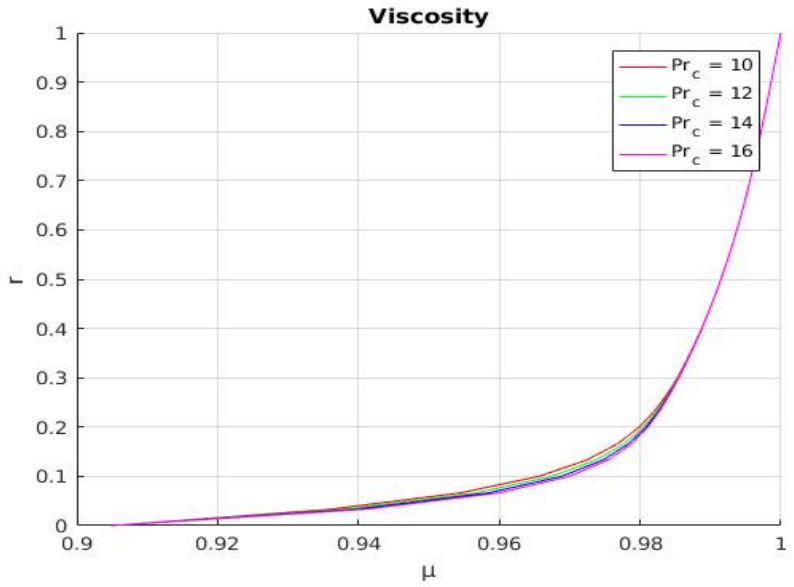

FIGURE 5.21: Prandtl vs Viscosity at Re = 2 plot.

At high values of the Deborah number viscosity dominates and at low Deborah numbers the elasticity is more pronounced. Due to an inverse relationship between viscosity and temperature, at slightly high values of the Deborah number, 0.5 to 1, on figure 5.22 the fluid is more viscous and hence the slight decrease in temperature. At a lower Deborah number, an increase in temperature is observed.

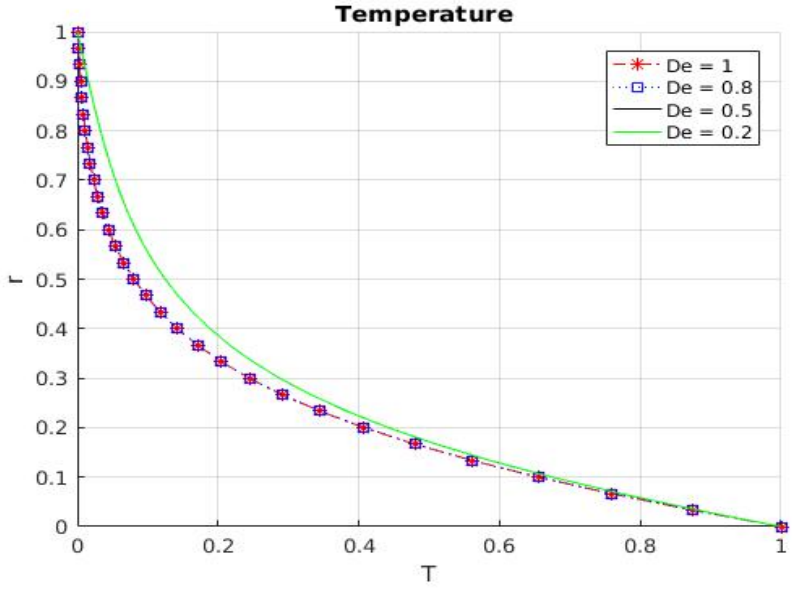

FIGURE 5.22: Effects of the Deborah number on temperature.

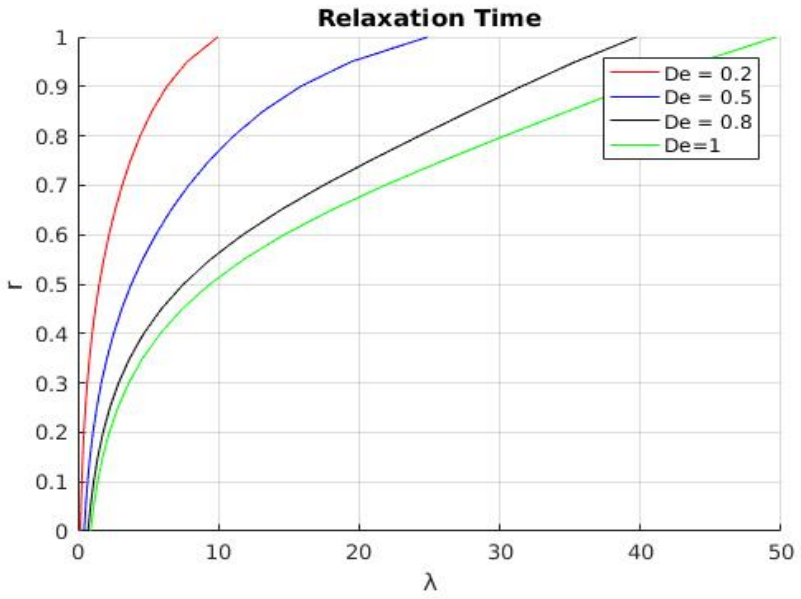

FIGURE 5.23: Effects of the Deborah number on Relaxation time.

Deborah number is the ratio of relaxation time of a material to the characteristic time. Figure 5.23 illustrates the direct proportionality relationship between relaxation time and Deborah number. The relaxation time increases as the Deborah number increases.

5.3 Shell fluid results

The cold shell fluid is solved without applying the SIMPLE algorithm. The fluid moves from right to left due to a positive pressure gradient which is shown in figure 5.26. The parabolic initial velocity which relates to the dimensionless basic velocity is given by equation (2.46) is graphically represented by figures 5.25. Unless otherwise stated, the parameter list presented above will be used to run the simulations. Similar results were obtained when a non-Newtonian shell fluid was considered.

5.3.1 Initial conditions

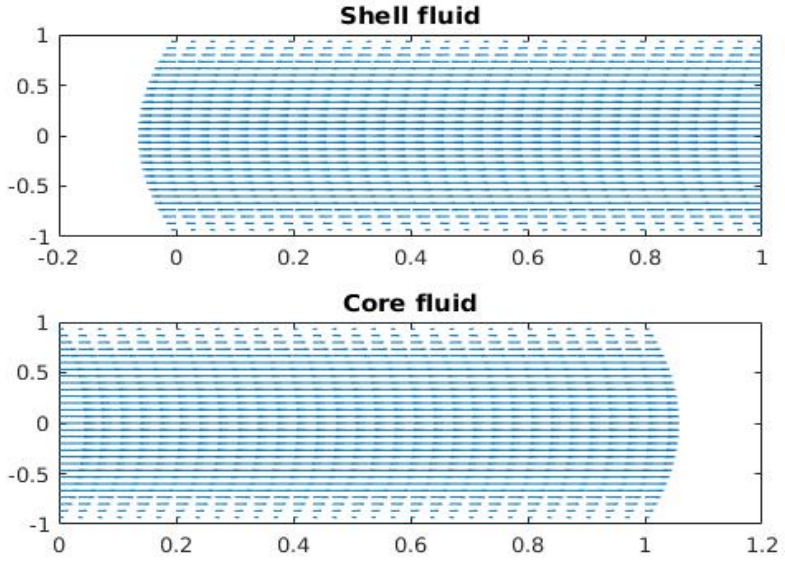

FIGURE 5.24: Initial velocity vector plot with a counter flow arrangement.

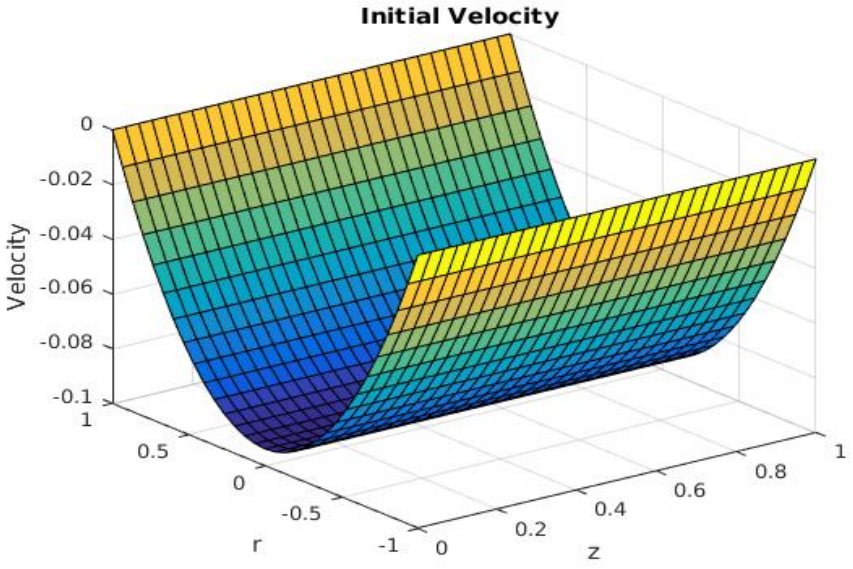

FIGURE 5.25: Shell fluid initial velocity surface plot.

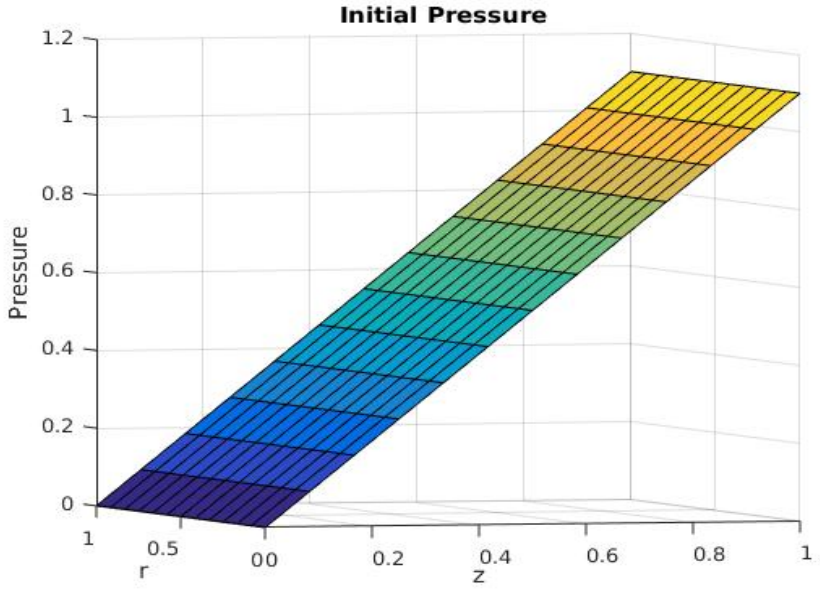

FIGURE 5.26: Shell fluid initial pressure surface plot.

5.3.2 Results at t = 0.3

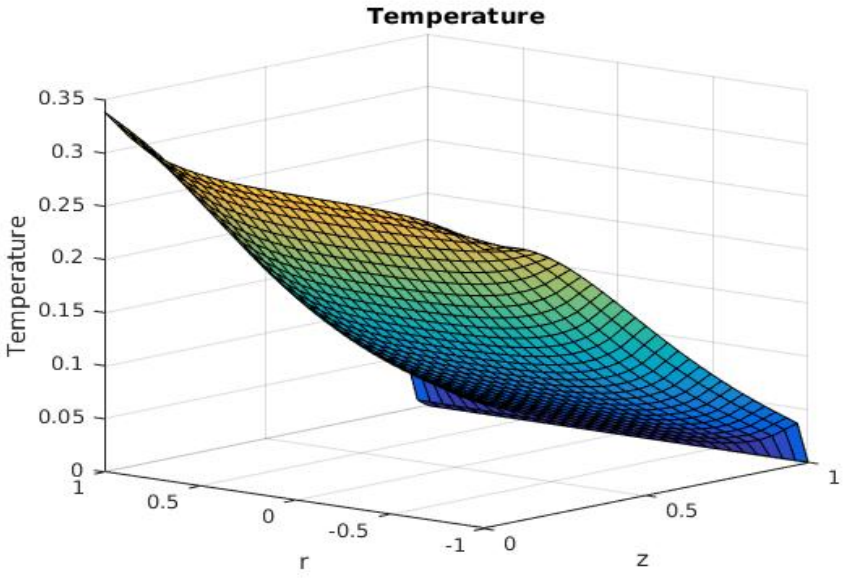

FIGURE 5.27: Shell fluid temperature surface plot.

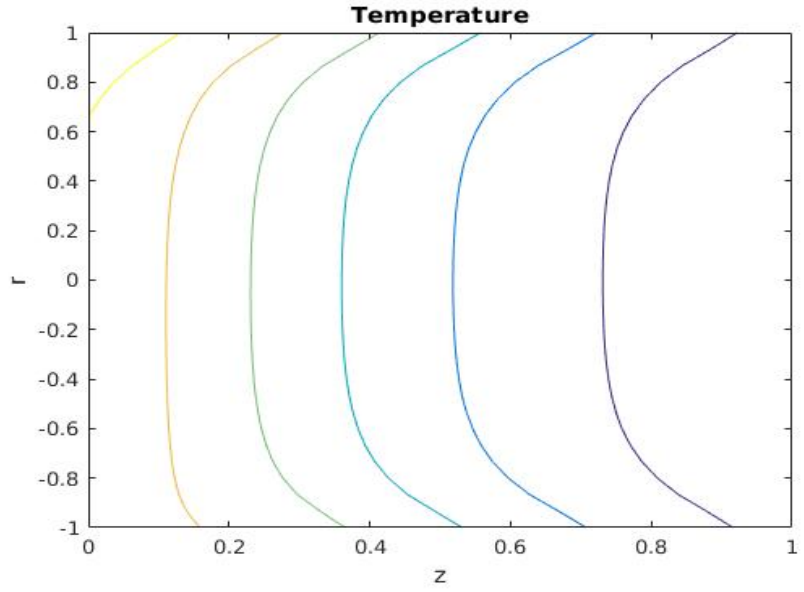

FIGURE 5.28: Shell fluid temperature contour plot.

In figures 5.27 - 5.28 an temperature increase in the Newtonian shell fluid which in the outer annulus of the double pipe heat exchanger is illustrated. The increase in temperature is observed to occur as the fluid traverses from the cold inlet channel to a warm outlet channel of the pipe.

Figures 5.29 and 5.30 show the velocity and pressure profiles of the shell fluid flow observed after a period of time, i.e, t = 0.3 respectively. The velocity and pressure profiles for both physical quantities remained unchanged as the fluid traversed through the pipe.

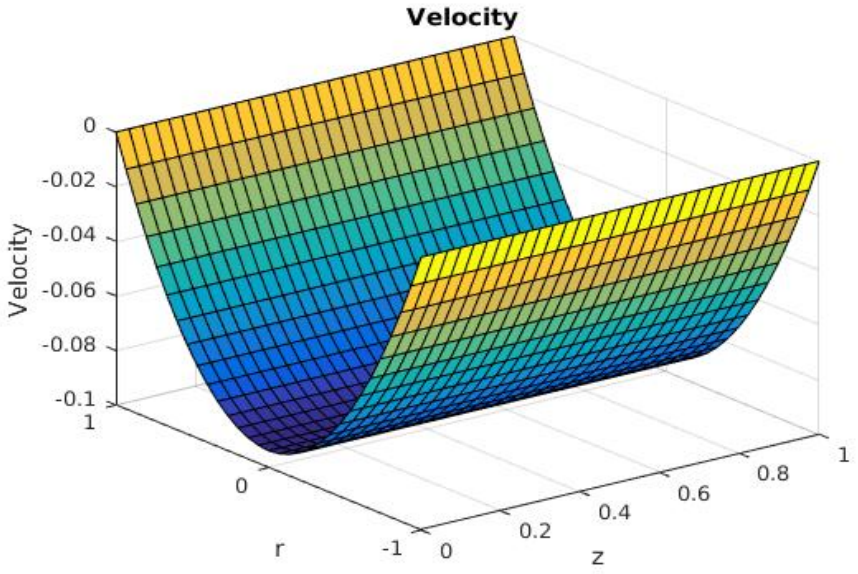

FIGURE 5.29: Shell fluid velocity at t = 0.3 plot.

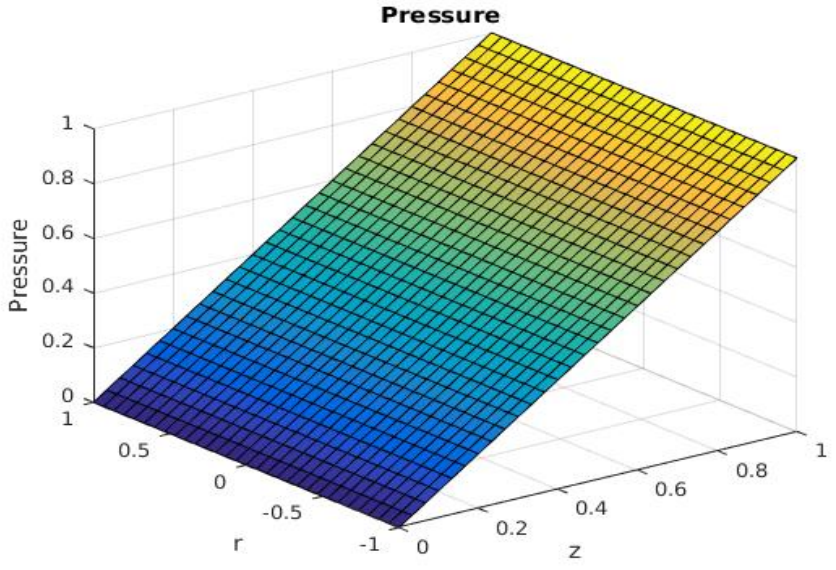

FIGURE 5.30: Shell fluid pressure at t = 0.3 plot.

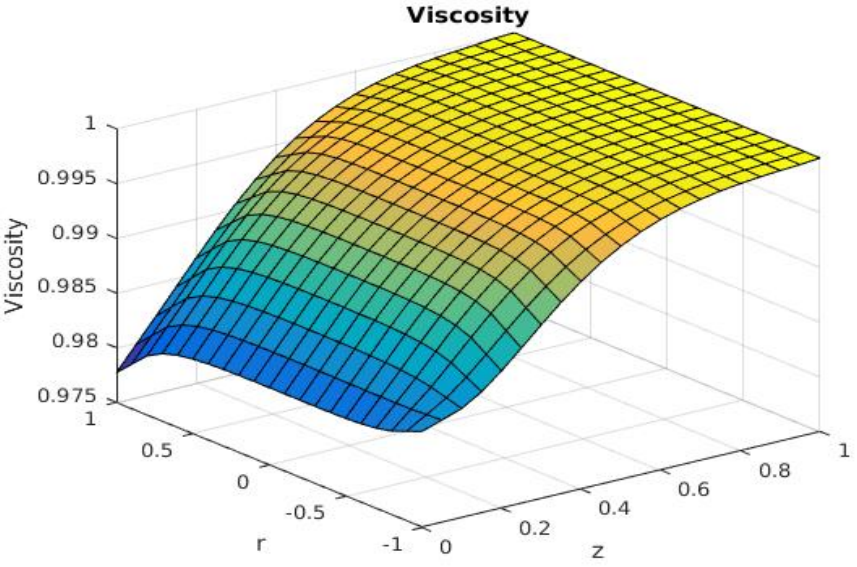

FIGURE 5.31: Shell fluid viscosity surface plot.

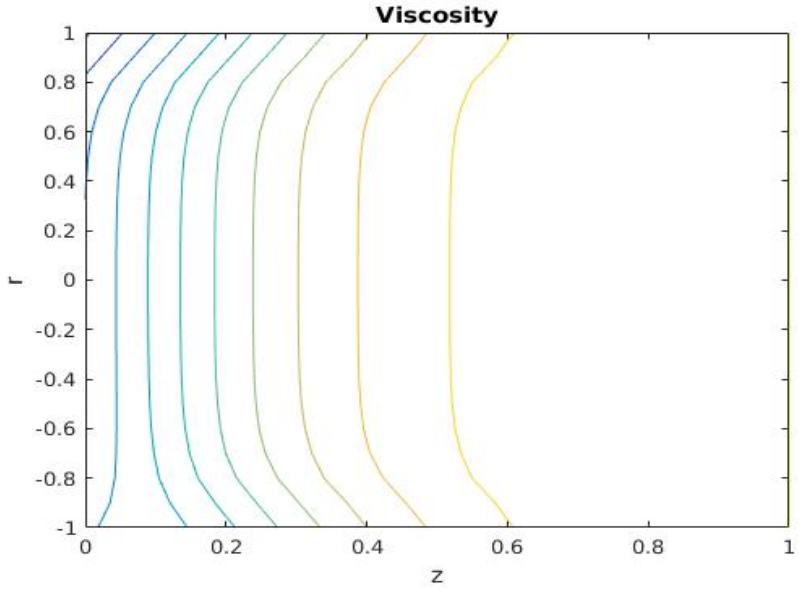

FIGURE 5.32: Shell fluid viscosity contour plot.

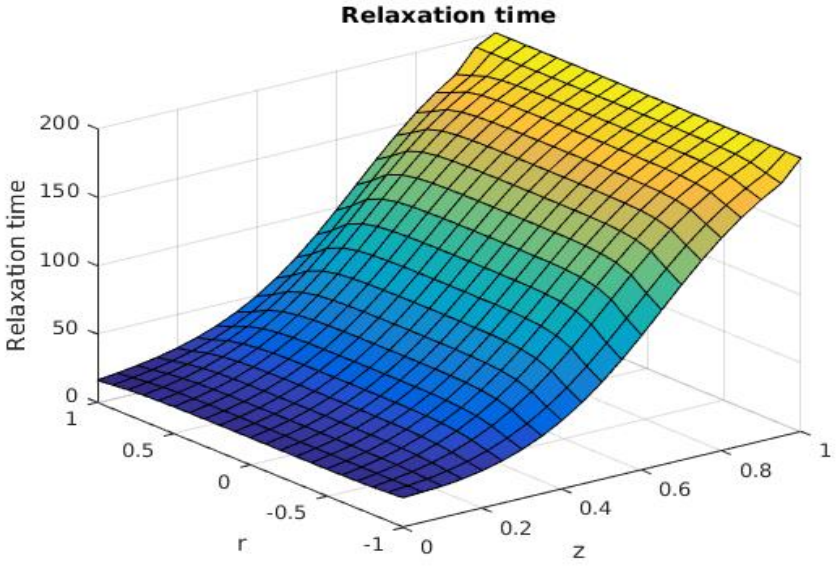

FIGURE 5.33: Shell fluid relaxation time surface plot.

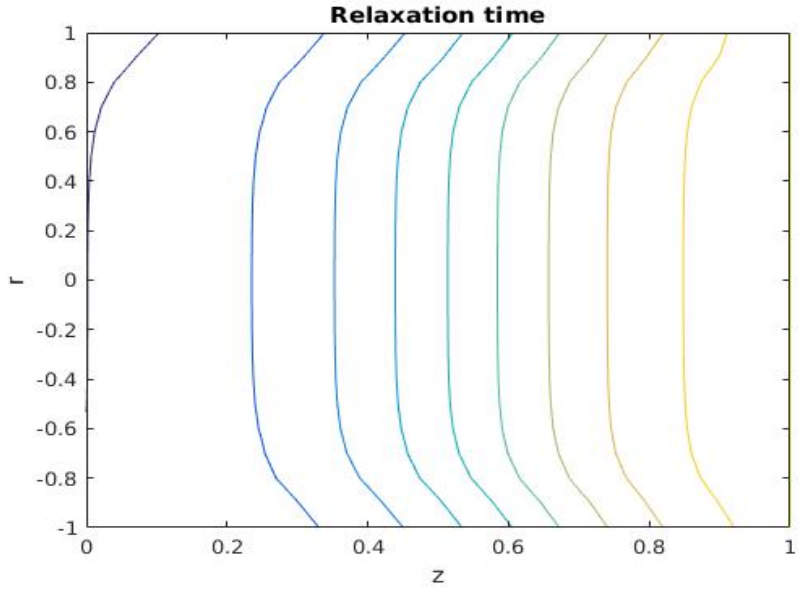

FIGURE 5.34: Shell fluid relaxation time contour plot.

5.3.3 Parallel flow and Counter flow arrangements comparison plots with respect to core fluid

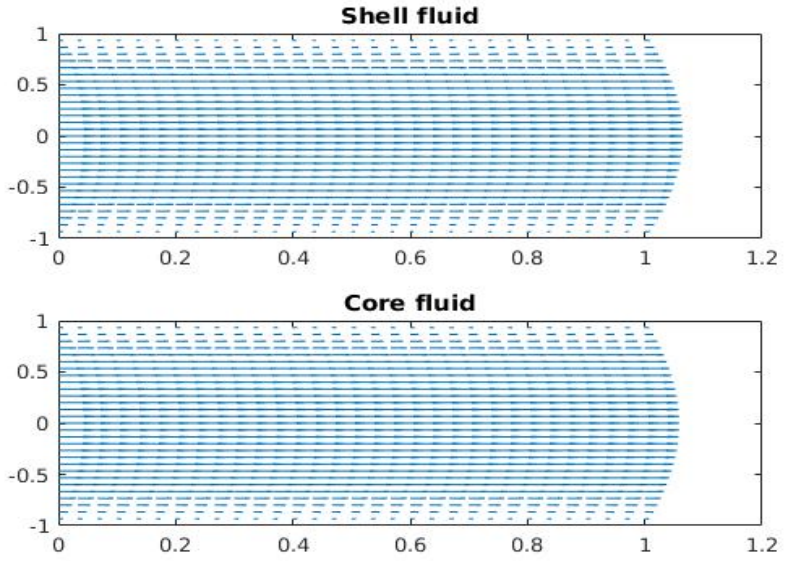

FIGURE 5.35: Parallel flow arrangement plot.

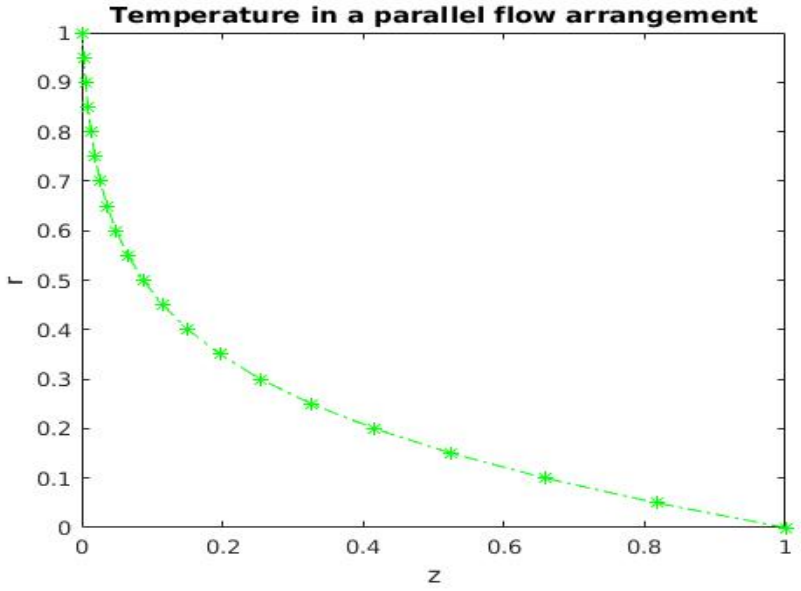

FIGURE 5.36: Parallel flow arrangement Temperature plot.

In figure 5.36 the maximum outlet temperature of the core fluid as it was flowing through the pipe is 0.0027072.

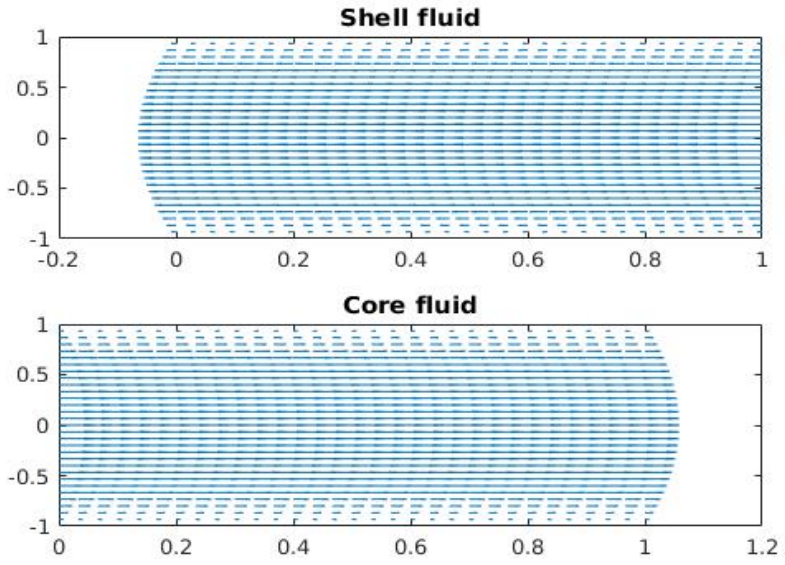

FIGURE 5.37: Counter flow arrangements plot.

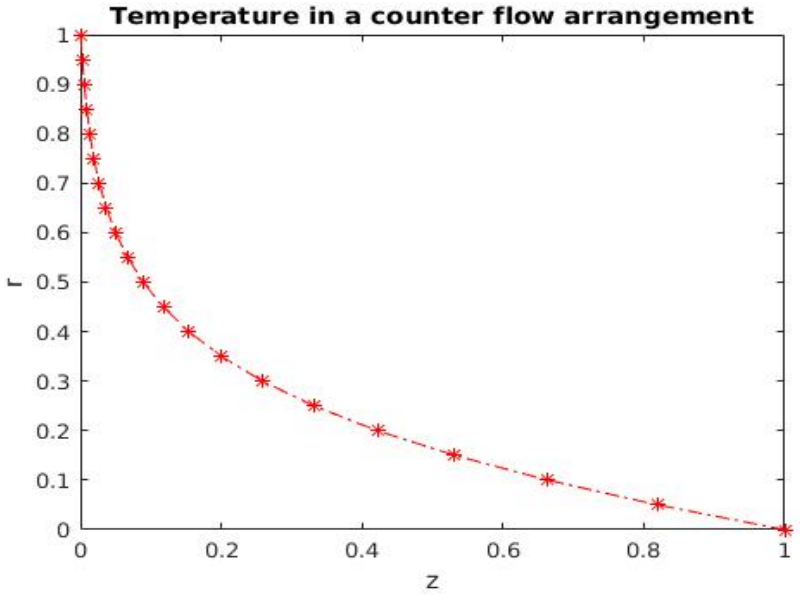

FIGURE 5.38: Counter flow arrangement core temperature plot .

In figure 5.38 the maximum outlet temperature of the core fluid as it was flowing through the pipe is 0.0027683

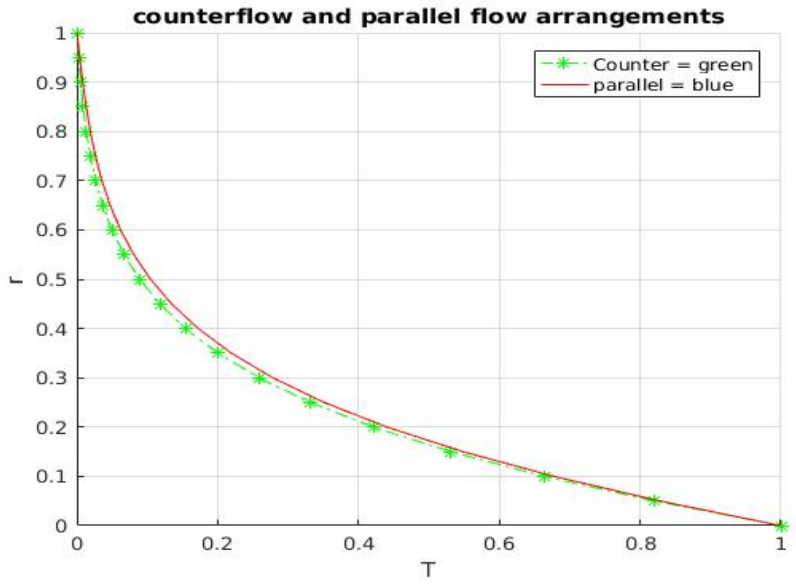

FIGURE 5.39: Parallel flow and Counter flow arrangements results plots.

Figure 5.39 a combination of plots 5.36 and 5.38, illustrates the difference in thermal heat transfer by convection between the counter flow and parallel flow configurations in the double pipe heat exchanger using core fluid as a case study. Simulation results as depicted in the figure show that the counterflow arrangement is more thermodynamically optimal as compared to the parallel flow set-up.

It was observed that the maximum outlet core temperature and average outlet core temperature obtained in the counter flow arrangement was 0.0027683 and 0.0021801 respectively. In the parallel flow set-up 0.0027072 and 0.0022317 were obtained respectively.

Furthermore in the shell fluid region, the maximum outlet core temperature and average outlet core temperature obtained in counterflow arrangement was 0.001669 and 0.00076989 respectively In the parallel flow set-up it was 0.0014836 and 0.00068236 respectively.

The graphical results were obtained when a non-Newtonian shell fluid was considered.

Chapter 6

Conclusion

In this concluding chapter, a summary of aims and objectives presented at the beginning of this research project is given.

6.1 Main objective

The main objective of this study was to computationally analyse the behaviour of a pressure driven viscoelastic fluid in a double pipe heat exchanger geometry. This study has significant industrial applications for both viscoelastic fluids and heat exchangers and these were explored extensively in the introductory chapter. The investigations were carried out by analysing the convective heat transfer from the core viscoelastic fluid to the Newtonian or non-Newtonian shell fluid flowing in the outer annulus of the heat exchanger. Furthermore the effects of several physical quantities on the temperature of the fluids were examined.

6.2 Computational Methods

The problem presented was mathematically modelled using complex, non-linear partial differential equations and the extra-stress equations were modelled using the non-isothermal Giesekus model. In chapter one, various methods which could be used to solve these type of equations were discussed. However in this study these equations were solved using the semi-implicit finite difference method which was found to be numerically unconditionally stable and efficient. That is due to its ability to combine the stability of an implicit method with the accuracy of a method that is second order in both space and time. Furthermore, the implementation of the Crank-Nicolson scheme on implicit terms increased stability. The SIMPLE algorithm was used to decoupled pressure-velocity components in the momentum equations. The algorithm was tested

for both spacial and temporal convergence. In terms of the treatment the convective terms using the upwind scheme, it was observed that in both the cases when it was not employed and employed, there were no significant changes in numerical results, they remained stable.

6.3 Parameter analysis

In the parameter analysis, it was observed that increase in both the Reynolds and Prandtl number resulted in a decrease in temperature in the viscoelastic core fluid region and as a consequence the Newtonian shell fluid in the outer annuls attained higher temperatures. However the Reynolds number was observed to have an inverse relationship with viscosity but a direct relationship with velocity and this had an influence on the temperature values attained in both the core fluid and shell fluid regions. Our results also showed an inverse relation between temperature and the Deborah number. This was directly related to the values of the Deborah number which had either an elastic or viscous effect on the fluid.

6.4 Simulation results

In terms of simulation results, we first considered an isothermal case and the results obtained agreed with those in literature. When a non-isothermal case was considered between a hot core viscoelastic fluid and a cold shell Newtonian or non-Newtonian fluid, it was observed that the core fluid reached lower temperatures than the shell fluid which had slightly higher temperature values as a result of the heat exchange. The influence of the heat exchanger flow arrangements which had an effect on the temperature differences between the two fluids were also considered. As expected the counter flow configuration was more thermodynamically optimal than the parallel flow configuration. These results match with those in previous work done by T. Chinyoka [3]. In closing, this project can serve as a foundation for future work which can be undertaken by using the Finite Volume Method integrated with various computational techniques.

Bibliography

[1] A.R. Khan-K.N Ahmad M.M.A. Bhutta N. Hayat, M.H. Bashir and S. Khan. Cfd applications in various heat exchangers design: A review. *Applied Thermal Engineering*, 32:1-12., 2012.

[2] R.K. Shah and D.P. Sekulic. Fundamentals of heat exchanger design (1st edition). *John Wiley & Sons*, 2003.

[3] T.Chinyoka. Viscoelastic effects in double-pipe single-pass counterflow heat exchangers. *International Journal for Numerical Methods in Fluids*, 59:677-690., 2008.

[4] J.M. Nóbrega I.M. Afonso L.F. Melo C.S. Fernandes, R.P. Dias and J.M. Maia. Thermal behaviour of stirred yoghurt during cooling in plate heat exchangers. *Journal of Food Engineering*, 76(3):433-439., 2005.

[5] T. Perrotin and D. Clodic. Thermal-hydraulic cfd study in louvered fin-and-flat-tube heat exchangers. *International Journal of Refrigeration*, 27(4):422-432., 2004.

[6] T. Chinyoka. Modeling of cross-flow heat exchangers with viscoelastic fluids. *NonlinearAnalysis:Real World Applications*, 10(6):3353-3359., 2009.

[7] B. Xia and Da-Wen Sun. Applications of computational fluid dynamics (cfd) in the food industry: a review. *Computers and Electronics in Agriculture*, 34:5-24., 2002.

[8] T. Hämäläinen M. Lyytikäinen and J. Hämäläinen. A fast modelling tool for plate heat exchangers based on depth-averaged equations. *International Journal of Heat and Mass Transfer*, 52(56.):1132-1137., 2009.

[9] J.C. Mandal P.K. Vijayan J.S. Jayakumar, S.M. Mahajani and R. Bhoi. Experimental and cfd estimation of heat transfer in helically coiled heat exchangers. *Chemical Engineering Research and Design*, 86(3):421-232., 2008.

[10] A.A. Mouza A.G. Kanaris and S.V. Paras. Flow and heat transfer prediction in a corrugated plate heat exchanger using a cfd code. *Chemical & Engineering Technology*, 29(8):923-930., 2006.

[11] Shao-Jie Chen Guang-Ming Chen Xiao-Hong Han, Li-Qi Cui and Qin Wang. A numerical and experimental study of chevron, corrugated-plate heat exchangers. *International Communications in Heat and Mass Transfer*, 37:1008-1014., 2010.

[12] S.D. Joshi. Heat transfer in in-tube flow of non-newtonian fluids. phd. thesis. *Digital Repository @ Iowa State University, http://lib.dr.iastate.edu/*, 1978.

[13] I.E.Ireka and T.Chinyoka. Non-isothermal flow of a johnsonsegalman liquid in a lubricated pipe with wall slip. *Journal of Non-Newtonian Fluid Mechanics*, 192: 20-28., 2012.

[14] O.D. Makinde and T. Chinyoka. Numerical study of unsteady hydromagnetic generalized couette flow of a reactive third-grade fluid with asymmetric convective cooling. *Computers and Mathematics with Applications*, 61:1167-1179., 2011.

[15] V. Casulli and R.T. Cheng. Semi implicit finite difference methods for threedimensional shallow water flow. *International Journal for Numerical Methods in Fluids*, 106:629-648., 1992.

[16] Sagar Chouhan M. Devakar, K. Ramesh and Ankush Raje. Fully developed flow of non-newtonian fluids in a straight uniform square duct through porous medium. *Journal of the Association of Arab Universities for Basic and Applied Sciences*, 23: 66-74., 2016.

[17] A. Matta G. Nagaraju and P. Aparna. Fully developed flow of non-newtonian fluids in a straight uniform square duct through porous medium. *International Journal of Advances in Applied Mathematics and Mechanics*, 3(1):77-86., 2015.

[18] J.A. Cuminato M.F. Tomé, N. Mangiavacchi and S. McKee A. Castelo. A finite difference technique for simulating unsteady viscoelastic free surface flows. *Journal of Non-Newtonian Fluid Mechanics*, 106:61-106., 2002.

[19] SHI Zai-hong NIU Jun and TAN. Wen-chang. Numerical simulation of thermal convection of viscoelastic fluids in an open-top porous medium with constant heat flux. *Journal of Hydrodynamics, Ser. B*, 27(1):52-61., 2015.

[20] B.E. Launder and D.B. Spalding. The mathematical modelling of turbulent flows. *Journal of Applied Mathematics and Mechanics*, 53(6):424-424., 1972.

[21] S.V. Patankar. Heat and mass transfer in turbulent boundary layers, phd. thesis. *Imperial College, London University, UK*, 1976.

[22] A.K. Runchal D.B. Spalding A.D. Gosman, W.M. Pun and M. Wolfshtein. Heat and mass transfer in recirculating flows. *International Journal of Heat and Mass Transfer*, 13(9):1509-1510., 1970.

[23] L. Mangani F. Moukalled and M. Darwish. The finite volume method in computational fluid dynamics. an advanced introduction with openfoam and matlab. *Springer*, 2015.

[24] J.A.M. Kuipers E.A.J.F. Peters S. De, S. Das and J.T. Padding. A coupled finite volume immersed boundary method for simulating 3d viscoelastic flows in complex geometries. *Journal of Non-Newtonian Fluid Mechanics*, 232:67-76., 2016.

[25] N. Phan-Thien S.-C. Xue and R.I. Tanner. Numerical study of secondary flows of viscoelastic fluid in straight pipes by an implicit finite volume method. *Journal of Non-Newtonian Fluid Mechanics*, 59:191-213., 1995.

[26] B. Karasozen K. Yapici and Y. Uludag. Finite volume simulation of viscoelastic laminar flow in a lid-driven cavity. *Journal of Non-Newtonian Fluid Mechanics*, 164:51-65., 2009.

[27] YIN Hong-jun SU Yu-chi FU Chun-quan, JIANG Hai-mei and ZENG Ye-ming. Finite volume method for simulation of viscoelastic flow through a expansion channel. *Journal of Hydrodynamics*, 21(3):360-365., 2009.

[28] F. Pimenta and M.A. Alves. Stabilization of an open-source finite-volume solver for viscoelastic fluid flows. *Journal of Non-Newtonian Fluid Mechanics*, 239:85-104., 2017.

[29] G. Raush J. Rigola, S. Morales and C.D. Pérez-Segarra. Analysis of two-phase flow in double-pipe condensers and evaporators with special emphasis on transition zones: Numerical model and experimental comparison. *International Refrigeration and Air Conditioning Conference, http://docs.lib.purdue.edu/iracc/658*, 2004.

[30] R.L. Taylor O.C. Zienkiewicz and P. Nithiarasu. The finite element method. ins basis and fundamentals, 6th edition. *Elsevier Ltd*, 2014.

[31] R.L. Taylor O.C. Zienkiewicz and J.Z. Zhu. The finite element method. ins basis and fundamentals, 6th edition. *Elsevier, Amsterdam*, 2005.

[32] H.C. Martin M.J. Turner, R.W. Clough and L.J. Topp. Stiffness and deflection analysis of complex structures. *Journal of the Aeronautical Sciences*, 23(9):805-823., 1956.

[33] O.C. Zienkiewicz and Y.K. Cheung. Finite elements in the solution of field problems, the engineer. pages 507-510., 1965.

[34] M. Vibiyayuthakorn and B. Caswbll. Finite element simulation of viscoelastic flow. *Journal of Non-Newtonian Fluid Mechanics*, 6:245-267., 1980.

[35] J.J. Feng C.F. Ollivier-Gooch P. Yue, C. Zhou and H.H. Hu. Phase-field simulations of interfacial dynamics in viscoelastic fluids using finite elements with adaptive meshing. *Journal of Computational Physics*, 219:47-67., 2006.

[36] D. Sahel H. Ameur M. Mellal, R. Benzeguir. Hydro-thermal shell-side performance evaluation of a shell and tube heat exchanger under different baffle arrangement and orientation. *International Journal of Thermal Sciences*, 121:138-149., 2017.

[37] R.Keunings and M.J.Crochet. Numerical simulation of the flow of a viscoelastic fluid through an abrupt contraction. *Journal of Non-Newtonian Fluid Mechanics*, 14:279-299., 1984.

[38] M.A.Hulsen Y.J. Choi and H.E.H.Meijera. An extended finite element method for the simulation of particulate viscoelastic flows. *Journal of Non-Newtonian Fluid Mechanics*, 165(607624.):11-12., 2010.

[39] R.C. Armstrong A.W. Liu, D.E. Bornside and R.A. Brown. Viscoelastic flow of polymer solutions around a periodic, linear array of cylinders: comparisons of predictions for microstructure and flow fields. *Journal of Non-Newtonian Fluid Mechanics*, 77:153-190., 1998.

[40] E. Castillo and R. Codina. Finite element approximation of the viscoelastic flow problem: A non-residual based stabilized formulation. *Computers and Fluids*, 142: 72-78., 2017.

[41] B.J. Edwards M. Dressler and H.C. Öttinger. Macroscopic thermodynamics of flowing polymeric liquids. *Rheologica Acta*, 38(2):117-136., 1999.

[42] M.A. Hulsen P. Wapperom and P.P.M. van der Zanden. A numerical method for steady and nonisothermal viscoelastic fluid flow for high deborah and pclet numbers. *Rheologica Acta*, 37(1):73-88., 1998.

[43] G.W.M Peters. Thermorheological modelling of viscoelastic materials. *IUTAM Symposium on Numerical Simulation of Non-Isothermal Flow of Viscoelastic Liquids*, 28:21-35., 1993.

[44] A. Wachs. Thermorheological models and numerical simulation of nonisothermal flows of viscoelastic fluids. phd. thesis. *Institut National Polytechnique de Grenoble, France*, 2000.

[45] J.R. Clermont A. Wachs and A. Khalifeh. Computations of nonisothermal viscous and viscoelastic flows in abrupt contractions using a finite volume method. *Engineering Computations*, 19(8):874-901., 2002.

[46] S. Neuner F. Habla, A. Woitalka and O. Hinrichsen. Development of a methodology for numerical simulation of non-isothermal viscoelastic fluid flows with application to axisymmetric 4:1 contraction flows. *Chemical Engineering Journal*, 207 -208:772 -784., 2012.

[47] D.O. Olagunju. Secondary flow in non-isothermal viscoelastic parallel-plate flow. *Journal of Engineering*, 51(04):325-338., 2005.

[48] R.M.Turian. Viscous heating in the cone-and-plate viscometer III, non-newtonian fluids with temperature-dependent viscosity and thermal conductivity. *Chemical Engineering Science*, 20(8):771-781., 1965.

[49] E. Becker and G.H. McKinley. The stability of viscoelastic creeping plane shear flows with viscous heating. *Journal of Non-Newtonian Fluid Mechanics*, 92(2-3): 771-781., 2000.

[50] R. Sureshkumar U. A. Al-Mubaiyedh and B. Khomami. Influence of energetics on the stability of viscoelastic taylorcouette flow. *Physics of Fluids*, 11:3217-3226., 1999.

[51] T. Chinyoka. Poisueille flow of a reactive phan-thien-tanner liquids in one dimension. *ASME Journal of Heat Transfer*, 132(11):1-7., 2010.

[52] T. Chinyoka. Suction and injection control of shear banding in non-isothermal and exothermic channel flow of johnson-segalman liquids. *ASME Journal of Fluids Engineering*, 133(7):1-12, 2011.

[53] T. Chinyoka. Two-dimensional flow flow of chemically reactive viscoelastic fluids with or without the influence of thermal convection. *Communications in nonlinear Science and Numerical Simulation*, 16(3):1387-1395., 2011.

[54] T. Chinyoka. Computational dynamics of a thermally decomposed viscoelastic lubricant under shear. *ASME Journal of Fluids Engineering*, 130(12):1-7., 2008.

[55] I.E. Ebubechukwu. Computational analysis of non-isothermal flow of non-newtonian fluids.phd. thesis. *University of Cape Town*, 2015.

[56] K.C. Su B. Khomami, Y. Renardy and M.A. Clarke. An experimental/theoretical investigation of interfacial stability in superposed pressure-driven channel flow of well-characterized viscoelastic fluids. part II: nonlinear stability. journal of non-newtonian fluid mechanics. *Journal of Non-Newtonian Fluid Mechanics*, 91:85-104., 2000.

[57] H.K. Versteeg and W. Malalasekera. An introduction to computational fluid dynamics (2nd edition): The finite volume method. *Pearson Education Limited*, 2007.

[58] P. Frolkovič and K. Mikula. Higher order semi-implicit schemes for linear advection equation on cartesian grids with numerical stability analysis. *Slovak University of Technology in Bratislava, Faculty of Civil Engineering*, 2016.

[59] H. Nam and S.J. Choi. Implementation of a semi-implicit time integration scheme in non-hydrostatic euler equations. *Journal of Applied Computational Mathematics*, 6(4), 2017.

[60] R.L. Street Y. Zang and J.R. Koseff. A non-staggered grid, fractional step method for time-dependent incompressible navier-stokes equations in curvilinear coordinates. *Journal Of Computational Physics*, 114(12):18-33., 1994.

[61] T. Chinyoka. Numerical simulation of stratified flows and droplet deformation in 2d shear flow of newtonian and viscoelastic fluids. phd. thesis, virginia polytechnic institute and state university. *http://scholar.lib.vt.edu/theses/available/etd-11292004-130236*, 2004.

[62] T. Chinyoka D.B. Khismatullin Y. Renardy, M. Renardy and J. Li. A viscoelastic vof-prost code for the study of drop deformation. *ASME Heat Transfer/Fluids Engineering Summer Conference,HTFED2004, Charlotte, North Carolina, U.S.A*, CDROM Track 5, 56114.pdf, 11 - 15 July 2004.

[63] T. Chinyoka and O.D. Makinde. On transient flow of a reactive variable viscosity third-grade fluid through a cylindrical pipe with convective cooling. *Meccanica*, 47 (3):667 - 685, 2012.

[64] X. Chen. Numerical modeling of fluid-structure interaction with rheologically complex fluids. *Technischen Universität*, 2014.

[65] C.A.J. Fletcher. Computational techniques for fluid dynamics 2 : Specific techniques for different flow categories. *Springer-Verlag*, 1991.

[66] T.V. Gerya T. Duretz, D.A. May and P.J. Tackley. Discretization errors and free surface stabilization in the finite difference and markerincell method for applied geodynamics: A numerical study. *Geochemistry, Geophysics, Geosystems*, 12(7), 2011.

[67] S. Mazumder. Numerical methods for partial differential equations:finite difference and finite volume methods. *Elsevier Science Publishing Co Inc*, 2016.

[68] C. Hirsch. Numerical computation of internal and external flows:fundamentals of computational fluid dynamics(3rd edition). *Butterworth-Heinemann*, 2007.

[69] O.V. Vasilyev Y.Morinishi, T.S. Lund and P. Moin. Fully conservative higher order finite difference schemes for incompressible flow. *Journal Of Computational Physics*, 143(1):90-124., 1998.

[70] M. Schäfer. Computational engineering : Introduction to numerical methods. *Springer-Verlag , Berlin*, 2006.

[71] L. Mangani and C. Bianchini. Heat transfer applications in turbomachinery. *OpenFOAM Conference, London United Kingdom*, 26 - 27 November 2007.

[72] J. H. Ferziger and M. Perić. Computational methods for fluid dynamics (3rd edition). *Springer-Verlag*, 2002.